



THE ROLE OF PLATELET GRANULES IN  
THROMBOSIS, HEMOSTASIS, STROKE AND  
INFLAMMATION

—  
ZUR ROLLE DER THROMBOZYTENGRANULA  
IN THROMBOSE, HÄMOSTASE,  
SCHLAGANFALL UND ENTZÜNDUNG

Doctoral thesis for a doctoral degree  
at the Graduate School of Life Sciences,  
Julius-Maximilians-Universität Würzburg,  
Section Biomedicine,  
submitted by

**Carsten Deppermann**  
from Frankfurt/Main, Germany

August 2015

Submitted on:

Members of the *Promotionskomitee*:

Chairperson:	Prof. Dr. Manfred Gessler
Primary Supervisor:	Prof. Dr. Bernhard Nieswandt
Supervisor (Second):	Prof. Dr. Georg Krohne
Supervisor (Third):	Dr. Paquita Nurden

Date of Public Defence:

Date of Receipt of Certificate:

# Contents

<b>Contents</b>	<b>iii</b>
<b>Summary</b>	<b>vi</b>
<b>Zusammenfassung</b>	<b>vii</b>
<b>1 Introduction</b>	<b>1</b>
1.1 Platelets . . . . .	1
1.2 Platelet activation and thrombus formation . . . . .	2
1.3 Platelet signaling upon activation . . . . .	3
1.4 Megakaryocytes . . . . .	7
1.4.1 Megakaryopoiesis . . . . .	9
1.4.2 Transcription factors in megakaryopoiesis . . . . .	9
1.5 Platelet granules . . . . .	10
1.5.1 Platelet granule content . . . . .	10
1.5.2 Platelet granule content in normal physiology and pathophysiology . . . . .	11
1.5.3 Biogenesis of platelet granules . . . . .	14
1.5.4 Platelet secretion . . . . .	15
1.5.5 Platelet granule disorders . . . . .	17
1.6 Aim of this study . . . . .	18
<b>2 Materials and Methods</b>	<b>20</b>
2.1 Materials . . . . .	20
2.1.1 Chemicals and reagents . . . . .	20
2.1.2 Antibodies . . . . .	21
2.1.3 Buffers . . . . .	22
2.1.4 Animals . . . . .	25
2.2 Methods . . . . .	26
2.2.1 Genotyping of mice . . . . .	26
2.2.2 Molecular biology and biochemistry . . . . .	28
2.2.3 <i>In vitro</i> analyses of platelet function . . . . .	29
2.2.4 <i>In vivo</i> analyses of platelet function . . . . .	32
2.2.5 MK analyses . . . . .	34
2.2.6 Electron microscopy . . . . .	35
2.2.7 Histology . . . . .	36

2.2.8	Statistical data analysis . . . . .	37
<b>3</b>	<b>Results</b>	<b>38</b>
3.1	Analysis of Munc13-4-deficient mice . . . . .	38
3.1.1	<i>Unc13d</i> <sup>-/-</sup> mice display unaltered platelet counts and granule numbers . . . . .	38
3.1.2	Abrogated ATP secretion and aggregation of <i>Unc13d</i> <sup>-/-</sup> platelets . . . . .	38
3.1.3	<i>Unc13d</i> <sup>-/-</sup> platelets show impaired P-selectin exposure and integrin activation after stimulation and adhesion to collagen under flow . . . . .	39
3.1.4	Defective <i>in vivo</i> thrombus formation and hemostasis in <i>Unc13d</i> <sup>-/-</sup> mice . . . . .	41
3.1.5	Reduced infarct size and no signs of hemorrhage in Munc13-4-deficient mice after tMCAO . . . . .	42
3.2	Analysis of <i>Nbeal2</i> -deficient mice . . . . .	46
3.2.1	<i>Nbeal2</i> <sup>-/-</sup> mice are macrothrombocytopenic and lack $\alpha$ -granules in MKs and platelets . . . . .	46
3.2.2	Defective adhesion and aggregate formation of <i>Nbeal2</i> <sup>-/-</sup> platelets under flow . . . . .	55
3.2.3	Severely defective arterial thrombus formation and hemostasis in <i>Nbeal2</i> -deficient mice . . . . .	57
3.2.4	<i>Nbeal2</i> <sup>-/-</sup> mice are protected in a model of ischemic stroke . . . . .	60
3.2.5	<i>Nbeal2</i> <sup>-/-</sup> mice show impaired dermal healing due to reduced TGF- $\beta$ release from mutant platelets . . . . .	61
3.2.6	Comparison of <i>Nbeal2</i> <sup>-/-</sup> and human GPS platelets and MKs . . . . .	62
3.3	Analysis of Munc13-4/ <i>Nbeal2</i> -deficient mice . . . . .	65
3.3.1	Macrothrombocytopenia but unaltered platelet glycoprotein expression in <i>Unc13d</i> <sup>-/-</sup> / <i>Nbeal2</i> <sup>-/-</sup> mice . . . . .	65
3.3.2	Abrogated P-selectin exposure and reduced integrin activation upon stimulation of Munc13-4/ <i>Nbeal2</i> -deficient platelets . . . . .	65
3.3.3	<i>Unc13d</i> <sup>-/-</sup> / <i>Nbeal2</i> <sup>-/-</sup> platelets show defective aggregation, adhesion to collagen under flow and PS exposure . . . . .	67
3.3.4	Munc13-4/ <i>Nbeal2</i> -deficient mice display impaired thrombosis and hemostasis <i>in vivo</i> . . . . .	69
3.3.5	<i>Unc13d</i> <sup>-/-</sup> / <i>Nbeal2</i> <sup>-/-</sup> mice maintain vascular integrity at sites of local inflammation but not ischemic stroke . . . . .	69
<b>4</b>	<b>Discussion</b>	<b>73</b>
4.1	Platelet dense granules in thrombosis, hemostasis and stroke . . . . .	73
4.2	Platelet $\alpha$ -granules in thrombosis, hemostasis and stroke . . . . .	74
4.2.1	The <i>Nbeal2</i> <sup>-/-</sup> mouse as a model for the gray platelet syndrome . . . . .	77
4.2.2	The role of NBEAL2 in $\alpha$ -granule biogenesis . . . . .	78
4.3	Combined deficiency of platelet $\alpha$ - and dense granule secretion . . . . .	79
4.4	Concluding remarks and outlook . . . . .	82

---

<b>Bibliography</b>	<b>84</b>
<b>5 Appendix</b>	<b>101</b>
5.1 Abbreviations . . . . .	101
5.2 Acknowledgements . . . . .	104
5.3 Curriculum vitae . . . . .	105
5.4 Publications . . . . .	107
5.4.1 Research articles . . . . .	107
5.4.2 Selected talks and presentations . . . . .	107
5.5 Affidavit . . . . .	109
5.6 Eidesstattliche Erklärung . . . . .	109

# Summary

Platelets are small anucleate cell fragments derived from bone marrow *megakaryocytes* (MKs) and are important players in hemostasis and thrombosis. Platelet granules store factors which are released upon activation. There are three major types of platelet granules:  $\alpha$ -granules, dense granules and lysosomes. While dense granules contain non-proteinaceous factors which support platelet aggregation and adhesion, platelet  $\alpha$ -granules contain more than 300 different proteins involved in various functions such as inflammation, wound healing and the maintenance of vascular integrity, however, their functional significance *in vivo* remains unknown. This thesis summarizes analyses using three mouse models generated to investigate the role of platelet granules in thrombosis, hemostasis, stroke and inflammation.

*Unc13d*<sup>-/-</sup> mice displayed defective platelet dense granule secretion, which resulted in abrogated thrombosis and hemostasis. Remarkably, Munc13-4-deficient mice were profoundly protected from infarct progression following *transient middle cerebral artery occlusion* (tMCAO) and this was not associated with increased intracranial bleeding indicating an essential involvement of dense granule secretion in infarct progression but not intracranial hemostasis during acute stroke with obvious therapeutic implications.

In the second part of this thesis, the role of platelet  $\alpha$ -granules was investigated using the *Nbeal2*<sup>-/-</sup> mouse. Mutations in *NBEAL2* have been linked to the *gray platelet syndrome* (GPS), a rare inherited bleeding disorder. *Nbeal2*<sup>-/-</sup> mice displayed the characteristics of human GPS, with defective  $\alpha$ -granule biogenesis in MKs and their absence from platelets. *Nbeal2*-deficiency did not affect MK differentiation and proplatelet formation *in vitro* or platelet life span *in vivo*. *Nbeal2*<sup>-/-</sup> platelets displayed impaired adhesion, aggregation, and coagulant activity *ex vivo* that translated into defective arterial thrombus formation and protection from thrombo-inflammatory brain infarction *in vivo*. In a model of skin wound repair, *Nbeal2*<sup>-/-</sup> mice exhibited impaired development of functional granulation tissue due to severely reduced differentiation of myofibroblasts.

In the third part, the effects of combined deficiency of  $\alpha$ - and dense granule secretion were analyzed using *Unc13d*<sup>-/-</sup>/*Nbeal2*<sup>-/-</sup> mice. Platelets of these mice showed impaired aggregation and adhesion to collagen under flow *ex vivo*, which translated into infinite tail bleeding times and severely defective arterial thrombus formation *in vivo*. When subjected to *in vivo* models of skin or lung inflammation, the double mutant mice showed no signs of hemorrhage. In contrast, lack of platelet granule release resulted in impaired vascular integrity in the ischemic brain following tMCAO leading to increased mortality. This indicates that while defective dense granule secretion or the paucity of  $\alpha$ -granules alone have no effect on vascular integrity after stroke, the combination of both impairs vascular integrity and causes an increase in mortality.

# Zusammenfassung

Thrombozyten sind kleine, kernlose Zellfragmente, die von *Megakaryozyten* (MKs) im Knochenmark gebildet werden und eine zentrale Rolle in Thrombose und Hämostase spielen. Thrombozytengranula speichern Faktoren, die nach Thrombozytenaktivierung freigesetzt werden. Die drei wichtigsten Thrombozytengranula sind  $\alpha$ - und dichte Granula, sowie Lysosomen. Während dichte Granula vor allem anorganische Faktoren enthalten, welche die Thrombozytenaktivierung und -aggregation fördern, speichern  $\alpha$ -Granula mehr als 300 verschiedene Proteine mit einer Vielzahl an Funktionen. Sie sind beispielsweise an Entzündungsprozessen, Wundheilung und der Aufrechterhaltung vaskulärer Integrität beteiligt. Die funktionelle Signifikanz dieser Faktoren, insbesondere *in vivo*, blieb bisher allerdings ungeklärt. Diese Doktorarbeit beschreibt die Analyse der Rolle von Thrombozytengranula in Thrombose, Hämostase, Schlaganfall und Entzündung unter Verwendung von drei Knockout-Mauslinien.

*Unc13d*<sup>-/-</sup> Mäuse dienten als Modell, um die Rolle der dichten Granulasekretion in Thrombose, Hämostase, Schlaganfall und der Aufrechterhaltung der vaskulären Integrität nach Thromboinflammation zu untersuchen. Die fehlende Freisetzung des Inhalts dichter Granula aus Thrombozyten dieser Mäuse führte zu defekter Thrombose und Hämostase. *Unc13d*<sup>-/-</sup> Mäuse zeigten deutlich kleinere Infarkte im tMCAO (*transient middle cerebral artery occlusion*)-Modell des ischämischen Schlaganfalls. Gleichzeitig wurde jedoch keine erhöhte Blutungsneigung im Gehirn nach Schlaganfall festgestellt. Dies deutet auf eine Schlüsselrolle der Sekretion dichter Granula in der Infarktentwicklung hin, die jedoch nicht die intrakranielle Hämostase während des akuten Schlaganfalls beeinflusst.

Der zweite Teil dieser Doktorarbeit behandelt die Rolle von  $\alpha$ -Granula unter Verwendung der *Nbeal2*<sup>-/-</sup> Maus. Vor Kurzem wurde gezeigt, dass Mutationen im *NBEAL2*-Gen das *Gray Platelet Syndrome* (GPS) hervorrufen. Das GPS ist eine seltene erbliche Blutungskrankheit mit Makrothrombozytopenie, defekter  $\alpha$ -Granulabiogenese in MKs und dem Fehlen thrombozytärer  $\alpha$ -Granula. *Nbeal2*-Defizienz führte zu unveränderter MK-Differenzierung, Proplättchenbildung *in vitro* und Thrombozytenlebensdauer *in vivo*. *Nbeal2*-defiziente Thrombozyten zeigten jedoch verringerte Adhäsion, Aggregation und Koagulation *ex vivo*, welche zu einer gestörten arteriellen Thrombusbildung und Schutz vor thromboinflammatorischem Schlaganfall nach zerebraler Ischämie führte. In einem Wundheilungsmodell der Haut zeigte sich bei *Nbeal2*-defizienten Mäusen eine verringerte Bildung von Granulationsgewebe während des Heilungsvorgangs. Die Ursache hierfür lag in der reduzierten Myofibroblastendifferenzierung aufgrund fehlender  $\alpha$ -Granulaausschüttung. Zusammengefasst zeigen diese Ergebnisse, dass  $\alpha$ -Granulabestandteile nicht nur für Thrombose und Hämostase, sondern auch für akute thromboinflammatorische Krankheitszustände und Geweberegeneration nach Verletzung essentiell sind.

Im dritten Teil dieser Arbeit wurde der Effekt einer kombinierten Sekretionsdefizienz von  $\alpha$ - und dichten Granula mithilfe von *Unc13d<sup>-/-</sup>/Nbeal2<sup>-/-</sup>* Mäusen untersucht. Thrombozyten dieser Mäuse zeigten verringerte Aggregation und Adhäsion an Kollagen unter Flussbedingungen *ex vivo*, sowie massiv verlängerte Blutungszeiten und defekte Thrombusbildung *in vivo*. Die defekte Granulafreisetzung in *Unc13d<sup>-/-</sup>/Nbeal2<sup>-/-</sup>* Mäusen führte zum Zusammenbruch der vaskulären Integrität im tMCAO-Modell des ischämischen Schlaganfalls und zu einer erhöhten Mortalitätsrate. Im Gegensatz dazu zeigten die doppeldefizienten Mäuse in *in vivo* Modellen der Haut- oder Lungenentzündung keine Einblutungen. Dies deutet darauf hin, dass die fehlende Sekretion dichter Granula oder die Abwesenheit von  $\alpha$ -Granula für sich genommen keinen Einfluss auf die Aufrechterhaltung der vaskulären Integrität nach Schlaganfall hat. Die Kombination beider Defekte führt jedoch zum Zusammenbruch der zerebrovaskulären Integrität und erhöhter Mortalität nach Schlaganfall.



# 1 Introduction

## 1.1 Platelets

Platelets are small, anucleate cell fragments that are derived from polyploid precursor cells called megakaryocytes (MKs) which reside predominantly in the bone marrow. Humans typically show platelet counts between 150,000 to 450,000/ $\mu\text{l}$  in the peripheral blood. Mice, which are an important model organism for the study of thrombosis and hemostasis, exhibit a platelet count of approximately 1,000,000/ $\mu\text{l}$ . The lifespan of a platelet is approximately 10 days in humans and about 5 days in mice [29, 51, 74].

As platelets lack a nucleus, they have only limited capacity for *de novo* protein synthesis. They contain, however, organelles including mitochondria, the *open canalicular system* (OCS), the dense tubular system and three different types of granules:  $\alpha$ -granules, dense granules and lysosomes. While dense granules contain mainly non-proteinaceous compounds that support platelet aggregation and lysosomes store proteolytic enzymes,  $\alpha$ -granules contain more than 300 different proteins involved in functions like coagulation, platelet adhesion, inflammation, wound healing and angiogenesis.

Platelets safeguard the integrity of the vascular system and are major players in hemostasis. In healthy individuals, however, most platelets never become activated and are cleared by the reticuloendothelial system in the spleen and liver at the end of their lifetime. As soon as platelets encounter a damaged vessel wall and the exposed components of the subendothelial *extracellular matrix* (ECM), they become rapidly activated and adhere tightly to both the vessel wall and to other platelets. Factors released from platelet granules and locally produced thrombin further enhance platelet activation in an autocrine and paracrine way thereby supporting thrombus formation.

Although the process of platelet adhesion and aggregation prevents excessive bleeding after injury, it can also cause damage in pathological situations, in which uncontrolled platelet aggregation and thrombus formation lead to occlusion of major vessels, e.g. during thrombosis or after rupture of an atherosclerotic plaque. The latter leads to exposure of thrombogenic material and is followed by platelet aggregation and formation of a thrombus that may either occlude the lumen or detach to embolize and block blood flow distal to its point of origin. Atherothrombosis elicits ischemia which can be fatal in case important organs or tissues are affected [73, 87, 131].

Cerebral ischemia accounts for about 80% of all strokes and is a leading cause of morbidity and mortality worldwide [126]. Atrial fibrillation and extracranial artery stenoses are the major

sources of thromboembolism to the brain. Occlusion of intracranial vessels deprives the respective brain territory of oxygen and glucose supply and leads to acute neurological defects like hemiparesis or aphasia.

Anti-coagulation or anti-platelet treatments are used for prevention of secondary stroke. Anticoagulation with warfarin (e.g. in patients with atrial fibrillation) carries a risk of bleeding complications. Novel oral anticoagulants specifically target thrombin or coagulation factor Xa and have a more favorable safety profile [43]. Platelet inhibitors such as *acetylsalicylic acid* (ASA) which inhibits *cyclooxygenase-1* and *-2* (COX-1 and -2) and thereby *thromboxane A2* (TxA<sub>2</sub>) production or clopidogrel which targets the platelet ADP receptor P2Y<sub>12</sub> are widely used. However, the mechanisms by which antiplatelet agents prevent thrombus growth within the brain microvasculature as well as the multifaceted role of platelets in acute stroke development remain unclear [172].

There is only one treatment option for acute stroke: thrombolysis with *tissue plasminogen activator* (tPA). Unfortunately, tPA application is restricted to the first 3-4.5 h after stroke, since afterwards bleeding complications outweigh the benefits of thrombolysis [71, 130]. Even if the thrombus is resolved, there is a significant incidence of infarct growth, a phenomenon termed "reperfusion injury". The molecular mechanisms involved are still poorly understood [172]. Therefore, investigations of the mechanisms that govern platelet activation and thrombus formation are of great importance to understand the role of platelets in acute stroke and to aid identification of targets that could lead to the development of safe and efficient treatments for (athero)thrombosis and stroke [189].

## 1.2 Platelet activation and thrombus formation

Platelet activation and thrombus formation at sites of vascular injury is a multi-step process that can be divided into three major steps (see figure 1.1): First, platelets encounter *von Willebrand Factor* (vWF), which is immobilized on collagen fibres after vessel injury. Interaction of vWF with the platelet receptor complex *glycoprotein* (GP) Ib-V-IX starts the platelet activation process and causes platelet tethering and rolling, which lead to platelet deceleration and enable further interactions of platelet receptors. The second step involves binding of the platelet-specific immunoglobulin superfamily receptor GPVI to the ECM protein collagen [129]. GPVI induces platelet activation by intracellular signaling processes via an *immunoreceptor tyrosine-based activation motif* (ITAM) in the associated *Fc receptor* (FcR)  $\gamma$ -chain. Platelet activation leads to the release of second wave mediators, most notably *adenosine diphosphate* (ADP), secreted by dense granules, and TxA<sub>2</sub>, synthesized by COX-1. Platelet activation also increases activity of platelet scramblases which causes exposure of negatively charged *phosphatidylserine* (PS) on the platelet surface. PS provides a surface for the assembly of two major coagulation factor complexes and subsequent thrombin production, which is amplified through the exposure of local *tissue factor* (TF) [32, 76]. ADP, thrombin and TxA<sub>2</sub> further enhance platelet activation via *G protein-coupled receptors* (GPCRs) and the downstream G proteins G<sub>q</sub>, G<sub>12/13</sub> and G<sub>i</sub>/G<sub>z</sub>

to induce full platelet activation [142] which enables recruitment of additional platelets from the blood stream into the growing thrombus.

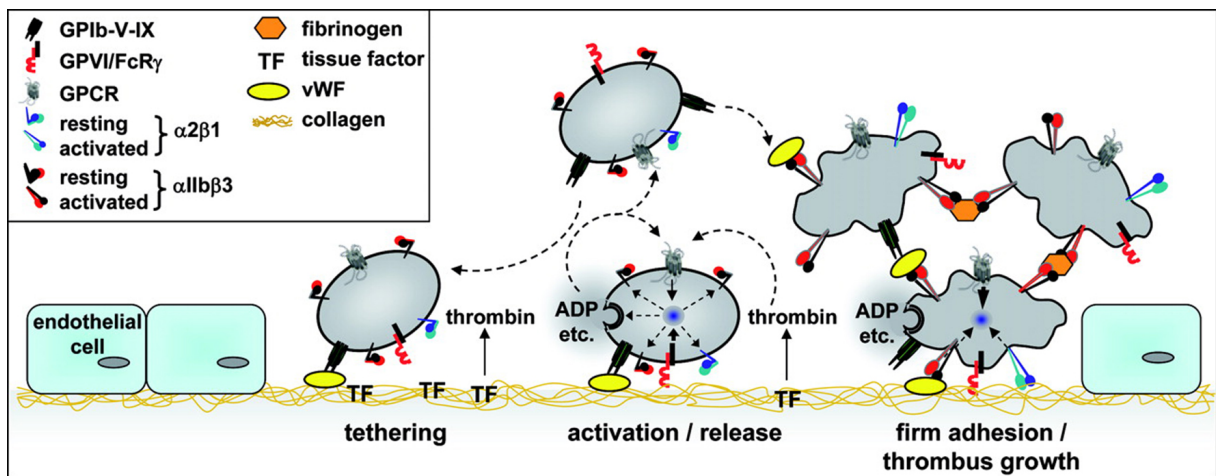


**Figure 1.1: Platelet adhesion and thrombus formation on components of the ECM.** Platelet tethering at sites of exposed ECM is mediated by GPIb-vWF interactions which causes platelets to slow down, roll along the vessel wall and form more stable interactions via the GPVI receptor that binds to exposed collagen fibres. Platelet activation by GPVI-collagen interactions causes integrins to shift from a low- to a high-affinity state and release of platelet granule content. Secondary mediators released from platelet granules such as ADP and locally produced thrombin further enhance platelet activation and thrombus growth. Image taken from [187].

All signaling events described converge in the final common pathway of platelet activation: Integrins on the platelet surface shift from a low to a high affinity state, which enables firm ligand binding. Platelets express three  $\beta 1$  integrins:  $\alpha 2\beta 1$ ,  $\alpha 5\beta 1$  and  $\alpha 6\beta 1$ , which bind to collagen, fibronectin and laminin, respectively, and two  $\beta 3$  integrins:  $\alpha v\beta 3$  which binds to vitronectin and  $\alpha IIb\beta 3$  [12]. The latter one is the most abundant integrin on the platelet surface and binds to fibrinogen, vWF, fibronectin, and vitronectin. Thereby it enables stable platelet-platelet interaction and adhesion to the ECM. Activated integrins transduce outside-in signals which cause cytoskeletal rearrangements, spreading and clot retraction [12, 191]. The importance of  $\alpha IIb\beta 3$  for stable platelet aggregation is illustrated by a disorder called Glanzmann thrombasthenia which is characterized by impaired  $\alpha IIb\beta 3$  expression or function that leads to severe bleeding in affected patients [140].

### 1.3 Platelet signaling upon activation

There are two major downstream signaling pathways that are activated after ligand binding to receptors on the platelet surface. Both culminate in the activation of *phospholipase C* (PLC) isoforms which is followed by an elevation of intracellular calcium levels ( $[Ca^{2+}]_i$ ). Increase in  $[Ca^{2+}]_i$  is a prerequisite for granule release, integrin activation and procoagulant activity (see figure 1.2).

As mentioned above, soluble factors such as ADP,  $TxA_2$  and thrombin activate platelets via GPCR-mediated signaling pathways that cause shape change, degranulation and activation of

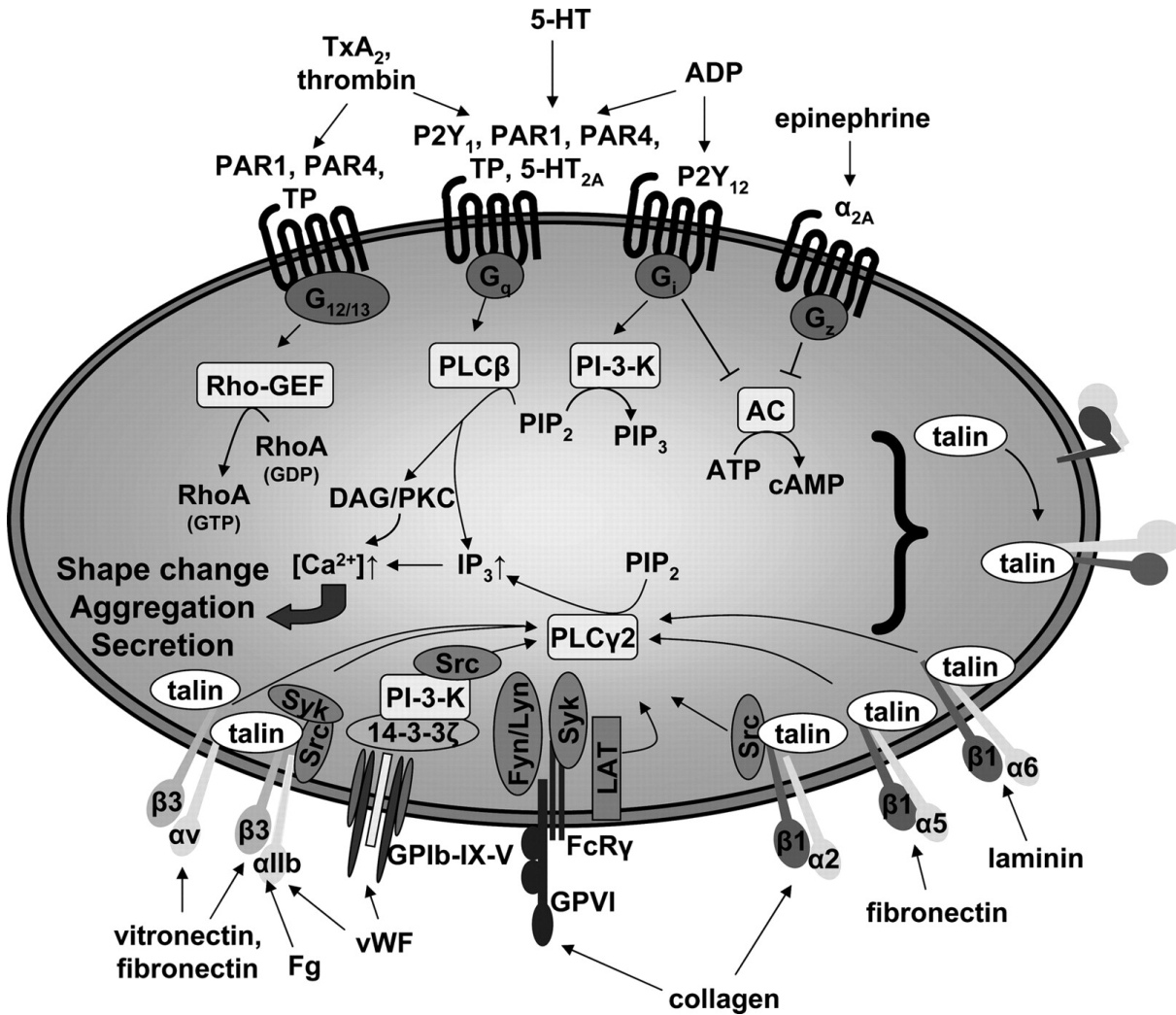


**Figure 1.2: Platelet signaling upon activation.** Soluble factors like ADP, TxA<sub>2</sub> and thrombin activate platelets via binding to *G-protein coupled receptors* (GPCRs) and stimulate G<sub>q</sub>, G<sub>12/13</sub> and G<sub>i</sub>. Signaling downstream of G<sub>q</sub> leads to activation of PLCβ. Furthermore, GPCRs induce activation of Rho GTPases leading to cytoskeletal rearrangements. Adhesion receptors, like the major collagen receptor GPVI and active integrins induce PLCγ2 activation upon ligand binding. PLCs generate *diacyl glycerol* (DAG) and *inositol-1,4,5-trisphosphate* (IP<sub>3</sub>) which induce an increase in intracellular Ca<sup>2+</sup> levels, which is crucial for platelet shape change, aggregation and granule secretion. PIP<sub>2</sub>, phosphatidylinositol-4,5-bisphosphate; PI-3-K, phosphoinositide-3-kinase; PKC, protein kinase C; PLC, phospholipase C. Image taken from [187].

integrin αIIbβ3 which leads to platelet aggregation. While ADP binds to the receptors P2Y<sub>12</sub> and P2Y<sub>1</sub> to activate G<sub>i</sub> and G<sub>q</sub>, TxA<sub>2</sub> binds to the *thromboxane receptor* (TP). The *protease-activated receptors* (PAR) 1 and 4 (human) or 3 and 4 (mouse) are activated by proteolytic cleavage of their N-terminus by thrombin, which exposes a so-called "tethered ligand" that activates the cleaved receptors to stimulate G<sub>q</sub> and G<sub>12/13</sub> [114].

The second pathway involves the major platelet collagen receptor GPVI and the *C-type lectin-like receptor 2* (CLEC-2), that binds the endogenous ligand podoplanin, which is not expressed within the vasculature, and the snake venom toxin rhodocytin [134, 177]. The GPVI receptor is non-covalently associated with an FcR γ-chain homodimer which serves as the signal trans-

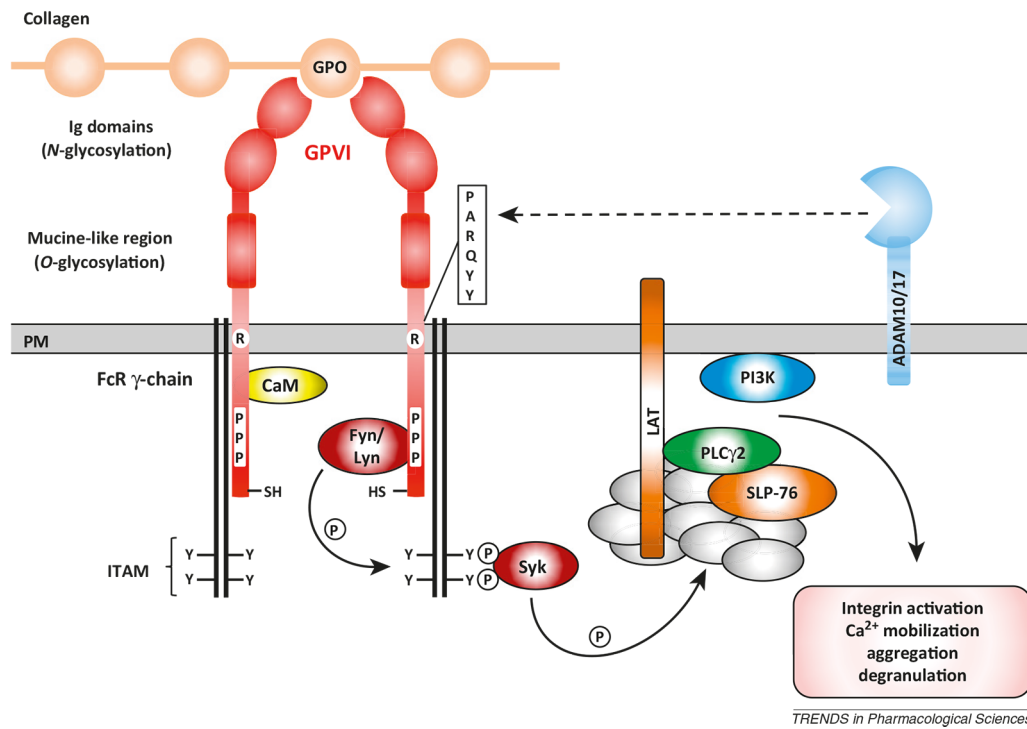


**Figure 1.3: Signaling of the GPVI/FcR  $\gamma$ -chain complex.** Crosslinking of GPVI dimers through binding to glycine–proline–hydroxyproline (GPO) motifs in collagen causes Fyn/Lyn-mediated phosphorylation of the FcR  $\gamma$ -chain ITAMs. This in turn initiates a Syk-dependent signaling cascade, ultimately leading to PLC $\gamma$ 2 and PI3K activation that triggers integrin activation, Ca<sup>2+</sup> mobilization, platelet aggregation and degranulation. Image taken from [38].

ducer of the receptor complex. GPVI recognizes *glycine–proline–hydroxyproline* (GPO) motifs within collagen, which spontaneously form helical structures. Collagen binding triggers receptor crosslinking, that leads to phosphorylation of the two tyrosine residues within the ITAM on the FcR  $\gamma$ -chain by the *Src family kinases* (SFKs) Fyn and Lyn [38, 134].

CLEC-2 contains a single conserved cytosolic YXXL sequence (hemITAM) which upon receptor multimerization is phosphorylated and enables receptor signaling. Phosphorylation of the (hem)ITAMs in the FcR  $\gamma$ -chain and CLEC-2 leads to recruitment, phosphorylation, and activation of the tyrosine kinase Syk. Syk initiates a downstream signaling cascade involving the adaptors *linker of activated T cells* (LAT) and *SH2 domain containing leukocyte protein of 76 kDa* (SLP-76) which leads to activation of PLC $\gamma$ 2 and *phosphoinositide-3 kinase* (PI3K) (see figure 1.3) [38, 134].

Activation of PLCs finally results in the production of *1,4,5-trisphosphate* (IP<sub>3</sub>) and *diacylglycerol* (DAG) by hydrolysis of *phosphatidylinositol 4,5-bisphosphate* (PIP<sub>2</sub>). IP<sub>3</sub> triggers Ca<sup>2+</sup> release from intracellular stores and in turn STIM1 opens Orai1 Ca<sup>2+</sup> channels in the plasma membrane, a process called *store-operated calcium entry* (SOCE). DAG on the other hand mediates non-SOCE through canonical *transient receptor potential channel 6* (TRPC6). Additionally, a direct *receptor-operated calcium* (ROC) channel, P2X<sub>1</sub> and a *Na<sup>+</sup>/Ca<sup>2+</sup> exchanger* (NCX) contribute to the elevation in [Ca<sup>2+</sup>]<sub>i</sub> [186] which is essential for platelet activation, gran-

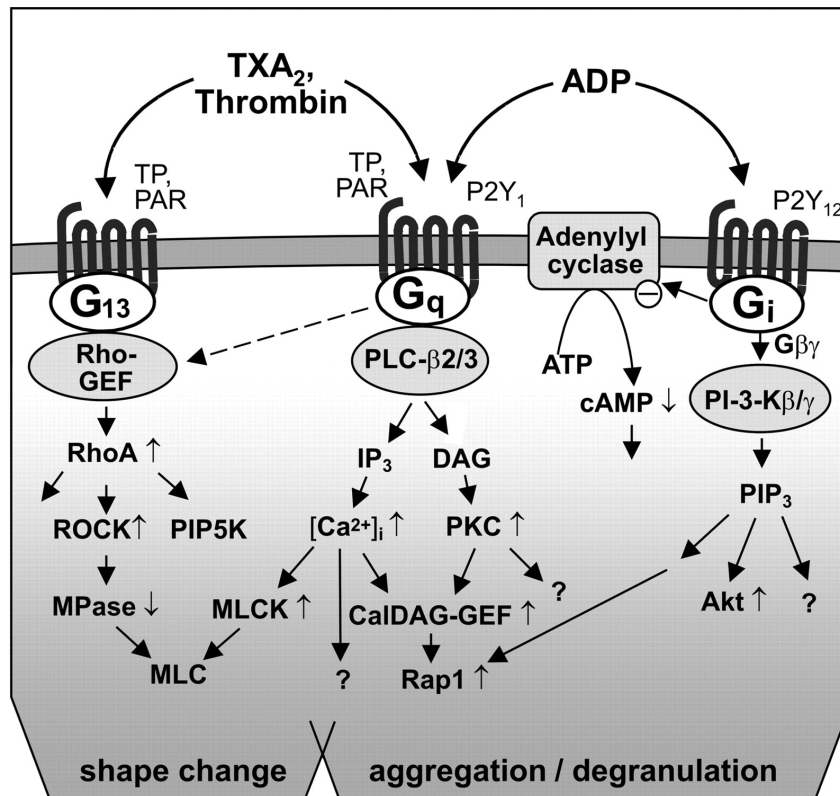


**Figure 1.4: Signaling pathways downstream of platelet GPCRs.** Shown are some of the signaling mechanisms linking the activation of GPCRs by ADP,  $\text{TxA}_2$ , and thrombin via the G proteins  $G_i$ ,  $G_q$  and  $G_{13}$  to the induction of platelet shape change, aggregation and degranulation. RhoGEF: Rho-guanine nucleotide exchange factor, PIP5K: phosphatidylinositol-4-phosphate 5-kinase, MPase: myosin phosphatase, MLCK: Myosin light chain kinase, DAG: diacyl glycerol, CalDAG-GEF: calcium and diacyl glycerol-regulated guanine nucleotide exchange factor, PIP3: phosphatidylinositol-3,4,5-trisphosphate. Image taken from [142].

ule secretion and aggregation [15].

There are several steps required for the activation of the integrin  $\alpha\text{IIb}\beta_3$  to take place:  $\text{Ca}^{2+}$  influx via SOCE and ROCE leads to the activation of *Ca<sup>2+</sup>- and DAG-regulated guanine nucleotide exchange factor 1* (CALDAG-GEF1) which converts RAP1 from its inactive GDP-bound form to its active GTP-bound form. PKC $\alpha$  facilitates CALDAG-GEF1 activation [165]. It is thought that in a next step the *Rap1-GTP-interacting adaptor molecule* (RIAM) and talin are recruited to the plasma membrane. Subsequently, talin binds to the  $\beta_3$  integrin subunit and activates integrin  $\alpha\text{IIb}\beta_3$  [165]. However, recently it has been reported that RIAM is dispensable for platelet integrin activation in mice [173]. Besides talin, it was shown that kindlin-3 is an essential regulator of integrin  $\beta_3$  and  $\beta_1$  activation and platelet aggregation. The exact role of kindlin-3 in integrin activation, however, remains unknown [124].

Platelet shape change is one of the first reactions of the cells to stimulation by thrombin,  $\text{TxA}_2$ , ADP and other agonists. It is mediated by *Myosin light chain* (MLC) phosphorylation which causes actomyosin contraction. MLC phosphorylation is controlled through a  $\text{Ca}^{2+}$ /calmodulin-dependent regulation of *MLC kinase* (MLCK) downstream of  $G_q$  and through a Rho/Rho-

kinase-mediated regulation of myosin phosphatase downstream of  $G_{12/13}$  [142]. Platelet activation involves a major reorganization of the cytoskeleton, including the formation of new actin filaments at the cytoplasmic side of the plasma membrane and centralization of  $\alpha$ - and dense granules enabling concerted degranulation (see figure 1.4). Depolymerization of the microtubule coil that surrounds the platelet enables shape change from discoid to spherical [75].

## 1.4 Megakaryocytes

Platelets are derived from precursor cells called *megakaryocytes* (MKs) that reside in the bone marrow. These specialized cells differentiate from *hematopoietic stem cells* (HSCs) and are capable of producing up to 10,000 platelets each [98, 111, 190]. During their development they undergo significant changes in morphology, size and DNA content.

Mature MKs show several unique characteristics, such as their size (50-100  $\mu\text{m}$  in diameter), the presence of a single, large multilobed nucleus and polyploidy. Polyploidization begins in immature MKs through a process called endomitosis, which is incompletely understood. Endomitosis is most likely caused by alterations in the regulation of the mitotic exit which causes abortive mitosis and a major defect in cytokinesis [188].

Furthermore, mature MKs express specific surface glycoproteins (e.g. GPIb, GPIX and GPV), show a large number of ribosomes that enable high protein synthesis rates and the presence of a *demarcation membrane system* (DMS) as well as  $\alpha$ - and dense granules. The DMS serves as a membrane reservoir during platelet formation. Secretory proteins, such as vWF, are synthesized and packed into granules, others, like fibrinogen are taken up via endocytosis and transported into platelet granules [143, 144, 161].

The exact mechanism of platelet formation by MKs has been discussed controversially over the last decades. Some groups support the idea of a fragmentation model according to which mature MKs “burst” into thousands of platelets in the bone marrow [103]. On the other hand, the flow model of platelet formation implies that mature MKs form pseudopodial extensions, so-called proplatelets, which extend into the bone marrow vascular sinusoids where they are released. Recent studies using *in vitro* and *in vivo* analyses consistently report proplatelet formation from MKs as a common feature of platelet biogenesis. *In vitro* cell culture systems have been instrumental in studying mechanisms of proplatelet formation [144, 161, 180]. Importantly, recent *in vivo* studies could show that, under physiological conditions, mature MKs shed proplatelet-like structures into sinusoids of the bone marrow which are then further fragmented to platelets by the shear forces present in blood vessels (see figure 1.5) [90, 201]. However, there are other very recent investigations using *in vivo* microscopy showing that IL-1 $\alpha$ -triggered MK rupture takes place upon acute platelet needs [133, 135]. Therefore, it is likely that both mechanisms exist in parallel but serve different functions: Continuous platelet release via proplatelet formation in normal physiology and MK rupture under conditions of increased platelet loss or consumption, e.g. as a result of excessive blood loss or in the setting of infection or inflammation.

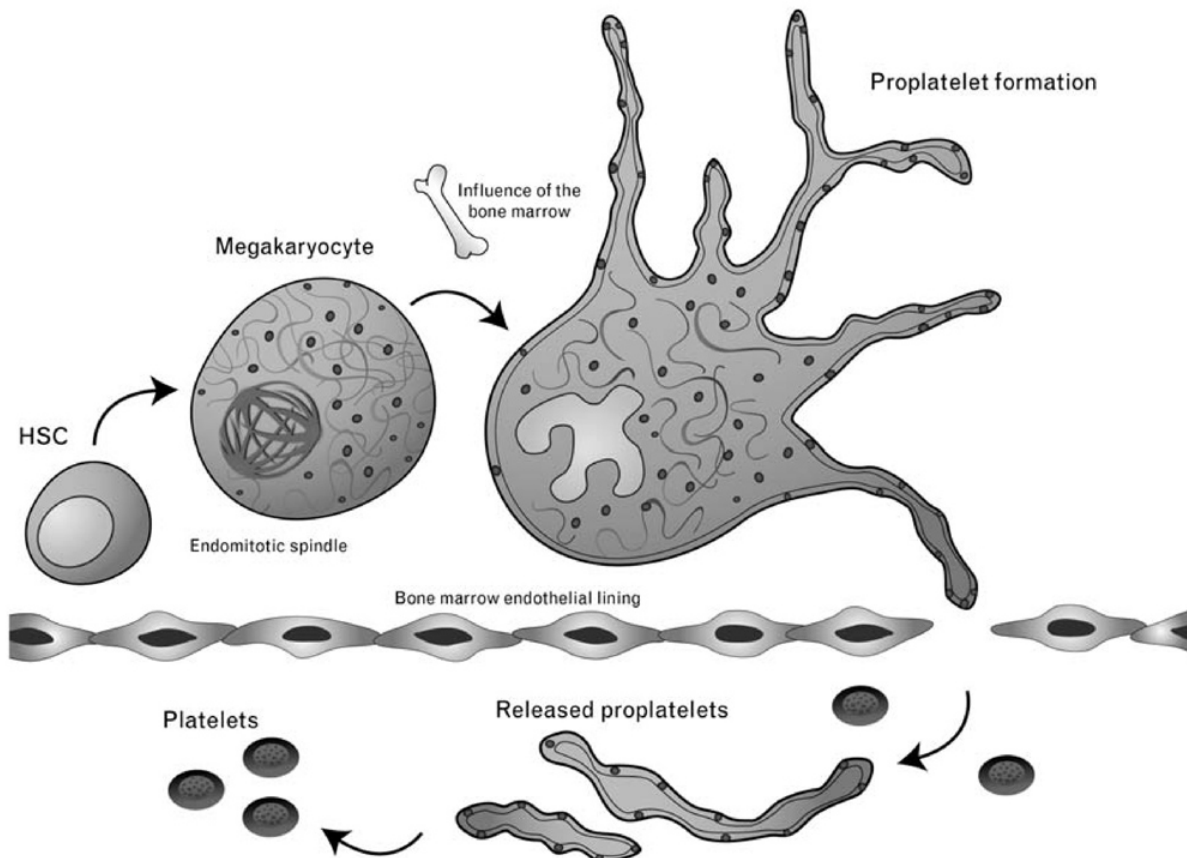


**Figure 1.5: Platelet release from megakaryocytes.** In the bone marrow, HSCs give rise to megakaryocytes. During maturation they undergo endomitosis, a dramatic increase in size, develop a demarcation membrane system and form granules. Following maturation, they produce extensions called proplatelets that reach into sinusoidal vessels. Platelets are then shed from proplatelets into the blood stream. Image taken from [9].

Cytoskeletal proteins play an important role during platelet formation. Proplatelets consist of actin-rich swellings which are connected by thin cytoplasmic strings or shafts that are lined by  $\beta 1$ -tubulin. Dynein and  $\beta 1$ -tubulin provide the force for proplatelet elongation. It is therefore not surprising that mice lacking  $\beta 1$ -tubulin exhibit platelet counts that are reduced by 60% and that the remaining platelets show structural and functional defects [9, 111, 144]. Proplatelet branching is regulated by actin and myosin while myosin IIa (encoded by *MYH9*) limits platelet formation. Mutations in the *MYH9* gene cause aberrant platelet shedding which leads to macrothrombocytopenia and a disease called the May-Hegglin syndrome [181]. The small Rho GTPase RhoA plays a central role in the organization of the actin cytoskeleton in various cell types. The function of RhoA in proplatelet formation, however, is discussed controversially. Studies using retroviral transfection of  $CD34^+$  cells could show that RhoA acts as a negative regulator of proplatelet formation [23]. In contrast, analyses using a MK-specific knockout mouse model revealed that absence of RhoA leads to severe macrothrombocytopenia [147, 175].



### 1.4.1 Megakaryopoiesis

Early HSCs develop into the *common lymphoid progenitor* (CLP) and the common myeloid progenitor (CMP). CMPs give rise to *granulocyte/macrophage progenitors* (GMP) and *megakaryocyte/erythrocyte progenitors* (MEP). The latter are committed to forming MKs and erythroid cells [9]. MK differentiation is driven by the cytokine *thrombopoietin* (TPO) and its receptor c-Mpl. Full knockout of either of the two results in a decrease in platelet and MK numbers to approximately 10% while their ultrastructures remain unaltered [70, 21]. Interestingly, conditional knockout of c-Mpl in the megakaryocytic lineage increases platelet numbers 10-fold due to an excess number of MKs and their progenitors [127]. Under normal conditions, TPO is continuously synthesized in the liver and the plasma level is maintained by its clearance from the circulation via binding of TPO to platelet c-Mpl receptors.

Another important regulator of megakaryopoiesis is *stromal cell-derived factor-1* (SDF-1, also called CXCL12) which is involved in the development, recruitment and homing of MKs. SDF-1 is thought to control the migration of MKs from the osteoblastic to the vascular niche during which MK maturation likely takes place [143]. However, this current model of MK migration and maturation has recently been challenged by the finding that the dense blood vessel network in the murine bone marrow spatially limits MK migration [van Eeuwijk et al, unpublished].

In addition, the cytokines GM-CSF, IL-3, IL-6, IL-11, IL-12 and *erythropoietin* (EPO) support proliferation of MK precursors while IL-1 $\alpha$  and *leukemia inhibitory factor* (LIF) induce MK maturation.

### 1.4.2 Transcription factors in megakaryopoiesis

Dimerization of the c-Mpl receptor causes auto-phosphorylation of *janus kinase 2* (JAK2) which in turn activates *mitogen-activated protein kinases* (MAPK), *phospho-inositol-3 kinase* (PI3K) and *signal transducers and activators of transcription* (STATs). This leads to the upregulation of genes that drive MK maturation [181]. Two of the most important genes are discussed below.

GATA1 is a zinc-finger transcription factor that binds the DNA sequence GATA as well as its co-factor *friend of GATA1* (FOG1). It is highly expressed in erythroid cells, mast cells and MKs. GATA1 targets the *CCND1* gene which encodes the cell cycle regulator cyclin D1 and facilitates MK polyploidization and cytoplasmic maturation.

RUNX1 belongs to the RUNT family of transcription factors and mutations in the *RUNX1* gene are frequently observed in acute leukemia. Full knockout of *RUNX1* almost completely abolishes hematopoiesis during development. Conditional *RUNX1* knockout causes reduced MK polyploidization and cytoplasmic maturation, comparable to that seen in *GATA1* knockout mice. As it has been shown that RUNX1 regulates myosin light chain 9 and non-muscle myosin IIa and IIb, the effects observed might be caused by cytoskeletal defects [111, 144, 181].

## 1.5 Platelet granules

Platelets contain three major types of granules:  $\alpha$ -granules, dense granules and lysosomes.  $\alpha$ -granules are the most abundant ones with 50-80/human platelet and account for approximately 10% of the total platelet mass. In addition, they provide a large reservoir (approximately  $14 \mu\text{m}^2$ ) of membrane, which is about the size of the OCS. Together,  $\alpha$ -granules and the OCS provide enough membrane to enable the increase in platelet size upon activation and spreading [16, 52].

Morphologically,  $\alpha$ -granules can be distinguished from other platelet structures using electron microscopy through the observation of the following features: a peripheral membrane, tubular and vesicular structures formed by large vWF multimers, an area with low electron density that contains fibrinogen and a small electron-dense spot comprising  $\beta$ -thromboglobulin, PF4 and proteoglycans [16, 99].

Dense granules occur less frequent (3-9/human platelet) than  $\alpha$ -granules and account for 1% of the total platelet volume. They are characterized by a large electron-dense spot seen in electron microscopic analysis, which is due to high concentrations of ADP, ATP,  $\text{Ca}^{2+}$ ,  $\text{Mg}^{2+}$  and serotonin [99].

Lysosomes contain various proteolytic enzymes which are active under acidic conditions. They cannot be distinguished from  $\alpha$ -granules in EM images, however, they can be identified using an acidic phosphatase staining [13]. Lysosomes contain glycosidases, proteases and bactericidal proteins. Prominent proteins present in the granule membrane are LIMP (CD63) and LAMP-1 and -2 [153].

### 1.5.1 Platelet granule content

Platelet  $\alpha$ -granules contain membrane proteins as well as soluble proteins which upon platelet activation are recruited to the plasma membrane or secreted into the extracellular space, respectively. While most of the membrane proteins stored in  $\alpha$ -granules, such as the tetraspanin CD9 and integrins  $\alpha\text{IIb}$ ,  $\alpha\text{6}$  and  $\beta\text{3}$  are already present on the platelet surface in the resting state, there are some (e.g. P-selectin) which are not. This allows the use of P-selectin surface expression as a marker for platelet  $\alpha$ -granule secretion. Additional recruitment of adhesion receptors such as integrin  $\alpha\text{IIb}\beta\text{3}$  might support platelet adhesion and aggregation at the site of vessel injury.

More than 300 different proteins are stored in  $\alpha$ -granules. They play a role in diverse processes such as platelet adhesion, coagulation, hemostasis, inflammation, wound healing, tumor growth and angiogenesis (see figure 1.6 and the following section) [16].

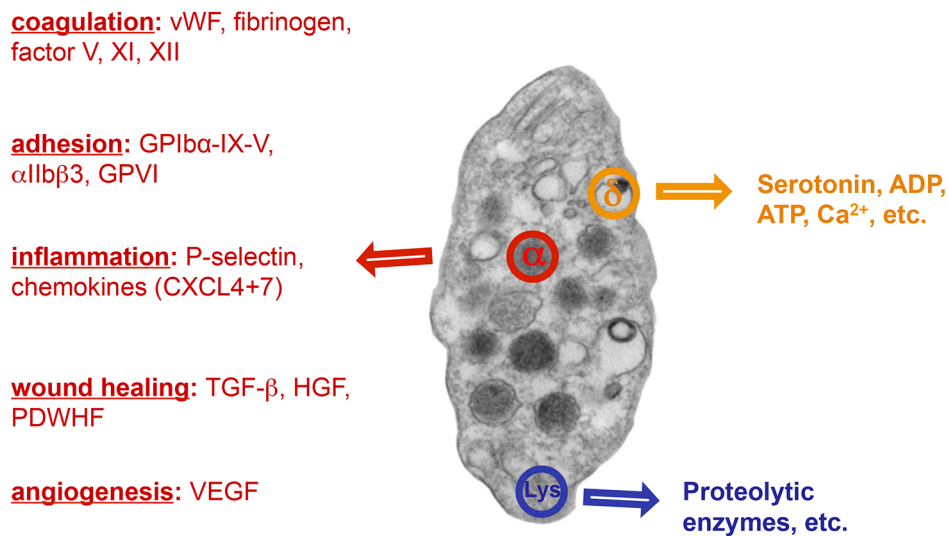


**Figure 1.6: Platelet granule content.** Platelets contain three major types of granules:  $\alpha$ -granules, dense granules and lysosomes. While dense granules contain mainly non-protein compounds such as ADP, ATP and Ca<sup>2+</sup> and lysosomes store proteolytic enzymes,  $\alpha$ -granules contain more than 300 different proteins involved in functions like coagulation, platelet adhesion, inflammation, wound healing and angiogenesis.

## 1.5.2 Platelet granule content in normal physiology and pathophysiology

### Hemostasis

Platelet  $\alpha$ -granules contain factors that are involved in secondary hemostasis: e.g. the coagulation factors V, XI and XIII. They also store factors like the *plasminogen activator inhibitor-1* (PAI-1), which inhibits the tPA, thereby limiting plasmin-mediated fibrinolysis, thus preventing removal of the hemostatic plug. However, platelet  $\alpha$ -granules also comprise numerous factors that counteract coagulation such as *tissue factor pathway inhibitor* (TFPI), protein S and plasmin(ogen). This exemplifies the function of platelets in the delicate task of fine-tuning the hemostatic and coagulation response [16, 61].

### Inflammation

Several soluble proteins and receptors stored in platelet  $\alpha$ -granules participate in inflammation. One of the most important proteins that mediates platelet-immune cell interaction is P-selectin, which is exposed on the platelet surface upon activation. P-selectin can bind to *P-selectin glycoprotein ligand-1* (PSGL1) on endothelial or immune cells and thereby enables platelets to bind to the inflamed endothelium, to recruit circulating monocytes, neutrophils and lymphocytes and to initiate an inflammation response at the site of injury. In addition, platelets secrete pro- and anti-inflammatory cytokines upon activation. The two most prominent cytokines stored in  $\alpha$ -granules are CXCL4 (PF4) and CXCL7 (platelet basic protein). CXCL4 has been shown to stim-

ulate neutrophil adhesion and degranulation as well as monocyte activation and recruitment. Furthermore, it is thought to be an important angiostatic factor as it inhibits endothelial cell proliferation. CXCL7 recruits neutrophils and facilitates their adhesion to the endothelium. Additionally, CXCL7 can be cleaved to give rise to several other chemokines (PBP, CTAP-III, b-TG, and NAP-2) of which NAP-2 is involved in chemotaxis of neutrophils [16, 58, 61, 97, 153, 163, 200].

Furthermore, platelet  $\alpha$ -granules contain CXCL1 (GRO- $\alpha$ ), CXCL5 (ENA-78), CXCL8 (IL-8), CXCL12 (SDF-1 $\alpha$ ), CCL2 (MCP-1), CCL3 (MIP-1 $\alpha$ ), and CCL5 (RANTES). CXCL5 was shown to regulate neutrophil migration and pulmonary host defense to bacterial infection. CCL5 is involved in monocyte recruitment and there are reports stating that it also enhances HIV infectivity [97, 156].

### Atherosclerosis

Atherosclerosis is characterized by an accumulation of lipids and immune cells (macrophages, T cells and mast cells) in the artery wall, thereby causing its thickening. This accumulation of cells is called atherosclerotic plaque and is covered by vascular smooth muscle cells and a fibrous cap containing collagen. While platelets play a major role in thrombus formation after rupture of the atherosclerotic plaque, there have also been reports stating that platelets and platelet-leukocyte/monocyte aggregates are involved in the process of atherosclerotic plaque formation [83]. The plaque formation is mediated by platelet-derived pro-inflammatory cytokines and platelet P-selectin. The chemokines CCL2, 3 and 4, as well as CXCL4 and CXCL12, that are stored in platelet  $\alpha$ -granules, have been detected in atherosclerotic plaques and their inhibition has been shown to dampen disease progression. As all of these factors, except CXCL4, are also secreted from immune cells, it is at this point unknown to which extent platelet chemokines are involved [16, 73, 83].

### Host defense against bacteria

Platelets play a role in host defense against bacterial infections by binding and internalizing pathogens via interactions of integrin  $\alpha$ IIb $\beta$ 3 with proteins on the pathogen surface [8, 84]. Through the release of antimicrobial proteins called thrombocidins that are stored in  $\alpha$ -granules, platelets are able to kill bacteria both *in vitro* and *in vivo*. Platelets were shown to efficiently kill *Staphylococcus aureus*, *Bacillus subtilis*, *Escherichia coli* and *Lactococcus lactis* [16, 102]. Beyond this, it was recently shown that platelets bind *Plasmodium falciparum*-infected erythrocytes and kill the parasite inside the cell [120]. During endotoxemia and sepsis, neutrophil-platelet interactions are required for the formation of *neutrophil extracellular traps* (NETs), which are DNA-based structures that capture and eliminate microbes [119].

### Angiogenesis

Platelet  $\alpha$ -granules contain both pro- and antiangiogenic factors, notably a number of growth factors: *vascular endothelial growth factor* (VEGF), *platelet-derived growth factor* (PDGF), *fi-*

*broblast growth factor* (FGF), *epidermal growth factor* (EGF), *hepatocyte growth factor* (HGF), and *insulin-like growth factor* (IGF). All of these are engaged in recruitment and growth of endothelial cells and fibroblasts. Furthermore,  $\alpha$ -granules also store angiopoietin, CXCL12 and matrix metalloproteinases [16, 138, 20]. Interestingly, at the same time platelets also store a number of anti-angiogenic factors, such as *thrombospondin* (TSP), CXCL4 (PF4), angiostatin and *tissue inhibitors of metalloproteinases* (TIMPs). TSP not only inhibits proliferation of endothelial cells, but also induces their apoptosis and CXCL4 prevents VEGF binding to its cellular receptor. Recently, there have been studies showing that pro- and antiangiogenic factors are packed differentially in  $\alpha$ -granules and are released in an agonist-dependent way [86, 85]. However, there are also reports which state that there is no functional coclustering of proteins in  $\alpha$ -granules [94].

### Wound healing

Wound healing is a multi-step-process comprising of inflammation, tissue formation and tissue remodeling. It involves the proliferation and the migration of *smooth muscle cells* (SMCs), fibroblasts and endothelial cells. Platelet releasate influences wound healing at several stages of the repair process. Platelets are among the first cells to act at sites of injury and restore vascular integrity by adhesion to the damaged endothelium and subsequent thrombus formation. Activated platelets secrete mediators that attract neutrophils, macrophages, endothelial cells and fibroblasts to the wound site. It is known that VEGF stimulates re-epithelialization and angiogenesis, while PDGF attracts fibroblasts and stimulates their proliferation. Platelet  $\alpha$ -granules contain TGF- $\beta$ , which is required for the differentiation of myofibroblasts, which produce the majority of extracellular matrix components that form the granulation tissue and the resulting scar. While the contribution of TGF- $\beta$  to the wound healing process is well established, the role of platelet  $\alpha$ -granule derived (growth) factors is unknown [40, 41, 42, 104, 136, 164, 192, 193].

### Metastasis

The first experimental evidence for the involvement of platelets in metastasis dates back to 1968 [55]. While this study only described the correlation between platelet count and the extent of tumor metastasis, other studies could later show the importance of platelet integrin  $\alpha$ IIb $\beta$ 3 binding to fibronectin or vWF during the metastatic process [96].

The function of the GPIb-V-IX complex in tumor metastasis is being discussed controversially since functional inhibition of GPIb $\alpha$  *in vivo* using Fab-fragments of a monoclonal antibody promoted melanoma metastasis indicating an inhibitory role of GPIb $\alpha$  [44]. In sharp contrast, reduced experimental metastasis was observed in mice deficient in the extracellular domain of GPIb $\alpha$  or the entire GPIb-V-IX complex [88]. To date, no convincing explanation for this discrepancy has been provided.

A recent publication indicates that platelet granule contents are crucial to prevent tumor hemorrhage, likely via angiopoietin or serotonin [80]. Besides serotonin, ATP is another important fac-

tor stored in platelet dense granules that was shown to play a role in tumor metastasis and vascular permeability. ATP secreted from platelets acts on the P2Y<sub>2</sub> receptor on endothelial cells to increase vascular permeability and allows tumor cell extravasation [162]. Generally, platelets likely influence tumor cell survival in the bloodstream and metastasis at different stages by platelet-leukocyte-tumor cell cohesion, coagulation, immune cell evasion and adhesion to the vessel wall [44, 56, 171].

### 1.5.3 Biogenesis of platelet granules

Platelet granule development begins in the MK residing in the bone marrow. Young MKs contain *multivesicular bodies* (MVBs) and have instead much less  $\alpha$ - and dense granules [77]. Platelet granules derive from MVBs, which serve as sorting stations. Cargo proteins are transferred to the MVBs in two ways. On the one hand proteins synthesized in the MK arrive at the *trans-Golgi network* (TGN) and are packed into vesicles which bud off and fuse with MVBs. On the other hand, proteins (e.g. fibrinogen) are taken up from the extracellular space via endocytosis and the endosomes formed also fuse with MVBs. This process has been shown to continue even in mature platelets [16, 99, 204].

As MKs mature, the number of  $\alpha$ - and dense granules increases while the number of MVBs decreases. At the same time the DMS is formed and granules are transported into the proplatelet territories [26]. While the exact mechanism of granule biogenesis and protein sorting in MKs remains incompletely understood, an increasing number of proteins that are involved in these processes is being identified. The *adaptor proteins* (AP) 1-3, for example, were shown to be expressed in platelets. While AP-1 is involved in protein transport from the TGN to MVBs, AP-2 plays a role in the endocytotic pathway and AP-3 deficiency has been shown to impair dense granule formation and to cause a storage pool disease [108, 203]. Both the synthetic and the endocytic pathway involve clathrin and recently it has been shown that VPS16B and VPS33B are important factors in  $\alpha$ -granule formation [50, 184]. Shortly before, it had been shown that mutations in *NBEAL2* cause the *gray platelet syndrome* (GPS) [5, 68, 91]. The GPS is a rare inherited platelet disorder characterized by defective  $\alpha$ -granule biogenesis. Its clinical features appear heterogenous but include a deficiency of most  $\alpha$ -granular proteins, a platelet aggregation defect, a mild to moderate bleeding tendency, macrothrombocytopenia, myelofibrosis and splenomegaly (see section 1.5.5). While mutations in *VPS16B* and *VPS33B* cause complete absence of  $\alpha$ -granules,  $\alpha$ -granules in platelets from GPS patients appear empty and vacuole-like, indicating that VPS16B and VPS33B act earlier in the process of granule biogenesis compared to NBEAL2.

Correct targeting of synthesized proteins to  $\alpha$ -granules is ensured by specific signal peptide sequences and for a number of proteins these have been identified. The core signal peptide sequence of CXCL4 consists of four amino acids (LKNG) that form a surface-exposed hydrophilic loop. A similar sequence was identified for RANTES and NAP-2 [39]. The exact mechanism by which soluble proteins are stored in platelet vesicles remains unclear, however, the proteoglycan serglycin was shown to be essential for the storage of CXCL4,  $\beta$ -TG and PDGF [195].

Once the granular proteins are packed into the respective granules, the granules themselves have to be transported to the correct location within the mature MK. Previously, it had been thought that the DMS divides the MK into future (pro)platelets. Today it is known that in normal physiology platelets are mostly released from the proplatelet extensions of MKs that reach into the bone marrow sinusoidal vessels. During proplatelet formation, organelles, such as granules and mitochondria are transported from the MK body to the proplatelets along the proplatelet shafts in a discontinuous fashion. Despite the bidirectional movement along shafts, the particles are eventually captured at the proplatelet tip. Immunofluorescence and electron microscopy studies indicate that organelles are in direct contact with microtubules, and their movement appears to be independent of actin. The motor protein kinesin is localized in a pattern that corresponds to that of organelles and granules and is probably responsible for transporting them along microtubules.

There are two mechanisms being discussed for the microtubule-associated bidirectional transport of organelles in proplatelets: (i) organelles are propelled along microtubules by motor proteins; (ii) organelles bind to microtubules that slide bidirectionally in relation to other filaments to indirectly move organelles along in a piggyback fashion [86, 90, 144, 154].

#### 1.5.4 Platelet secretion

Fusion of vesicles with the plasma membrane is required for a plethora of processes in different cell types, such as the release of neurotransmitters, cytokine release from mast cells or platelet degranulation. It is therefore not surprising that a common mechanism evolved which is largely conserved among eukaryotes and involves the *SNAP receptor* (SNARE) protein family. SNAREs were first analyzed by their interaction with NSF (N-ethylmaleimide sensitive factor) and SNAP (soluble NSF attachment protein), which are required for vesicle fusion with the plasma membrane. According to the SNARE hypothesis, three t-SNAREs on the target membrane bind one v-SNARE on the vesicular membrane, forming the trans-SNARE complex consisting of a four-helix bundle. The SNARE proteins then generate the force needed to fuse the membranes in a zipper-like fashion [169, 174].

There are three major classes of SNARE proteins: *synaptosomal-associated proteins* (SNAPs), *vesicle-associated membrane proteins* (VAMPs) and syntaxins. SNAPs contain two SNARE motifs, but lack a transmembrane domain and instead are anchored via palmitoylated cysteine residues or interactions with other SNAREs. All syntaxins contain one SNARE motif and are transmembrane proteins with their C-terminus forming the lipid anchor. The only exception is syntaxin 11 which does not have a transmembrane domain. VAMPs contain a SNARE motif and a transmembrane domain and are rather small with most members of this family consisting of less than 120 amino acids. On the other hand, syntaxins are larger than 230 amino acids [81].

Identification of the first SNARE proteins in platelets dates back to 1997 [106]. Today it is known that platelets contain a large number of SNAREs and associated proteins that tightly regulate

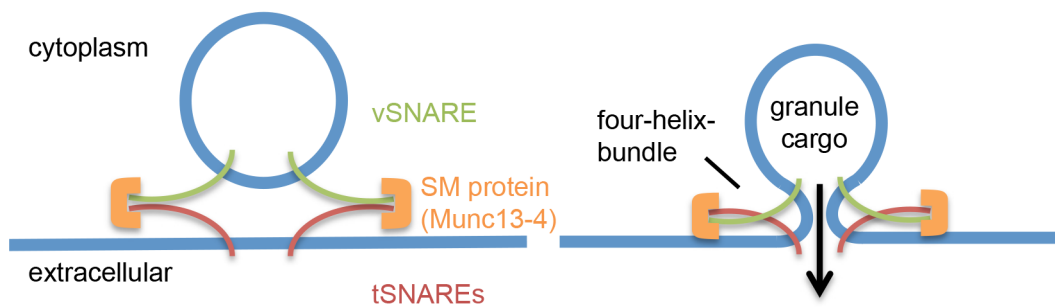


**Figure 1.7: The platelet secretory machinery.** The platelet secretory machinery consists of three major components: v-SNAREs on the granule membrane, t-SNAREs on the cytoplasmic side of the plasma membrane and SM (sec/munc-like) proteins that facilitate binding of the SNARE proteins and formation of a four-helix bundle. The most abundant SM protein in platelets is Munc13-4.

the secretion process. VAMP8 was shown to be involved in platelet granule secretion and mice deficient in VAMP8 were protected in an *in vivo* thrombosis model [60, 63, 150, 152]. For a long time it was unclear which syntaxin plays the most important role in platelet secretion. Recently, it has been demonstrated that *STX11*, the gene encoding for syntaxin 11 is mutated in patients with *Familial Haemophagocytic Lymphohistiocytosis 4* (FHL4), a rare auto-immune disease. Patients with FHL4 show reduced erythrocyte and platelet numbers. Syntaxin11-deficient platelets display abrogated  $\alpha$ - and dense granule release, although platelet granule number and content were unaltered [199]. There are reports which used an *in vitro* exocytosis assay to show that SNAP-23 is an important SNAP isoform in platelets, however, direct evidence is missing since the full knockout is embryonic lethal and the platelet-specific knockout has not been analyzed yet [24, 60].

SM (sec/munc-like) proteins or STXBPs (syntaxin binding proteins) regulate the vesicle release process by binding to the SNARE proteins in the four-helix bundle [4, 60, 113, 174]. STXBP2 for instance binds to syntaxin 11 and a mutation in the *STXBP2* gene causes FHL5 and a defective platelet secretion [4]. Munc13-4 is the most abundant protein of the UNC13 family in platelets and was first identified as a Rab27 interactor. Later, it was shown that it is crucial for the release of cytolytic granules at the immunological synapse. Interestingly, the lytic granules of the *cytotoxic T lymphocytes* (CTL) and *natural killer* (NK) cells defective in this protein accumulate at the plasma membrane, but are unable to secrete their content, indicating a defect in vesicle priming. Mutations in *UNC13D* cause FHL3 which is associated with defective cytotoxic activity in CTLs and NK cells [48, 112]. *Unc13d<sup>jinx</sup>* knockout mice in which a frameshift mutation in the *Unc13d* gene causes absence of the Munc13-4 protein show an abrogated platelet dense granule secretion and reduced  $\alpha$ -granule release that leads to protection not only from thrombosis *in vitro* and *in vivo* [151, 159], but also from tumor metastasis [162] due to increased vascular permeability.



### 1.5.5 Platelet granule disorders

There are two types of inherited platelet disorders that involve platelet granules: those that show a defect in granule biogenesis and those that are characterized by defects in proteins which are part of the granule secretory machinery. The former render the platelet deficient of a certain granule subtype or reduce its content, while the latter show normal granule counts and morphology, but are unable to secrete the content of those granules.

The *Platelet storage pool disease* (SPD) is a heterogeneous group of platelet disorders characterized by a reduction in the number or content of dense granules. Key features of the *Hermansky-Pudlak syndrome* (HPS) involve moderate bleeding and oculocutaneous albinism while some subtypes show more severe deficiencies. The 9 genes found to be mutated in HPS (*HPS1 to HPS6, DTNBP1, BLOC1S3 and BLOC1S6 (PLDN)*) are involved in the biogenesis or the function of *lysosome-related organelles* (LROs). LROs share certain features with lysosomes (e.g. low pH, common biogenesis pathway), but have distinct morphologies and functions. Examples of LROs are melanosomes, lytic granules in cytotoxic T cells, basophil granules in mast cells, platelet dense granules and Weibel-Palade bodies in endothelial cells [82]. Every mutation gives rise to a certain subtype of HSP. The most severe subtype is HSP1 with associated immunodeficiencies, Crohn's disease and pulmonary fibrosis [115, 140].

The *Chediak-Higashi syndrome* (CHS) is associated with bleeding, progressive neurological dysfunctions and severe immunological defects including severe infections with *Staphylococcus aureus*, *Streptococcus*, *Candida* or *Aspergillus*, especially in children. These defects are caused by reduced leukocyte migration, abnormal NK cell function and reduced platelet dense granule content, which leads to impaired platelet aggregation. About 85% of the CHS patients develop lymphohistiocytosis, which is caused by dysregulated lymphocyte proliferation and can lead to fever, anemia, neutropenia, thrombocytopenia, hepatosplenomegaly, and lymphadenopathy. CHS is caused by mutations in *LYST*, which encodes for the *lysosomal trafficking regulator* (LYST), also known as the Chediak-Higashi Syndrome 1 (CHS1) protein. LYST is a 429 kDa member of the Beige and Chediak (BEACH) protein family. It contains a PH-like domain, *Armadillo* (ARM) and HEAT motifs, a C-terminal WD40 domain, a *Concanavalin A* (ConA)-like lectin domain and a BEACH motif [27, 137].

*Pleckstrin homology* (PH) domains are present in proteins involved in intracellular signaling and cytoskeletal proteins. While the sequence homology of this domain is rather low, the three-dimensional structure is very well conserved. PH domains bind to phospholipids, especially phosphoinositides. A WD40 repeat is a short sequence that normally ends with a tryptophan and aspartic acid dipeptide. A WD40 domain is formed by 4 to 16 of these repeats and shows a  $\beta$ -propeller structure. WD40 repeat proteins are involved in a number of functions, such as cell cycle control, signal transduction and, most importantly, vesicle trafficking. ConA-like domains were proposed to be involved in oligosaccharide binding and protein sorting during secretion and to play a role in the vesicle fusion machinery [22].

Members of the BEACH family are large proteins involved in vesicle transport, apoptosis, mem-

brane dynamics and receptor signaling. They are receiving increasing attention because several of them have been associated with diseases. Besides *LYST*, there are eight other proteins in this family: *neurobeachin* (*NBEA*), *neurobeachin-like 1* and *2* (*Nbeal1* and *Nbeal2*), *lipopolysaccharide-responsive, beige-like anchor protein* (*LRBA*), *WD and FYVE zinc finger domain containing protein 3* and *4* (*WDFY3* and *WDFY4*), *neutral sphingomyelinase activation-associated factor* (*NSMAF*) and *WD repeat domain 81* (*WDR81*). While *LYST* mutations cause the CHS, it was shown that mutations in *LRBA* are associated with autoimmune diseases, that *NBEA* is potentially involved in autism and that *NBEAL1* is upregulated in glioma. Only recently it was demonstrated that mutations in *NBEAL2* cause the GPS [5, 68, 91, 82].

As mentioned above, the GPS is a rare inherited platelet disorder characterized by defective  $\alpha$ -granule biogenesis. Its clinical features appear heterogenous but include a gray appearance of platelets on May-Grünwald-Giemsa stained blood smears, a deficiency in most  $\alpha$ -granular proteins (e.g. fibrinogen, vWF, PF4, PDGF and  $\beta$ -TG), an unaltered expression of major glycoproteins on the platelet surface, a mild to moderate bleeding phenotype, macrothrombocytopenia, myelofibrosis, emperipolesis and splenomegaly. Platelets from GPS patients lack  $\alpha$ -granules and instead show an increased number of vacuoles. They have severe platelet aggregation defects and platelets are unable to spread on poly-L-lysine, collagen and fibrinogen [145, 140]. The dramatic reduction in  $\alpha$ -granular proteins and some of the other symptoms are thought to be caused by the defective packaging or sorting of proteins into  $\alpha$ -granules in the MKs. However, direct experimental evidence is lacking [139].

FHL is a severe syndrome of immune dysregulation. It is the primary form of *haemophagocytic lymphohistiocytosis* (HLH) and is caused by mutations in genes that are involved in the cytolytic activity of NK cells and cytotoxic T cells. FHL consists of a family of disorders characterized by *hemophagocytic syndrome* (HS). Central to HS is impaired lymphocyte homeostasis which is caused by defective cytotoxic granule secretion, multisystemic inflammation and organ infiltration by activated CD8<sup>+</sup> T cells and macrophages [31].

The genetic cause for FHL1 has not been identified, but it is known that FHL2 is related to mutations in perforin. Recently, a new FHL subtype has been identified that is not caused by mutations in perforin but by mutations in *UNC13D*. The Munc13-4 protein enables release of lytic granules docked at the plasma membrane of cytotoxic T lymphocytes and natural killer cells in a way similar to that described in platelets [48, 121].

### 1.6 Aim of this study

An increasing number of studies suggests that the role of platelets extends beyond their function in thrombosis and hemostasis and that platelets take part not only in (thrombo-)inflammatory processes that occur following ischemia, sepsis and wound healing, but also in tumor cell migration and metastasis. While there are several receptors expressed on the platelet surface that are involved in these pathological conditions, it has also been shown that the contents of platelet granules contribute to these processes [61, 130, 162, 171, 194].

Under conditions of inflammation, platelets prevent hemorrhage [59] and it was shown that (hem)ITAM signaling of GPVI and CLEC-2 is important for this process [18]. While the downstream effectors remained elusive, it was speculated that vasoactive mediators released from platelet granules might play an important role.

Therefore, the aim of this study was to investigate the role of platelet dense and  $\alpha$ -granules in thrombosis, hemostasis, (thrombo-)inflammation and maintaining vascular integrity during inflammation. *Unc13d*<sup>-/-</sup> and *Nbeal2*<sup>-/-</sup> mice were used to study the effects of defective dense and  $\alpha$ -granule release on *in vitro* and *in vivo* thrombosis and hemostasis models. Using *Nbeal2*<sup>-/-</sup> mice a proof-of-concept study was performed using a reverse genetics approach to unravel whether *Nbeal2* knockout causes GPS in mice. This enabled us to specifically decipher the defects that are caused by *Nbeal2*-deficiency and to correlate these findings with the GPS phenotype described in humans.

Furthermore, to study the role of platelet dense granule content and the plethora of proteins stored in  $\alpha$ -granules on thromboinflammation after ischemic stroke and wound healing as well as their role in maintaining the vascular integrity during inflammation, single and double deficient animals were subjected to *in vivo* models of ischemic stroke, skin and lung inflammation and the extent of hemorrhage was quantified.

## 2 Materials and Methods

### 2.1 Materials

#### 2.1.1 Chemicals and reagents

**Table 2.1:** Chemicals and reagents

<b>Reagent</b>	<b>Manufacturer</b>
3,3,5,5-tetramethylbenzidine (TMB)	BD Biosciences (Heidelberg, Germany)
Adenosine diphosphate (ADP)	Sigma-Aldrich (Schnelldorf, Germany)
Agarose	Roth (Karlsruhe, Germany)
Amersham Hyperfilm ECL	GE Healthcare (Little Chalfont, UK)
Ammonium peroxodisulfate (APS)	Roth (Karlsruhe, Germany)
Apyrase (grade III)	Sigma-Aldrich (Schnelldorf, Germany)
Bovine serum albumin (BSA)	AppliChem (Darmstadt, Germany)
Calcium chloride	Roth (Karlsruhe, Germany)
Chrono-Lume luciferase reagent	Chrono-log (Havertown, PA, USA)
Complete mini protease inhibitors	Roche Diagnostics (Mannheim, Germany)
Convulxin (CVX)	Enzo Lifesciences (Lörrach, Germany)
Cyclosporin A	Calbiochem (Bad Soden, Germany)
dNTP mix	Fermentas (St. Leon-Rot, Germany)
ECL solution	PerkinElmer LAS (Boston, USA)
Ethylenediaminetetraacetic acid (EDTA)	AppliChem (Darmstadt, Germany)
Fat-free dry milk	AppliChem (Darmstadt, Germany)
Fentanyl	Janssen-Cilag (Neuss, Germany)
Fibrillar type I collagen (Horm)	Nycomed (Munich, Germany)
Flumazenil	Delta Select (Dreieich, Germany)
Isofluran CP	cp-pharma (Burgdorf, Germany)
GeneRuler 1kbp DNA Ladder	Fermentas (St. Leon-Rot, Germany)
GeneRuler 100bp DNA Ladder	Fermentas (St. Leon-Rot, Germany)
Heparin sodium	Ratiopharm (Ulm, Germany)
Human fibrinogen	Sigma-Aldrich (Schnelldorf, Germany)
IGEPAL CA-630	Sigma-Aldrich (Schnelldorf, Germany)
Immobilon-P transfer membrane	Millipore (Schwalbach, Germany)

Continued on next page

Table 2.1 – continued from previous page

Reagent	Manufacturer
Indomethacin	Alfa Aesar (Karlsruhe, Germany)
Medetomidine (Dormitor)	Pfizer (Karlsruhe, Germany)
Midazolam (Dormicum)	Roche (Grenzach-Wyhlen, Germany)
Midori Green DNA stain	Nippon Genetics (Düren, Germany)
Naloxon	Delta Select (Dreieich, Germany)
N-ethylmaleimide (NEM)	Calbiochem (Bad Soden, Germany)
PageRuler prestained protein ladder	Fermentas (St. Leon-Rot, Germany)
Phalloidin atto647N	Sigma (Deisenhofen, Germany)
Phenol/chloroform/isoamyl alcohol	Roth (Karlsruhe, Germany)
Phorbol 12-myristate 13-acetate (PMA)	Sigma (Schnelldorf, Germany)
Pluronic F-127	Invitrogen (Karlsruhe, Germany)
Prostacyclin (PGI <sub>2</sub> )	Sigma (Schnelldorf, Germany)
Protease inhibitor cocktail (100x)	Sigma-Aldrich (Schnelldorf, Germany)
Proteinase K	Fermentas (St. Leon-Rot, Germany)
Protein G Sepharose 4 Fast Flow	GE Healthcare (Freiburg, Germany)
Rotiphorese gel 30 acrylamide	Roth (Karlsruhe, Germany)
Sodium orthovanadate	Sigma (Schnelldorf, Germany)
Triton X-100	AppliChem (Darmstadt, Germany)
Taq polymerase	Fermentas (St. Leon-Rot, Germany)
Taq polymerase buffer (10x)	Fermentas (St. Leon-Rot, Germany)
Tetramethylethylenediamine (TEMED)	Roth (Karlsruhe, Germany)
Thapsigargin (TG)	Invitrogen (Karlsruhe, Germany)
Thrombin (20 U/ml)	Roche Diagnostics (Mannheim)
Tween 20	Roth (Karlsruhe, Germany)
U46619	Enzo Lifesciences (Lörrach, Germany)
Uranylacetate	EMS (Hatfield, USA)
Vectashield mounting medium	Vector Laboratories (Burlingame, USA)

*Collagen-related peptide* (CRP) was kindly provided by Prof. Dr. S. Watson (University of Birmingham, UK). Rhodocytin was a generous gift from Prof. Dr. J. Eble (University Hospital Frankfurt, Germany). All other non-listed chemicals were obtained from AppliChem (Darmstadt, Germany), Sigma (Schnelldorf, Germany) or Roth (Karlsruhe, Germany).

## 2.1.2 Antibodies

### Monoclonal antibodies

The monoclonal antibodies listed in table 2.2 were generated/modified in our laboratory and labeled with *fluorescein isothiocyanate* (FITC) or with *phycoerythrin* (PE) using commercial kits

and following manufacturer's protocols.

Annexin-A5 was purified in our laboratory and coupled to DyLight488.

**Table 2.2:** Monoclonal antibodies generated in our laboratory

Antibody	Clone	Isotype	Antigen	Source
p0p/A	92H12	IgG2b	GPIb	unpublished
p0p/B	57E12	IgG2b	GPIb	[116]
p0p4	15E2	IgG2b	GPIb	[128]
p0p6	56F8	IgG2b	GPIX	[128]
DOM2	89H11	IgG2a	GPV	[128]
ULF1	96H10	IgG2a	CD9	[128]
JAQ1	98A3	IgG2a	GPVI	[132]
JON6	14A3	IgG2b	$\alpha$ IIb $\beta$ 3	unpublished
LEN1	12C6	IgG2b	$\alpha$ 2	[66]
INU1	11E9	IgG1	CLEC-2	[117]
JON/A	4H5	IgG2b	$\alpha$ IIb $\beta$ 3	[14]
WUG 1.9	5C8	IgG1	P-selectin	unpublished
EDL-1	57B10	IgG2a	$\beta$ 3 integrin	[128]
BAR-1	25B11	IgG1	$\alpha$ 5 integrin	[66]

## Commercial antibodies

**Table 2.3:** Commercial antibodies

Antibody	Manufacturer
Anti-Munc13-4	Everest Biotech (Oxfordshire, UK)
Anti-mouse CD11b (M1/70)	Biologend (Fell, Germany)
Anti-mouse CD3 (17A2)	Biologend (Fell, Germany)
Anti-mouse CD45R/B220 (RA3-6B2)	Biologend (Fell, Germany)
Anti-mouse Ly-6G/C (RB6-8C5)	Biologend (Fell, Germany)
Anti-mouse TER-119	Biologend (Fell, Germany)
Anti-Nbeal2	Thermo Fisher (Braunschweig, Germany)
Anti-rabbit IgG HRP	Dako (Hamburg, Germany)
Anti-tubulin Alexa 488	Invitrogen (Karlsruhe, Germany)
Anti-vWF HRP (#A0226)	Dako (Hamburg, Germany)
Anti-vWF (#A0082)	Dako (Hamburg, Germany)

### 2.1.3 Buffers

All buffers were prepared using deionized water obtained from a MilliQ Water Purification System (Millipore, Schwalbach, Germany). pH was adjusted using HCl or NaOH.

- **Blocking solution for immunoblotting**

Washing buffer (TBS-T)	—
BSA or fat-free dry milk	5%

<b>• Cell culture medium</b>	
RPMI	—
FCS	10%
Sodium pyruvate (100 mM)	1%
L-Glutamine (200 mM)	1%
Non-essential amino acids	1%
β-mercaptoethanol	30 μM
Penicillin/streptomycin	100 U/ml
<b>• Coating buffer, pH 9.6</b>	
Na <sub>2</sub> CO <sub>3</sub>	15 mM
NaHCO <sub>3</sub>	85 mM
<b>• Fixation buffer I (electron microscopy)</b>	
Sodium cacodylate, pH 7.2	0.1 M
Glutaraldehyde	2.5%
Formaldehyde	2%
<b>• Fixation buffer II (electron microscopy)</b>	
Sodium cacodylate, pH 7.2	50 mM
Osmium tetroxid	2%
<b>• Laemmli buffer for SDS-PAGE</b>	
TRIS	40 mM
Glycine	0.95 mM
SDS	0.5%
<b>• Lysis buffer (for DNA isolation), pH 7.2</b>	
TRIS base	100 mM
EDTA	5 mM
NaCl	200 mM
SDS	0.2%
Proteinase K	100 μg/ml
<b>• MK Medium</b>	
IMDM	—
FCS	10%
Penicillin-Streptomycin	1%
(TPO	50 ng/ml)
<b>• PHEM, pH 7.2</b>	
PIPES	60 mM
HEPES	25 mM
EGTA	10 mM
MgSO <sub>4</sub>	2 mM

- **Phosphate buffered saline (PBS), pH 7.14**

NaCl	137 mM
KCl	2.7 mM
KH <sub>2</sub> PO <sub>4</sub>	1.5 mM
Na <sub>2</sub> HPO <sub>4</sub>	8 mM
- **Sample buffer for agarose gels, 6x**

Tris buffer (150 mM)	33%
Glycerine	60%
Bromophenol blue (3',3'',5',5''-tetrabromophenol-sulfonphthalein)	0.04%
- **SDS sample buffer, 4x**

β-mercaptoethanol (reducing conditions)	20%
TRIS buffer (1 M), pH 6.8	20%
Glycerine	40%
SDS	4%
Bromophenol blue	0.04%
- **Separating gel buffer (Western blot), pH 8.8**

TRIS/HCl	1.5 M
----------	-------
- **Stacking gel buffer (Western blot), pH 6.8**

TRIS/HCl	0.5 M
----------	-------
- **Stripping buffer (Western blot), pH 2.0**

PBS (1x)	—
Glycine	25 mM
SDS	1%
- **TAE buffer, 50x, pH 8.0**

TRIS	0.2 M
Acetic acid	5.7%
EDTA	50 mM
- **TE buffer, pH 8.0**

TRIS base	10 mM
EDTA	1 mM
- **Transfer buffer**

Tris Ultra	50 mM
Glycine	40 mM
Methanol	20%
- **Tris-buffered saline (TBS), pH 7.3**

NaCl	137 mM
TRIS/HCl	20 mM



- **Tyrode's buffer, pH 7.3**

NaCl	137 mM
KCl	2.7 mM
NaHCO <sub>3</sub>	12 mM
NaH <sub>2</sub> PO <sub>4</sub>	0.43 mM
CaCl <sub>2</sub>	0 or 2 mM
MgCl <sub>2</sub>	1 mM
HEPES	5 mM
BSA	0.35%
Glucose	1%

- **Washing buffer for immunoblotting (TBS-T)**

TBS (1x)	—
Tween 20	0.1%

- **Washing buffer for ELISA (PBS-T)**

PBS (1x)	—
Tween 20	0.1%

#### 2.1.4 Animals

All animal studies were approved by the district government of Lower Franconia (Bezirksregierung Unterfranken). Specific pathogen free C57BL/6J mice were purchased from JANVIER LABS (Saint Berthevin, France). 6-10-week-old mice were used for experiments, unless stated otherwise.

*Unc13d*<sup>tm1(KOMP)Vlcg</sup> ES cells were obtained from KOMP (University of California, Davis, USA) and injected into C57BL/6 blastocysts. Germ line transmission was obtained by backcrossing the resulting chimeric mice with C57BL/6 mice.

*Nbeal2*<sup>+/-</sup> mice on a C57BL/6J background, in which exons 4 through 11 were targeted by homologous recombination, were obtained from MMRRC (University of California, Davis, USA) and intercrossed to generate *Nbeal2*<sup>-/-</sup> mice.

*Unc13d*<sup>-/-</sup>/*Nbeal2*<sup>-/-</sup> mice were generated by intercrossing *Unc13d*<sup>-/-</sup> and *Nbeal2*<sup>-/-</sup> single knock-out mice.

#### Generation of bone marrow chimeric mice

6-week-old recipient C57BL/6 mice were lethally irradiated with a single dose of 10 Gy. The femur and tibia of donor mice were prepared and bone marrow was flushed with a 22G needle into prewarmed DMEM supplemented with 10% FCS and 1% penicillin/streptomycin. Bone marrow cells from donor mice were injected i.v. into the irradiated mice (4x10<sup>6</sup> cells per mouse). All recipient mice received water containing 2 g/l neomycin sulfate for 2 weeks after transplantation.

## 2.2 Methods

### 2.2.1 Genotyping of mice

#### Isolation of genomic DNA from mouse tissue

Using an ear punch device, a small part of the mouse ear was excised and incubated in 500  $\mu$ l DNA lysis buffer at 1,000 rpm, overnight (o/n) at 56°C. The next day, 500  $\mu$ l phenol/chloroform were added, the samples were mixed and afterwards centrifuged at 11,000 rpm for 10 min at *room temperature* (RT). The upper phase was carefully transferred into a new tube containing 500  $\mu$ l isopropanol. Following vigorously shaking, samples were centrifuged at 14,000 rpm for 10 min at 4°C. After washing the resulting pellet with 1 ml 70% ethanol, the samples were centrifuged again at 14,000 rpm for 10 min. Finally, the DNA pellet was dried at 37°C and then resuspended in 80  $\mu$ l TE buffer.

#### Genotyping of *Unc13d*<sup>-/-</sup> mice

##### Primers WT-PCR:

Unc13d-TUF: 5'- GGG ACG CCG TGT CTT TCT AC -3'

Unc13d-TUR: 5'- ACA CTC TCC CAA CAT CTC CTC TTA C -3'

Predicted band size: 73 bp

##### Primers KO-PCR:

Unc13d-SU: 5'- CTC TCC CCA GAG CCT CCG TG -3'

Unc13d-LacZrev: 5'- GTC TGT CCT AGC TTC CTC ACT G -3'

Predicted band size: 392 bp

##### PCR mix

Reagent	Amount
dNTP	1 $\mu$ l
Buffer	5 $\mu$ l
MgCl <sub>2</sub>	5 $\mu$ l
FP-SU	0.1 $\mu$ l
LacZrev	0.1 $\mu$ l
TUF	0.1 $\mu$ l
TUR	0.1 $\mu$ l
H <sub>2</sub> O	36.1 $\mu$ l
Taq	0.5 $\mu$ l

PCR program

	Temperature	Duration	
1	96°C	3:00 min	
2	94°C	0:30 min	
3	68°C	0:30 min	Repeat steps 2-4: 35 cycles.
4	72°C	1:00 min	
5	72°C	10:00 min	
6	15°C	∞	

**Genotyping of *Nbeal2*<sup>-/-</sup> mice**Primers WT-PCR:

Forward primer: 5' – GTC CTG CTT GAC CTA CCG TC – 3'

Reverse primer: 5' – CAG GGA GGA TAA CGA GAT AGT CTT – 3'

Predicted band size: 223 bp

Primers KO-PCR:

Forward primer: 5' – GTC CTG CTT GAC CTA CCG TC – 3'

IRES-GT: 5' – CCT AGG AAT GCT CGT CAA GA – 3'

Predicted band size: 401 bp

PCR mix

Reagent	Amount
dNTP	1 µl
Buffer	5 µl
MgCl <sub>2</sub>	5 µl
Forward primer	0.3 µl
Reverse primer	0.1 µl
IRES-GT	0.1 µl
H <sub>2</sub> O	36.1 µl
Taq	0.5 µl

### PCR program

	Temperature	Duration
1	96°C	3:00 min
2	94°C	0:30 min
3	51.4°C	0:30 min
4	72°C	1:00 min
5	72°C	10:00 min
6	15°C	∞

Repeat steps 2-4 35 cycles.

### Genotyping of *Nbeal2*<sup>-/-</sup>/*Munc13-4*<sup>-/-</sup> mice

Double-deficient mice were genotyped like the single-deficient mice.

### Agarose gel electrophoresis

To analyze the PCR product, agarose gels were used. The concentration of agarose (1-2%) was adapted to the expected size of the PCR products. Agarose was dissolved in 1x TAE buffer by boiling the solution in a microwave. Afterwards, the solution was cooled down to approx. 60°C and 5 µl Midori green per 100 ml were added. The solution was poured into a tray with a comb to congeal. The tray was positioned in an electrophoresis chamber containing 1x TAE buffer and the comb was removed. The PCR products were mixed with 6x sample loading buffer and 20 µl were loaded into the slots of the gel. Samples were run for approximately 30 min at 100-160 V. A 1 kbp or 100 bp DNA ladder was used to estimate the size of the DNA bands under UV light later on.

## 2.2.2 Molecular biology and biochemistry

### Preparation of platelet lysates

Washed platelets ( $5 \times 10^5/\mu\text{l}$ ) were prepared as described in the next section and were incubated in lysis buffer containing 1% Igepal for 20 min at 4°C, and centrifuged 5 min at 22,000 g. Supernatants were transferred into a new tube and frozen at -80°C.

### Western blotting

Cell lysates were mixed with 4x SDS sample buffer and boiled for 5 min at 95°C. For SDS-PAGE, 20 µl per sample were loaded onto a gel with a 4% stacking gel and a 10 or 12% separating gel, provided in a gel chamber filled with Laemmli buffer. Alternatively, NuPAGE Tris-Acetate Pre-Cast gels were used.

The gel was run at 25 mA for 1.5 h. After separation, the proteins were transferred onto a *polyvinylidene difluoride* (PVDF) membrane by semidry immunoblotting at 65 mA per gel. Afterwards, the membrane was incubated in blocking buffer in order to avoid unspecific binding

of the primary antibody. Subsequently, the membrane was incubated with the primary antibody o/n at 4°C. To remove the unbound antibody, the membrane was washed three times for 10 min with washing buffer. Next, membranes were incubated with the appropriate HRP-coupled secondary antibodies for 1 h at RT. The membrane was washed three times, 10 min each to remove unbound secondary antibody. The proteins were visualized using ECL solution and X-ray films.

To strip the membranes from bound antibodies, the membranes were incubated with stripping buffer for 20-25 min at RT under rotation. Afterwards, membranes were washed briefly several times in TBS-T to remove residual stripping buffer. Next, the membranes were blocked again and incubated with antibodies as described.

### **Quantification of vWF, fibrinogen, and PF4 content by ELISA**

For determination of vWF or fibrinogen content, ELISA plates were coated with 10 µg/ml rabbit anti-human vWF or 10 µg/ml rabbit anti-human fibrinogen antibody, respectively, o/n at 4°C and blocked with 5% BSA. Serial 1:2 dilutions of the samples (heparinized plasma or platelet lysates) were prepared, transferred onto the ELISA plates and incubated for 2 h at 37°C. After washing with TBS 0.1% Tween, samples were incubated with HRP-coupled rabbit anti-human vWF antibody (1:3,000) or rabbit anti-human fibrinogen-FITC-Fab fragments followed by rabbit anti-FITC-HRP (1:1,000). After washing, ELISAs were developed using TMB ONE substrate, and plates were read at 450 nm. The amount of plasma PF4 was quantified using a PF4 ELISA (RayBiotech) following the manufacturer's instructions.

### **2.2.3 *In vitro* analyses of platelet function**

#### **Platelet isolation**

Mice were bled under isoflurane anesthesia from the retroorbital plexus. 700 µl blood were collected into 300 µl heparin in TBS (20 U/ml, pH 7.3). 200 µl heparin were added and blood was centrifuged at 800 rpm (Eppendorf Centrifuge 5415C) for 5 min at RT. The upper phase and buffy coat were carefully transferred into a new tube containing 200 µl heparin and centrifuged at 800 rpm for 7 min at RT to obtain *platelet-rich plasma* (PRP). To obtain washed platelets, PRP was centrifuged at 2,800 rpm for 5 min at RT in the presence of *prostacyclin* (PGI<sub>2</sub>) (0.1 µg/ml) and apyrase (0.02 U/ml) and the pellet was resuspended in 1 ml Tyrode's buffer w/o Ca<sup>2+</sup> containing PGI<sub>2</sub> and apyrase. After 10 min incubation at 37°C, the sample was centrifuged at 2,800 rpm for 5 min. After resuspending the platelets once more in 1 ml Tyrode's buffer w/o Ca<sup>2+</sup>, the platelet numbers were determined. To this end, a 1:1 dilution of the platelet suspension in PBS was analyzed using a Sysmex KX-21N automated hematology analyzer. After a final centrifugation step at 2,800 rpm for 5 min, the pellet was resuspended in the appropriate volume of Tyrode's buffer to reach the platelet concentration required for the experiment. Apyrase was added and the platelet suspension was incubated for 30 min at 37°C to allow the platelets to rest.

### Plasma preparation

Mice were bled under isoflurane anesthesia from the retroorbital plexus. 700  $\mu$ l blood were collected into 300  $\mu$ l heparin in TBS (20 U/ml, pH 7.3). The heparinized blood was centrifuged at 2,800 rpm for 5 min and the supernatant was transferred into a new tube. After centrifugation at 10,000 rpm for 5 min, the supernatant was collected. The plasma was either used directly or stored at  $-80^{\circ}\text{C}$ .

### Platelet counting

To determine platelet count and size, mice were bled under isoflurane anesthesia from the retroorbital plexus. 50  $\mu$ l blood were collected into a reaction tube containing 300  $\mu$ l heparin in TBS (20 U/ml, pH 7.3) using heparinized microcapillaries. PBS was added to receive a final dilution of 1:20. The sample was analyzed using a Sysmex KX-21N automated hematology analyzer.

### Flow cytometric analysis of platelets

To determine the expression levels of major platelet surface glycoproteins, mice were bled under isoflurane anesthesia from the retroorbital plexus. 50  $\mu$ l of blood were collected into a reaction tube containing 300  $\mu$ l heparin in TBS (20 U/ml, pH 7.3) using heparinized microcapillaries. One ml Tyrode's buffer w/o  $\text{Ca}^{2+}$  was added and 50  $\mu$ l of diluted blood were stained with saturating amounts of fluorophore-conjugated antibodies for 15 min at RT in the dark. 500  $\mu$ l of PBS were added to stop the staining reaction and the platelets were analyzed directly using a FACSCalibur flow cytometer with Cell Quest software (BD Biosciences, Heidelberg, Germany).

To analyze integrin  $\alpha\text{IIb}\beta_3$  activation and P-selectin exposure upon platelet activation, heparinized blood samples were washed twice (2,800 rpm, 5 min, RT) in Tyrode's buffer w/o  $\text{Ca}^{2+}$  and finally resuspended in Tyrode's buffer containing 2 mM  $\text{Ca}^{2+}$ . Platelets were activated with agonists for 7 min at  $37^{\circ}\text{C}$  followed by 7 min at RT in the presence of saturating amounts of PE-coupled JON/A (4H5) and FITC-coupled anti-P-selectin (5C8) antibodies. The reaction was stopped by addition of 500  $\mu$ l PBS and samples were analyzed. Platelets were identified by their forward/side scatter (FSC/SSC) characteristics. FACS settings are detailed in tables 2.4, 2.5 and 2.6.

**Table 2.4:** Detector/amplifier settings for the flow cytometer

Parameter	Detector	Voltage
P1	FSC	E01
P2	SSC	380
P3	FL1	650
P4	FL2	580
P5	FL3	150

**Table 2.5:** Threshold settings for the flow cytometer

Parameter	Value
FSC-H	253
SSC-H	52
FL1-H	52
FL2-H	52
FL3-H	52

**Table 2.6:** Compensation settings for the flow cytometer

Parameter	Value
FL1	2.4% of FL2
FL2	7.0% of FL1
FL3	0% of FL3
FL4	0% of FL2

### Determination of phosphatidylserine exposure

Washed platelets were resuspended to a concentration of  $5 \times 10^4/\mu\text{l}$  in Tyrode's buffer containing 2 mM  $\text{Ca}^{2+}$ . 50  $\mu\text{l}$  of this suspension were used for activation with agonists for 15 min at  $37^\circ\text{C}$  in the presence of DyLight488-coupled Annexin-A5. The reaction was stopped by adding Tyrode's buffer with 2 mM  $\text{Ca}^{2+}$  and the samples were immediately analyzed using a flow cytometer.

### Aggregation studies

Washed platelets were resuspended to a concentration of  $5 \times 10^5/\mu\text{l}$  in Tyrode's buffer w/o  $\text{Ca}^{2+}$ . 50  $\mu\text{l}$  of this platelet suspension or heparinized PRP (when using ADP as agonist) were transferred into a cuvette containing 110  $\mu\text{l}$  Tyrode's buffer with 2 mM  $\text{Ca}^{2+}$  and 100  $\mu\text{g}/\text{ml}$  human fibrinogen (no fibrinogen was added when using thrombin as agonist). Agonists were added and light transmission was recorded over 10 min with an Apect 4-channel optical aggregation system (APACT, Hamburg, Germany). Before starting the measurement, Tyrode's buffer or plasma was set as 100% aggregation and washed platelet suspension or PRP was set as 0% aggregation.

### ATP release

Washed platelets were resuspended to a concentration of  $5 \times 10^5/\mu\text{l}$  in Tyrode's buffer w/o  $\text{Ca}^{2+}$ . 80  $\mu\text{l}$  of this platelet suspension were diluted into 160  $\mu\text{l}$  Tyrode's buffer with 2 mM  $\text{Ca}^{2+}$ . After addition of 25  $\mu\text{l}$  Chrono-lume luciferase reagent, agonists were added to the continuously stirred (1,000 rpm) platelet suspension. Light transmission and luminescence were recorded on a 700 Whole Blood/Optical Lumi-Aggregometer (Chrono-log) over 10 min. Results were expressed in arbitrary units with buffer representing 100% transmission and washed platelet suspension 0% transmission. ATP release was calculated using an ATP standard and the AggroLink 8 software.

### **Static adhesion (spreading) to fibrinogen**

Rectangular glass coverslips (24x50 mm) were coated with 100 µg/ml human fibrinogen under humid conditions at 4°C o/n. The next day the slides were blocked for at least 1 h at RT with 1% BSA in sterile PBS. The coverslips were rinsed with warm Tyrode's buffer with Ca<sup>2+</sup>. Washed platelets (3x10<sup>5</sup>/µl in Tyrode's buffer with 2 mM Ca<sup>2+</sup>) were stimulated with thrombin (0.01 U/ml) and immediately applied to the fibrinogen surface. Platelets were allowed to spread at RT for 5-30 min, after which the process was stopped by adding 300 µl 4% PFA/PBS. Excessive liquid was removed and platelets were visualized by *differential interference contrast* (DIC) microscopy with a Zeiss Axiovert 200 inverted microscope. Representative images were taken using a CoolSNAP-EZ camera (Visitron, Munich, Germany) and evaluated according to different platelet spreading stages with ImageJ (National Institutes of Health, Bethesda, MD, USA).

### **Adhesion to collagen under flow**

Rectangular glass cover slips (24x60 mm) were coated with 200 µg/ml fibrillar type I collagen o/n at 37°C. The next day, the slides were blocked with 1% BSA for at least 1 h. Platelets were labeled by incubation with DyLight488-conjugated anti-GPIX antibody (0.2 µg/ml) for 5 min at 37°C. Heparinized whole blood was diluted 2:1 in Tyrode's buffer with 2 mM Ca<sup>2+</sup>) and perfused over collagen-coated coverslips through a transparent flow chamber at wall shear rates of 1,700 s<sup>-1</sup>, 1,000 s<sup>-1</sup> or 150 s<sup>-1</sup>. Phase-contrast and fluorescence images were obtained from at least 7 different representative collagen-containing visual fields for each sample using a Zeiss Axiovert 200 inverted microscope. Analysis of surface coverage and thrombus volume was performed using Metavue software (Visitron).

### **Phosphatidylserine exposure under flow**

Heparinized whole blood was supplemented with an additional 10 U/ml heparin. Adhesion experiments under flow conditions (shear rate 1,000 s<sup>-1</sup>) were performed as described above. The flow chamber was rinsed for 4 min with Tyrode's buffer with 2 mM CaCl<sub>2</sub>, 10 U/ml heparin, and 0.25 µg/ml Annexin-A5-DyLight488. Afterwards, it was rinsed for an additional 2 min with Tyrode's buffer supplemented with 2 mM CaCl<sub>2</sub> and 10 U/ml heparin, before phase-contrast and fluorescence images were obtained and analyzed as detailed above.

## **2.2.4 *In vivo* analyses of platelet function**

### **Determination of platelet life span**

Mice were injected i.v. under isoflurane anesthesia with DyLight488-conjugated anti-GPIX antibody (0.5 µg/g body weight). 60 min after injection, mice were bled from the retroorbital plexus. 50 µl of blood were collected into a reaction tube containing 300 µl heparin in TBS (20 U/ml,



pH 7.3) using heparinized microcapillaries. Thereafter, mice were bled every day for 5 days and the percentage of fluorescently labeled platelets was determined using flow cytometry.

### **Anesthesia**

Mice were anesthetized by intraperitoneal injection of a combination of midazolam, medetomidine and fentanyl (5, 0.5 and 0.05 mg/kg body weight). Mice were placed on a heating mat to prevent hypothermia. After 5 min corneal and crossed extensor reflexes were tested to assure proper anesthesia.

### **Tail bleeding time**

Mice were anesthetized, and a 1 mm segment of the tail tip was removed using a scalpel. Tail bleeding was monitored by gently absorbing blood drops on filter paper every 20 s without making contact with the wound site. Bleeding was determined to have ceased when no blood was observed on the paper. Experiments were stopped after 20 min.

### **FeCl<sub>3</sub>-induced thrombus formation in small mesenteric arterioles**

Four-weeks-old mice were anesthetized, and the mesentery was exteriorized through a midline abdominal incision. Arterioles (35-60  $\mu\text{m}$  diameter) were visualized with a Zeiss Axiovert 200 inverted microscope (x10/0.3 NA objective) (Carl Zeiss) equipped with a 100-W HBO fluorescent lamp source and a CoolSNAP-EZ camera (Visitron). Digital images were recorded and analyzed using Metavue software. The injury was induced by topical application of a 3 mm<sup>2</sup> filter paper saturated with 20% FeCl<sub>3</sub> for 10 sec. Adhesion and aggregation of fluorescently labeled platelets (DyLight488-conjugated anti-GPIX antibody) in arterioles were monitored for 40 min or until complete vessel occlusion occurred (blood flow stopped for more than 1 min). FeCl<sub>3</sub>-injury experiments shown in this study were performed and evaluated by Martina Morowski or Ina Thielmann in our research group.

### **Mechanical injury of the abdominal aorta**

The abdominal cavity of 8-12-weeks-old anesthetized mice was opened by a longitudinal incision. An ultrasonic flow probe (Transonic Flowprobe 0.5, Transonic Systems) was placed around the exposed abdominal aorta. Thrombosis was induced by a single firm compression using forceps. Blood flow was monitored until complete blood vessel occlusion occurred for a minimum of 5 min. Otherwise the experiment was stopped after 30 min. Aorta injury experiments shown in this study were performed and evaluated by Martina Morowski, Ina Thielmann or Karen Wolf in our research group.

### **Transient middle cerebral artery occlusion (tMCAO) model**

Experiments were conducted by Dr. Peter Kraft and colleagues in the group of Prof. Dr. Guido Stoll (Department of Neurology, University Hospital, Würzburg) according to the recommendations for research in mechanism-driven basic stroke studies [36]. tMCAO was induced in 8-12-weeks-old mice under inhalation anesthesia using the intraluminal filament technique [25]. Briefly, a midline neck incision was made and a standardized silicon rubber-coated 6.0 nylon monofilament (6021PK10, Doccol, Redlands, CA, USA) was inserted into the right common carotid artery and advanced via the internal carotid artery to occlude the origin of the middle cerebral artery. After 60 min, the filament was removed to allow reperfusion. 24h after tMCAO the global neurological status was assessed using the Bederson score [10]. Motor function and coordination were evaluated using the grip test [122]. For determination of the ischemic brain infarct volume, mice were euthanized 24h after induction of tMCAO and brain sections were stained with 2% 2,3,5-triphenyltetrazolium chloride. Planimetric measurements were performed using ImageJ software to calculate lesion volumes, which were corrected for brain edema as described [178].

### **Reverse passive Arthus (rpA) reaction of the skin**

Mice were anesthetized and shaved using a Contura HS61 hair cutter (Wella, Schwalbach, Germany). The rpA reaction was elicited by intradermal injection of anti-BSA antibody (5 µg/µl) using a 30-G needle followed by intravenous injection of BSA (75 µg protein/g mouse in PBS). Mice were killed and skinned 4 h later. Skins were photographed and analyzed. For hemoglobin quantification punch biopsies of inflamed skin areas were homogenized in 500 µl PBS. The homogenate was cleared by centrifugation at 15,000g for 10 min and the supernatant used for analysis. The optical density at 405 nm was measured to quantify hemoglobin.

### **LPS-induced inflammation of the lung**

Mice were anesthetized and inoculated intranasally with 10 µg LPS. 6h later, *bronchoalveolar lavage* (BAL) was performed by cannulating the trachea and lungs were lavaged with 1 ml PBS. Hemoglobin concentration in the lavage was quantified as described above.

## **2.2.5 MK analyses**

### **Culture of MKs derived from fetal liver progenitors**

Fetal livers were isolated on embryonic day 13.5 to 14.5 from time-mated females. Livers were homogenized by aspirating the suspension 10 times each using 19G and 22G needles and a 1 ml syringe. Afterwards the cell suspension was centrifuged 5 min at 900 rpm (RT). The cells were resuspended in 2 ml MK medium (+50 ng/ml TPO) and incubated at 37°C, 5% CO<sub>2</sub>. After three days of culture, mature MKs were enriched using a 2-step density gradient consisting of 1.5% and 3% BSA. The MKs were resuspended in 1 ml MK medium and cultured

for another day. On day 4, the percentage of proplatelet-forming MKs was determined using a light microscope.

### **Culture of MKs derived from bone marrow progenitor cells**

Hematopoietic stem cells were isolated by flushing bone marrow cells from femurs of 6-8-weeks-old male mice followed by a negative selection using a MACS system (Miltenyi Biotec) with the Dynal Mouse T Cell Negative Isolation Kit according to the manufacturer's protocol (Invitrogen) in combination with rat-anti-mouse antibodies directed against CD45R/B220, TER-119, CD3, Ly-6G/C and CD11b (0.5 mg/10<sup>7</sup> cells). Cells were cultured in MK medium (+50 ng/ml TPO) supplemented with 50 µg/ml recombinant hirudin at 37°C, 5% CO<sub>2</sub> for 3 days, prior to MK purification using a 1.5%–3% BSA gradient.

### **Fluorescent staining of MKs**

Cultured MKs were spun down onto a microscope slide using a cytocentrifuge (Cytospin, Thermo Scientific), fixed in 4% PFA, and permeabilized with 1% Igepal.  $\alpha$ -granular vWF was stained with an anti-vWF-FITC antibody. Tubulin was visualized using an anti- $\alpha$ -tubulin antibody (clone B-5-1-2, Invitrogen), and polymerized actin was stained with phalloidin-Atto647N (Sigma). MKs were visualized using a Leica TCS SP5 confocal microscope (Leica Microsystems) and further processed with ImageJ software (NIH).

## **2.2.6 Electron microscopy**

### ***Transmission electron microscopy (TEM) of resting platelets***

Washed platelets (3x10<sup>5</sup>/µl in Tyrode's buffer w/o Ca<sup>2+</sup>) were fixed with 2.5% glutaraldehyde in 0.1 M cacodylate buffer, pH 7.2 for 10 min at 37°C, followed by incubation at RT for 1h. Samples were stored at 4°C until further processing. Samples were spun at 5,000 rpm for 1 min and washed twice by gently resuspending in 500 µl 50 mM cacodylate buffer. Afterwards 450 µl of 1% osmium tetroxide in 50 mM cacodylate buffer were added, incubated for 1h at RT, washed twice with 400 µl 50 mM cacodylate buffer and washed twice with 400 µl ddH<sub>2</sub>O. Next, 400 µl 2% uranyl acetate in ddH<sub>2</sub>O were added and incubated at 4°C, followed by washing three times with 400 µl ddH<sub>2</sub>O.

For dehydration, samples were incubated with 70% (3x5 min), 95% (3x15 min) and 100% (3x15 min) EtOH (each step 400 µl), followed by incubation with 400 µl of 100% propylene oxide (2x10 min) and 400 µl of a 1:1 mixture of propylene oxide/epon (1x1 h) under rotating conditions. After 2 incubation steps in epon at RT (first step: o/n, second step: 2-3 h) samples were embedded in gelatine capsules and left to dry for 48 h at 60°C. 50 nm thin sections were cut using a ultra microtom (Leica Ultracut UCT). Thin sections were stained with 2% uranyl acetate (in 100% ethanol) and lead citrate and examined under an EM900 transmission electron microscope (Carl Zeiss).

### **TEM of bone marrow MKs**

Femora of 6-8-weeks-old mice were prepared and stored temporary in PBS. Fixation was performed by incubation in 10 ml fixation buffer I per femur for 10 min rotating at RT, followed by o/n incubation at 4°C without rotation. For decalcification, femora were incubated for 5 days in 10% EDTA/PBS (10 ml per femur) with buffer exchange every day.

Next, the samples were washed three times for 10 min with 50 mM cacodylate buffer at 4°C, followed by incubation in fixation buffer II for 2h at 4°C. Following washing with ddH<sub>2</sub>O and staining by incubation in 0.5% uranyl acetate/ddH<sub>2</sub>O at 4°C o/n the samples were washed again three times with 400 µl each and spun down at 5,000 rpm for 1 min at RT. Dehydration, embedding, cutting and analysis were performed as described above.

### **2.2.7 Histology**

#### **Preparation of paraffin sections**

Different organs (spleen, liver, lung, brain, small intestine, femur) from adult mice were prepared, washed in PBS and fixed o/n in 4% PFA/PBS. The next day, organs (except femora) were washed three times with PBS, dehydrated and embedded in paraffin. For decalcification, fixed femora were incubated for 5 days in 10% EDTA/PBS (10 ml per femur) with buffer exchange every day. Afterwards, femora were embedded in paraffin. Organs were cut using a Microm Cool Cut microtome (Thermo Scientific, Braunschweig, Germany) to prepare 5 µm thin sections and dried at 37°C o/n.

#### **Hematoxylin/Eosin staining of paraffin sections**

Sections were deparaffinized by incubation in xylene (2x3 min). Rehydration was carried out using decreasing EtOH concentrations (100%, 90%, 80% and 70%) followed by incubation in ddH<sub>2</sub>O with 2 min incubation time in each solution. Afterwards sections were stained 30 sec in hematoxylin solution, followed by a 10 min incubation step in running tap water. This neutralizes the acid and enables formation of an insoluble blue aluminium haematin complex ("blueing"). Next, the sections are stained for 2 min with 0.05% Eosin G. The sections were washed shortly in ddH<sub>2</sub>O and dehydrated using the same ethanol series and xylene as described above, but in reverse order. Finally, the sections were dried and mounted using Eukitt medium. Samples were analyzed using a Leica DHI 4000B inverse microscope.

#### **Cryo sectioning and staining**

Fresh tissues were embedded in Tissue-Tek (Sakura) and flash-frozen swimming on liquid nitrogen. 5 µm sections were cut and stored at -20°C. Sections were stained using an anti-CD105 (anti-endoglin, BioLegend) antibody which was labeled using the Alexa 647 labeling kit (Invitrogen) and rabbit anti-human-vWF antibody (DAKO) plus goat anti-rabbit Alexa 488 (Invitrogen)

secondary antibody and visualized using a Leica TCS SP5 confocal microscope (Leica Microsystems).

### **2.2.8 Statistical data analysis**

Results are presented as means  $\pm$  SD or dot blots if not stated differently. Differences between two groups were assessed using the Welch's test or if applicable with the Mann Whitney U test. Infarct volumes and functional data obtained from tMCAO experiments were tested for Gaussian distribution with the D'Agostino and Pearson omnibus normality test and then analyzed using the two-tailed Student's t test. Differences between more than two groups were analyzed by one-way analysis of variance (ANOVA) with Dunnetts T3 as post-hoc test.  $p < 0.05$  was considered as statistically significant (\*),  $p < 0.01$  (\*\*) and  $p < 0.001$  (\*\*\*)

## 3 Results

### 3.1 Analysis of Munc13-4-deficient mice

#### 3.1.1 *Unc13d*<sup>-/-</sup> mice display unaltered platelet counts and granule numbers

To test the biological significance of dense granule secretion in thrombosis, hemostasis and ischemic stroke, Munc13-4-deficient (*Unc13d*<sup>-/-</sup>) mice were generated using *Unc13d*<sup>tm1(KOMP)Vlcg</sup> ES cells. Mice homozygous for the *Unc13d* knockout mutation were born in the expected Mendelian ratios, developed normally and did not show any signs of spontaneous bleeding. Western blot analysis confirmed the absence of Munc13-4 in platelets of *Unc13d*<sup>-/-</sup> mice (see figure 3.1 A).

TEM revealed no alterations in the ultrastructure of *Unc13d*<sup>-/-</sup> platelets and normal numbers of  $\alpha$ - and dense granules (see figure 3.1 B). Munc13-4-deficient mice had normal blood parameters like platelet count and size, *white blood cell* (WBC) count, *red blood cell* (RBC) count, *hemoglobin* (HGB) concentration, *hematocrit* (HCT) and surface expression of prominent platelet receptors like GPIb, GPVI, integrin  $\alpha$ IIb $\beta$ 3 or CLEC-2 (see table 3.1 and figure 3.1).

	Wildtype	<i>Unc13d</i> <sup>-/-</sup>	Significance
Plt count [nl <sup>-1</sup> ]	750 $\pm$ 80.83	645 $\pm$ 66.08	n.s.
Plt size [fl]	5.73 $\pm$ 0.16	6.09 $\pm$ 0.48	n.s.
WBC [x10 <sup>3</sup> / $\mu$ l]	4.76 $\pm$ 1.35	6.44 $\pm$ 1.94	n.s.
RBC [x10 <sup>6</sup> / $\mu$ l]	8.56 $\pm$ 1.40	9.5 $\pm$ 1.00	n.s.
HGB [g/dl]	13.44 $\pm$ 2.6	14.8 $\pm$ 1.48	n.s.
HCT [%]	46.2 $\pm$ 7.62	51.2 $\pm$ 5.10	n.s.

**Table 3.1: Basic blood parameters of *Unc13d*<sup>-/-</sup> mice.** Basic blood parameters were assessed in diluted whole blood using a Sysmex hematology analyzer. Results are expressed as mean  $\pm$  SD. n=4 mice per group and are representative of 3 independent experiments. n.s., not significant.

#### 3.1.2 Abrogated ATP secretion and aggregation of *Unc13d*<sup>-/-</sup> platelets

However, in line with previous reports of *Unc13d*<sup>Jinx/Jinx</sup> mice [151], which have a point mutation in the *Unc13d* gene, resulting in the absence of Munc13-4 in platelets, ATP secretion was completely abolished in *Unc13d*<sup>-/-</sup> platelets in response to stimulation with major platelet agonists like thrombin or CRP (see figure 3.2). Platelet aggregation which is a direct consequence of platelet activation and strongly depends on second wave mediators released by activated

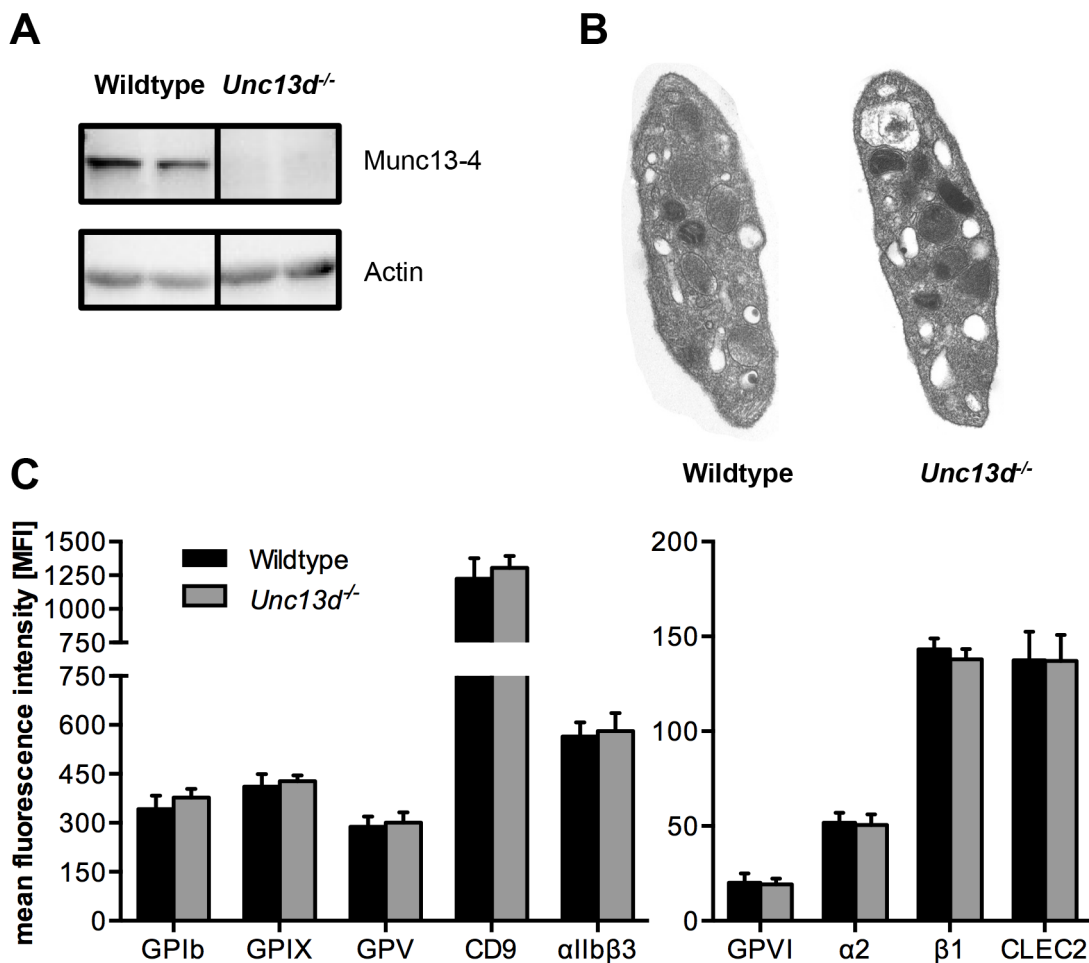


**Figure 3.1: Knockout of *Unc13d* does not alter platelet morphology or expression levels of major platelet glycoproteins.** (A) Western blot analysis of Munc13-4 expression in platelets of wildtype and *Unc13d*<sup>-/-</sup> mice. Actin was used as loading control. (B) Representative TEM images of resting wildtype and *Unc13d*<sup>-/-</sup> platelets. (C) Expression levels of major surface glycoproteins of platelets from Munc13-4-deficient and wildtype mice as determined by flow cytometry in diluted whole blood. Values are mean  $\pm$  SD. n=4 mice per group; representative of 3 independent experiments. Parts published in [170].

platelets was measured using a Born aggregometer in which an increase in light transmission is indicative of platelet aggregation. *Unc13d*<sup>-/-</sup> platelets displayed defective aggregation upon stimulation with different concentrations of several platelet agonists including collagen, thrombin and CRP (see figure 3.2).

### 3.1.3 *Unc13d*<sup>-/-</sup> platelets show impaired P-selectin exposure and integrin activation after stimulation and adhesion to collagen under flow

Platelet activation was further investigated using flow cytometry: P-selectin surface exposure as a marker of  $\alpha$ -granule release and integrin  $\alpha$ IIb $\beta$ 3 activation were assessed using wildtype and mutant platelets. *Unc13d*<sup>-/-</sup> platelets showed significantly reduced P-selectin exposure upon ac-

tivation with strong agonists, namely a combination of ADP and U46 (U46619, a stable  $\text{TxA}_2$  analog), high and intermediate concentrations of thrombin, high concentrations of CRP and the snake venom toxins *rhodocytin* (RC) and *convulxin* (CVX)(see figure 3.3 A). Integrin activation was impaired following activation with the combination of ADP and U46, low and intermediate doses of thrombin, high and intermediate doses of CRP and convulxin. Interestingly, no defect was observed upon stimulation with high-dose thrombin or rhodocytin (see figure 3.3 B). This indicates that there is a broad activation defect downstream of both (hem)ITAM receptors and GPCRs that leads to reduced degranulation and integrin activation. The defective integrin activation can be overcome by strong stimulation either by high-dose thrombin or rhodocytin (see figure 3.3).

Next, *Munc13-4*-deficient platelets were analyzed for their capacity to adhere to collagen under flow. To this end, diluted heparinized whole blood was perfused over collagen coated slides at a shear rate of  $1,000 \text{ s}^{-1}$  using a flow chamber device. Surface coverage and thrombus volume were assessed by fluorescent labeling of platelets and quantification of the area covered

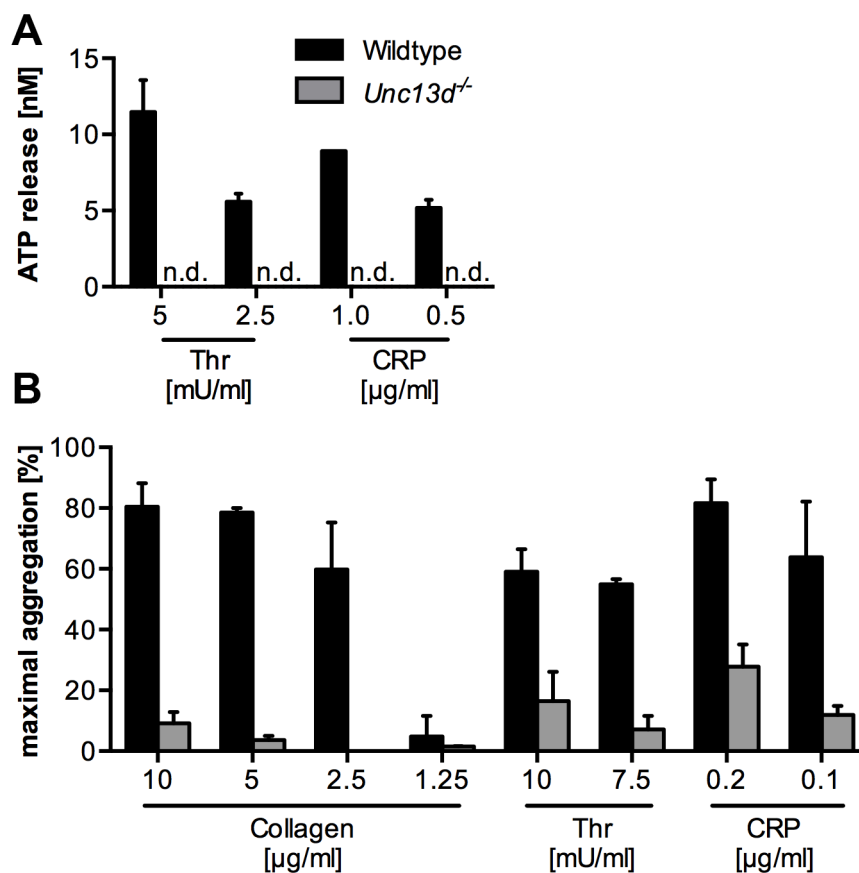


**Figure 3.2: Munc13-4-deficiency abrogates ATP secretion and impairs platelet aggregation** (A) ATP release from wildtype and *Unc13d<sup>-/-</sup>* platelets after thrombin (Thr) or *collagen-related peptide* (CRP) stimulation was assessed using a luciferase assay. (B) Platelet aggregation of wildtype and *Unc13d<sup>-/-</sup>* mice after stimulation with different agonists was measured using a Born aggregometer. Results are shown as mean  $\pm$  SD.  $n=4$  mice per group, representative of 3 independent experiments. n.d., not detectable. Parts published in [170].



by platelets as well as the fluorescence intensity, which directly correlates with the thrombus volume. Wildtype platelets rapidly adhered and formed three-dimensional thrombi resulting in a surface coverage of 42%. In sharp contrast, *Munc13-4*-deficient platelets were unable to adhere and form stable thrombi, resulting in a surface coverage of only 4%. Similarly, thrombus volume was also significantly reduced indicating that thrombus formation under flow *in vitro* is markedly impaired by the absence of ADP secretion in *Munc13-4*-deficient platelets (see figure 3.4).

### 3.1.4 Defective *in vivo* thrombus formation and hemostasis in *Unc13d*<sup>-/-</sup> mice

To test whether defective dense granule secretion also translates into an *in vivo* phenotype, *Unc13d*<sup>-/-</sup> mice were subjected to an *in vivo* model of arterial thrombosis. Platelet accumulation at sites of ferric chloride-induced arteriole injury was monitored using intravital fluorescence microscopy. Interestingly, beginning of thrombus formation followed similar kinetics in both wildtype and *Unc13d*<sup>-/-</sup> mice, indicating that dense granule secretion is dispensable for

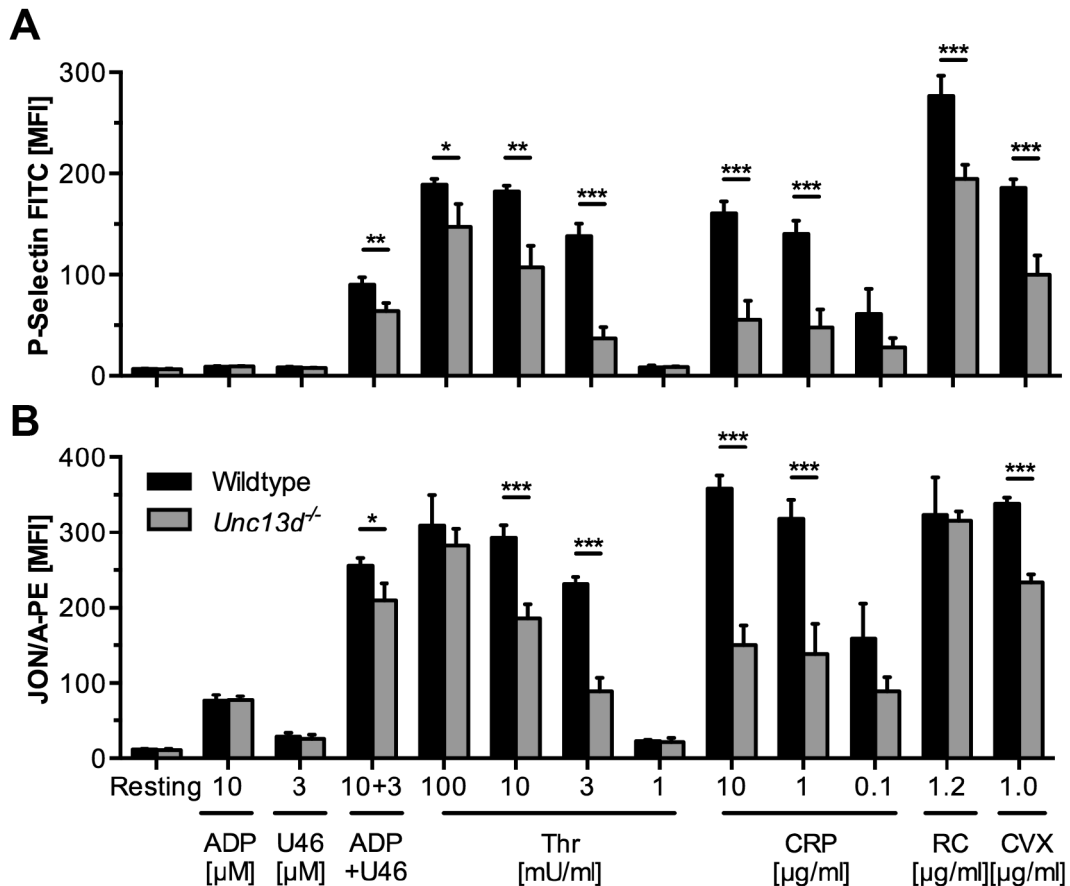


**Figure 3.3: Knockout of *Unc13d* impairs P-selectin exposure as well as integrin activation.** Flow cytometric analysis of P-selectin exposure (A) and activation of integrin  $\alpha$ IIb $\beta$ 3 (B, binding of JON/A-PE antibody) upon stimulation with the indicated agonists in washed platelets of wildtype and *Unc13d*<sup>-/-</sup> mice. Results are presented as MFI  $\pm$  SD. n=5 mice per group, representative of 3 independent experiments. U46, U46619; Thr, thrombin; RC, rhodocytin; CVX, convulxin. \*, p<0.05; \*\*, p<0.01; \*\*\*, p<0.001.

initial platelet adhesion in this setting. Following appearance of first thrombi, wildtype mice showed rapid thrombus growth which finally led to full vessel occlusion after approximately 10 min. In contrast, thrombus growth in *Unc13d*<sup>-/-</sup> mice was limited to small aggregates and no occlusion occurred during the observation period of 40 min (see figure 3.5 A+B).

A second model of arterial thrombosis in which the aorta is mechanically injured with a forceps was used to confirm whether thrombosis in larger vessels is also defective. In this assay, blood flow was monitored with an ultrasonic flow probe. All wildtype mice rapidly formed occlusive thrombi, while 7 out of 8 *Unc13d*<sup>-/-</sup> mice analyzed were unable to fully occlude the vessel within the observation period of 30 minutes (see figure 3.5 C+D).

The effect of defective thrombus formation on hemostasis was investigated by subjecting the mice to a tail bleeding model in which 1 mm of the tail tip is removed and the time until cessation of bleeding is monitored. All *Unc13d*<sup>-/-</sup> mice analyzed were unable to stop bleeding within the observation period (see figure 3.5 E).

### 3.1.5 Reduced infarct size and no signs of hemorrhage in *Munc13-4*-deficient mice after tMCAO

To investigate whether the severely impaired *in vitro* and *in vivo* thrombus formation capacity in *Unc13d*<sup>-/-</sup> mice leads to protection from ischemic stroke, wildtype mice and *Unc13d*<sup>-/-</sup> mice were subjected to the *transient middle cerebral artery occlusion* (tMCAO) stroke model. In this model, a filament is advanced through the carotid artery to reduce cerebral blood flow in the

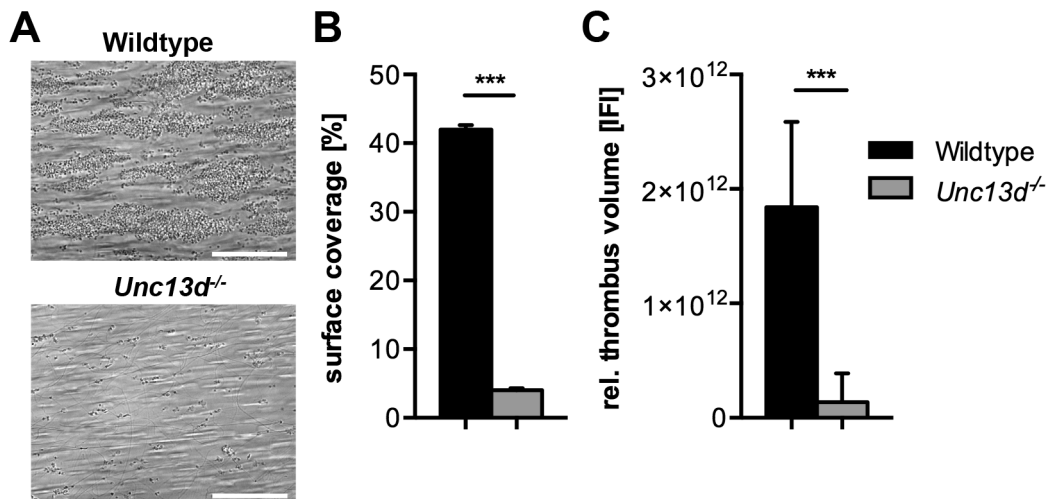


**Figure 3.4: Knockout of *Unc13d* markedly reduces platelet adhesion to collagen under flow.** Diluted whole blood was perfused over collagen under flow at a shear rate of 1000 s<sup>-1</sup>. (A) Representative pictures. Note the absence of any thrombus formation of *Munc13-4*-deficient platelets. Scale bar 50 μm. Quantification of the surface coverage (B) revealed an eightfold decrease for *Munc13-4*-deficient platelets compared to wildtype platelets and a strong reduction in relative thrombus volume (C, measured as integrated fluorescence intensity). n=5-6 mice per group, representative of 3 independent experiments. \*, p<0.05; \*\*, p<0.01; \*\*\*, p<0.001.

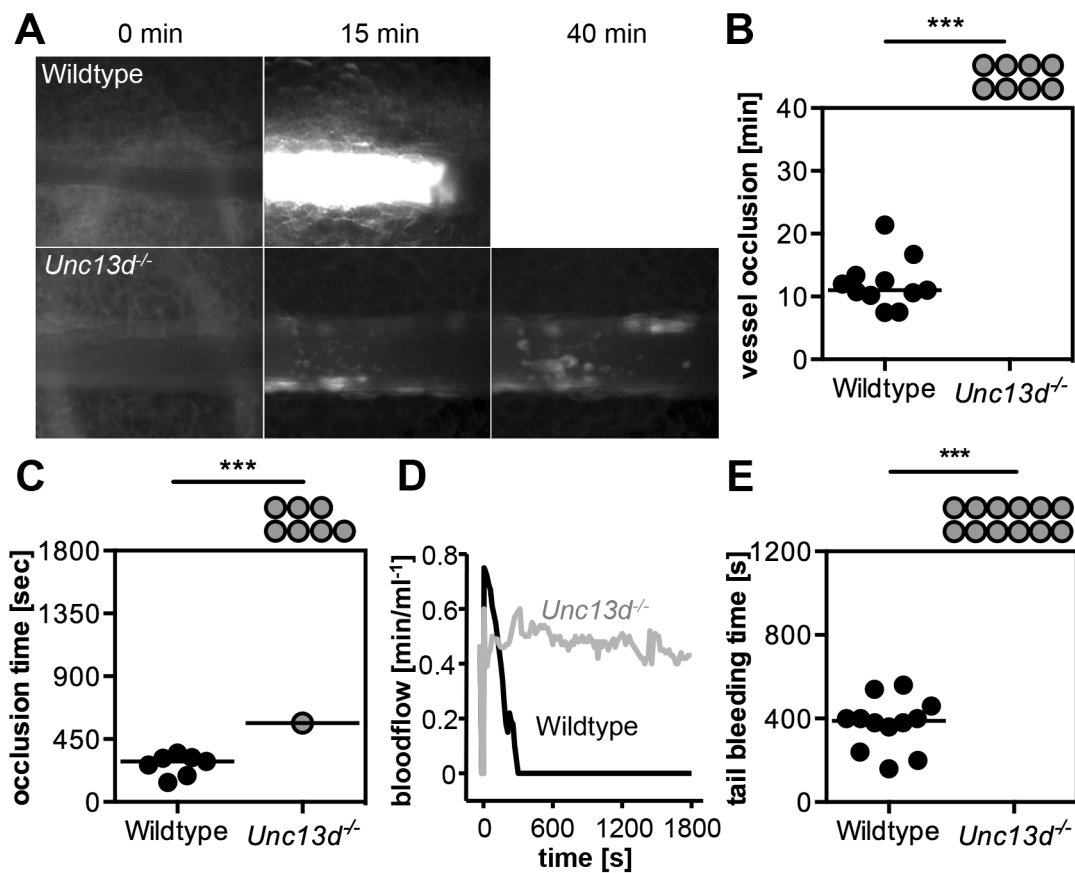


**Figure 3.5: *Unc13d* knockout leads to protection from thrombosis and infinite tail bleeding times.** Thrombus formation in small mesenteric arterioles of wildtype and *Unc13d<sup>-/-</sup>* mice was induced by topical application of 20% FeCl<sub>3</sub>. (A) Representative images at the indicated time points after injury. (B) Time to stable vessel occlusion is depicted, each symbol represents one arteriole. (C) In an aorta injury model the blood flow was monitored for 30 min or until complete occlusion occurred. Time to stable vessel occlusion is depicted; each symbol represents one animal. (D) Representative blood flow traces. (E) Tail bleeding time was assessed in wildtype and knockout animals. Each symbol represents one animal. \*\*\*,  $p < 0.001$ . Parts published in [170].

*middle cerebral artery* (MCA). The filament is removed after 60 min to allow reperfusion. 24 h after reperfusion, the infarct volumes are quantified using a 2,3,5-triphenyltetrazolium chloride (TTC) staining. The infarct volumes in *Unc13d<sup>-/-</sup>* mice were significantly reduced to 38% of the volumes of wildtype mice ( $34.60 \pm 13.53 \text{ mm}^3$  vs.  $90.34 \pm 41.79 \text{ mm}^3$ ;  $p < 0.001$ ; see figure 3.6 A and B).

The reduced infarct size also led to improved neurological outcome as the Bederson score which assesses global neurological function was significantly better in *Unc13d<sup>-/-</sup>* mice (see figure 3.6 C). The grip test, which is used to specifically analyze motor function and coordination displayed a similar tendency, however, did not reach statistical significance (see figure 3.6 D). *Magnetic resonance imaging* (MRI) of live mice confirmed the protective effect of *Munc13-4*-deficiency on infarct development (see figure 3.7 A). This data indicates that impaired dense granule secretion protects mice from infarct progression following tMCAO.

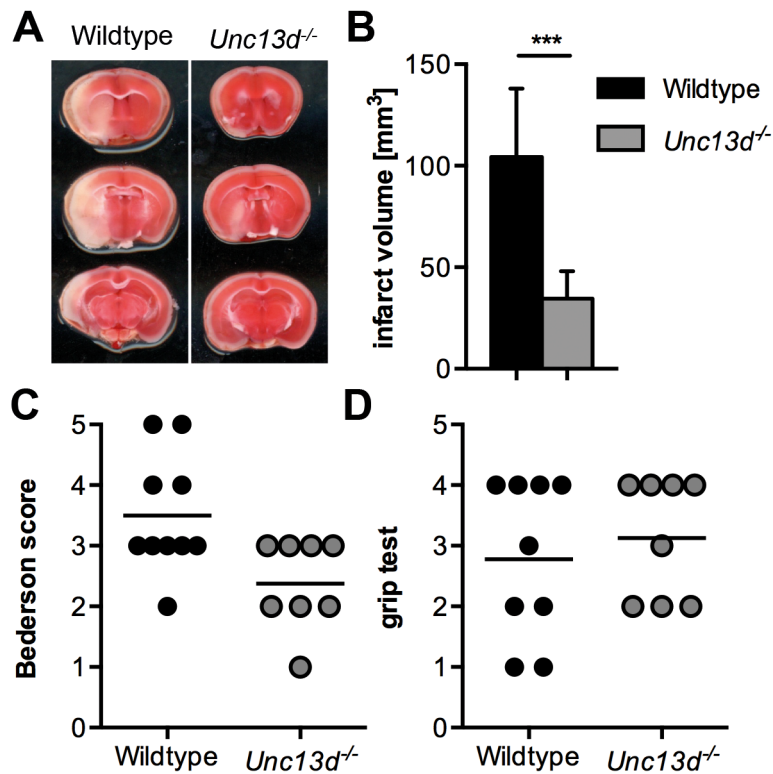


**Figure 3.6: Knockout of *Unc13d* protects from ischemic stroke.** Mice were subjected to 60 min tMCAO. (A) Representative images of 3 coronal sections stained with TTC 24 h after tMCAO. (B) Brain infarct volumes ( $n > 6$ ) were measured by planimetry. Results are shown as mean  $\pm$  SD. (C) Bederson score and (D) Grip test determined 24 h after tMCAO as measures of the neurological outcome. Each symbol represents one individual.  $n = 8-10$  mice per group, on 3 individual experimental days. \*,  $p < 0.05$ ; \*\*,  $p < 0.01$ ; \*\*\*,  $p < 0.001$ . Published in [170].

In a next step we aimed to investigate whether there is an increased incidence of *intracranial hemorrhages* (ICH) in *Unc13d*<sup>-/-</sup> after tMCAO due to impaired hemostasis. GPIIb/IIIa blockade was used as a positive control since application of 100  $\mu$ g anti-GPIIb/IIIa F(ab)<sub>2</sub> per mouse leads to receptor blockade of more than 95% and a high incidence of ICH after tMCAO [101]. Indeed, massive hemorrhage was observed in brains from mice treated with anti-GPIIb/IIIa F(ab)<sub>2</sub> (see figure 3.7 B). In sharp contrast, no signs of ICH were visible in brains of *Unc13d*<sup>-/-</sup> mice after tMCAO (see figure 3.7 B). Likewise, no hypointense areas, indicating ICH, were detectable in MRI of Munc13-4-deficient mice after ischemic stroke (see figure 3.7 A). This data excludes an increased rate of ICH in Munc13-4-deficient mice and confirms the observation that *Unc13d*<sup>-/-</sup> mice do not show spontaneous bleedings.

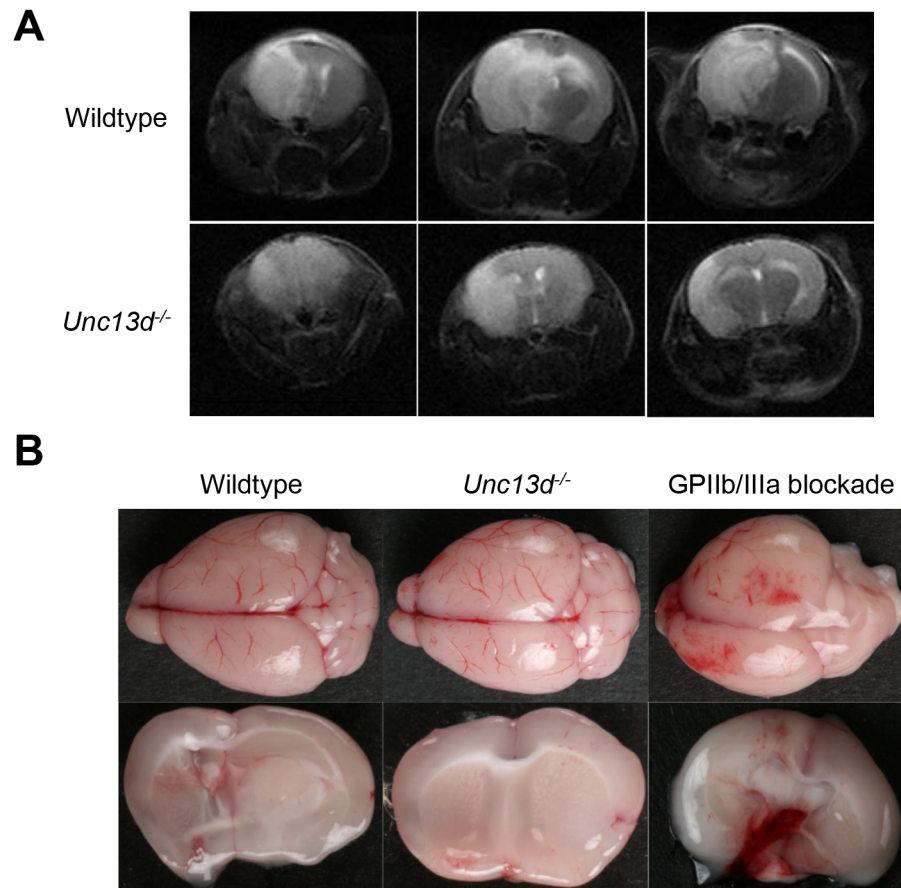


**Figure 3.7: Knockout of *Unc13d* does not cause intracranial bleeding after ischemic stroke.**

(A) MRI of cerebral infarcts 24 h after tMCAO in wildtype and *Unc13d*<sup>-/-</sup> mice ( $n > 6$ ). Representative images are shown. T2-weighted gradient echo MRI shows bright ischemic lesions in wildtype mice (top) and *Unc13d*<sup>-/-</sup> mice (bottom). Note that infarcts are smaller in *Unc13d*<sup>-/-</sup> mice compared to wildtype mice. Hypointense (dark) areas indicative of *intracranial hemorrhage* (ICH) were not detectable in both *Unc13d*<sup>-/-</sup> and wildtype controls. (B) Representative images of whole brain (top) and corresponding coronal brain sections (bottom) from wildtype, *Unc13d*<sup>-/-</sup> and wildtype mice treated with 100  $\mu$ g anti-GPIIb/IIIa F(ab)<sub>2</sub> (more than 95% receptor blockade), prior to 60 min of tMCAO. Note the massive hemorrhage in the infarcted brain area of anti-GPIIb/IIIa treated mice, which was absent in all other mice. Published in [170].

## 3.2 Analysis of *Nbeal2*-deficient mice

### 3.2.1 *Nbeal2*<sup>-/-</sup> mice are macrothrombocytopenic and lack $\alpha$ -granules in MKs and platelets

To analyze the role of *Nbeal2* in platelet biogenesis, hemostasis, thrombosis and inflammatory settings, the *Nbeal2* gene was disrupted in mice. The absence of the *Nbeal2* protein in platelets was confirmed using Western blotting (see figure 3.8 A). *Nbeal2*-deficient mice were born in expected Mendelian ratios, developed normally, were viable and fertile, and showed no signs of spontaneous bleeding. *Nbeal2*-deficient mice showed a moderate macrothrombocytopenia, with platelet size increased by 14% and a platelet count reduced by 40% compared to wildtype (see figure 3.8 B). A mild increase in the relative spleen weight was observed in 6-week-old mice, which did not develop further in older mice (see figure 3.8 C). Analysis of the spleen and bone marrow revealed an almost twofold increase in the number of splenic MKs and a minor

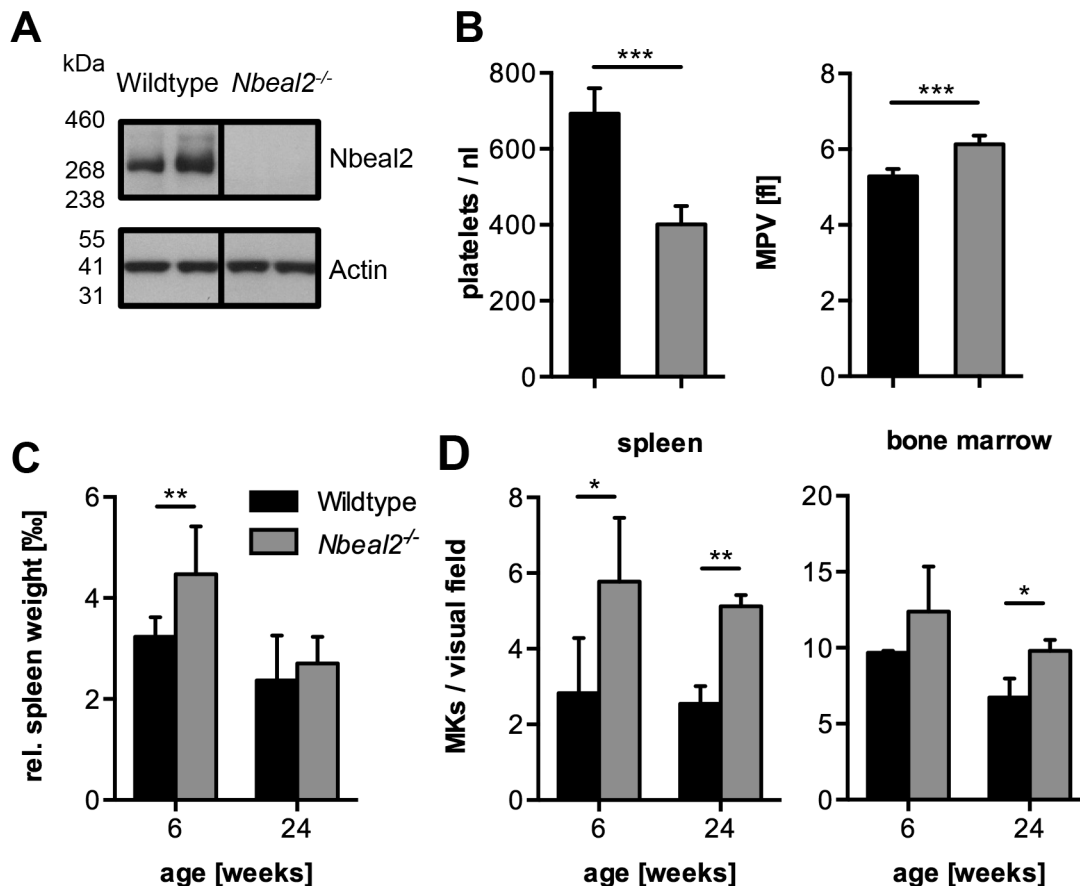


**Figure 3.8: Knockout of *Nbeal2* causes macrothrombocytopenia.** (A) Western blot analysis of *Nbeal2* expression in platelets of wildtype and *Nbeal2*<sup>-/-</sup> mice. Actin was used as loading control. (B) Platelet counts and mean platelet volume (MPV) of wildtype and *Nbeal2*-deficient mice. (C) Spleen-to-body-weight ratio in young (6 weeks) and old (24 weeks) mice. (D) Quantification of MK numbers per visual field (294 x 221  $\mu$ m) in hematoxylin and eosin stained sections of old and young mice. Values are mean  $\pm$  SD. n=4 mice per group and are representative of 3 independent experiments. \*, p<0.05; \*\*, p<0.01; \*\*\*, p<0.001. Parts published in [34].

increase in the number of bone marrow MKs in both young and older mice that lack *Nbeal2* (see figure 3.8 D).

Of note, *Nbeal2*-deficient platelets showed a life span that was similar to that of wildtype platelets as assessed by injection of a fluorescently labeled anti-platelet antibody and quantification of the percentage of labeled platelets over time. This excluded increased platelet clearance as a cause of the thrombocytopenia observed in these mice (see figure 3.9).

To assess whether *Nbeal2*-deficiency causes global defects on the hematopoietic system, basic blood parameters of wildtype and *Nbeal2*-deficient mice were analyzed using a Sysmex hematology analyzer. RBC and WBC count, HGB concentration and HCT were unaltered in *Nbeal2*<sup>-/-</sup> mice (see table 3.2). Next, the effect of *Nbeal2*-deficiency on certain immune cell populations was investigated. B cell, T cell and granulocyte subpopulations were analyzed using flow cytometry and found to be unaltered in *Nbeal2*-deficient mice.

Expression levels of major platelet surface glycoproteins were comparable to those of wildtype platelets, except for slight elevations in GPIb, GPIX,  $\alpha$ IIb $\beta$ 3, and CD9 expression, which correlated well with the increased platelet size (see table 3.2 and figure 3.8).

	Wildtype	<i>Nbeal2</i> <sup>-/-</sup>	Significance
WBC [x10 <sup>3</sup> / $\mu$ l]	6.3 $\pm$ 2.5	7.5 $\pm$ 2.8	n.s.
RBC [x10 <sup>6</sup> / $\mu$ l]	6.8 $\pm$ 0.7	7.2 $\pm$ 1.6	n.s.
HGB [g/dl]	10.6 $\pm$ 1.0	12.2 $\pm$ 2.4	n.s.
HCT [%]	36.2 $\pm$ 3.5	40.1 $\pm$ 9.8	n.s.
GPIb [MFI]	325 $\pm$ 9	365 $\pm$ 4	**
GPV [MFI]	261 $\pm$ 9	268 $\pm$ 5	n.s.
GPIX [MFI]	362 $\pm$ 9	410 $\pm$ 11	***
CD9 [MFI]	1149 $\pm$ 18	1226 $\pm$ 44	*
GPVI [MFI]	43 $\pm$ 1	42 $\pm$ 2	n.s.
$\alpha$ 2 [MFI]	47 $\pm$ 3	46 $\pm$ 1	n.s.
$\beta$ 1 [MFI]	140 $\pm$ 12	135 $\pm$ 4	n.s.
$\alpha$ IIb $\beta$ 3 [MFI]	552 $\pm$ 38	632 $\pm$ 37	**
CLEC-2 [MFI]	112 $\pm$ 8	123 $\pm$ 8	n.s.
B cells [%]	50.4 $\pm$ 3.6	53.1 $\pm$ 4.9	n.s.
CD4 <sup>+</sup> T cells [%]	16.2 $\pm$ 2.5	14.7 $\pm$ 1.4	n.s.
CD8 <sup>+</sup> T cells [%]	9.9 $\pm$ 1.7	11.3 $\pm$ 3.0	n.s.
Gr1 <sup>+</sup> CD11b <sup>+</sup> [%]	7.3 $\pm$ 1.5	8.0 $\pm$ 3.6	n.s.
Gr1 <sup>low</sup> CD11b <sup>+</sup> [%]	7.1 $\pm$ 1.8	5.1 $\pm$ 1.2	n.s.
Gr1 <sup>neg</sup> CD11b <sup>low</sup> [%]	3.4 $\pm$ 2.0	4.0 $\pm$ 1.0	n.s.

**Table 3.2: Basic blood parameters of *Nbeal2*<sup>-/-</sup> mice.** Basic blood parameters were assessed by analyzing diluted whole blood using a Sysmex hematology analyzer. For other values, diluted whole blood (major platelet glycoproteins) or blood lysed in ACK buffer (immune cells) was analyzed by flow cytometry. Results are expressed as mean  $\pm$  SD. n=4 mice per group and are representative of 3 independent experiments. \*, p < 0.05; \*\*, p < 0.01; \*\*\*, p < 0.001; n.s., not significant.

TEM analyses were performed to study the ultrastructure of platelets and MKs and confirmed the absence of  $\alpha$ -granules in platelets of *Nbeal2*<sup>-/-</sup> mice, while dense granules were not affected. *Nbeal2*-deficient platelets showed increased numbers of vacuoles, which appeared empty, with

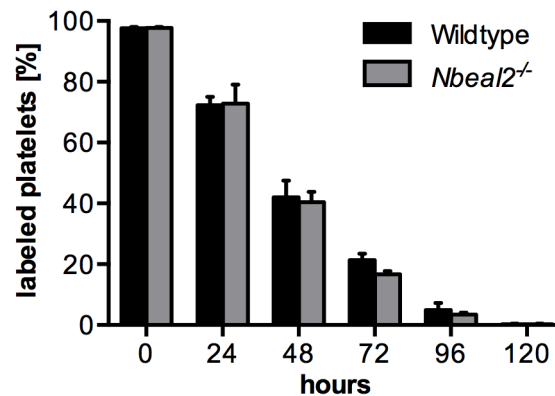


**Figure 3.9: *Nbeal2* knockout does not affect platelet lifespan *in vivo*.** To measure platelet lifespan, mice were injected i.v. with DyLight488-conjugated anti-GPIX. Afterwards blood was collected daily and the percentage of labeled platelets was analyzed. Results are presented as mean  $\pm$  SD. n=4 mice per group and are representative of 3 independent experiments. Published in [34].

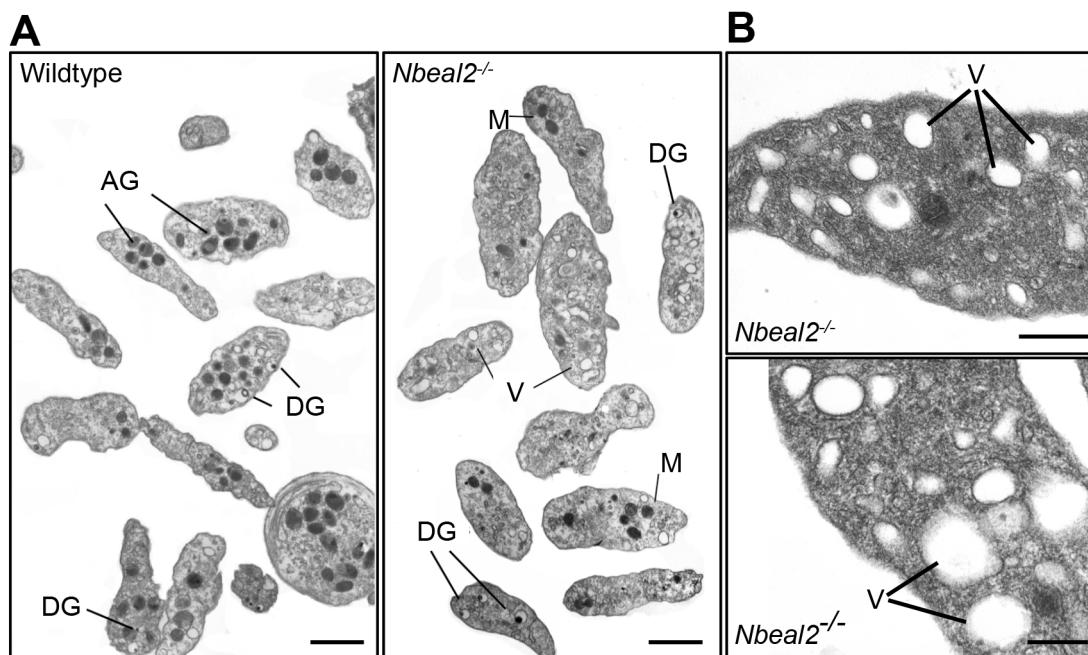


**Figure 3.10: *Nbeal2*<sup>-/-</sup> platelets show defective  $\alpha$ -granule biogenesis.** (A) Representative TEM images of wildtype and *Nbeal2*-deficient platelets. Note complete lack of  $\alpha$ -granules in knockout platelets. AG,  $\alpha$ -granules; DG, dense granules; M, mitochondria; V, vacuoles. Scale bar 1  $\mu$ m. (B) Ultrastructure of *Nbeal2*<sup>-/-</sup> platelets. Note the large vacuoles. Scale bar: 0.5  $\mu$ m (upper), 0.25  $\mu$ m (lower). Published in [34].



no electron-dense material present (see figure 3.10 A and B). In some knockout samples, there were structures present that could be described as  $\alpha$ -granule remnants and were partially filled with diffuse electron-dense material. This is in agreement with observations in platelets from GPS patients [118]. Immunofluorescent staining of vWF in spread platelets showed typical centralization of vWF-positive ( $\alpha$ -)granules in wildtype platelets, while the protein was virtually absent in *Nbeal2*-deficient platelets (see figure 3.11 A). Quantification of the total platelet vWF content using an ELISA system confirmed that *Nbeal2*-deficient platelets contain only 11% of the vWF present in wildtype platelets (see figure 3.11 B). Interestingly, fibrinogen levels were affected to a similar extent.

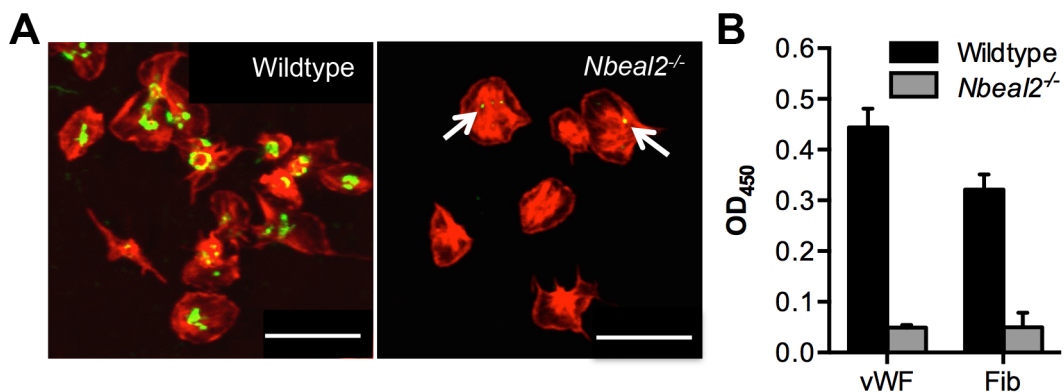


**Figure 3.11: *Nbeal2* knockout causes absence of  $\alpha$ -granular proteins in platelets.** (A) Actin (red) and vWF (green) staining on spread (30 min on fibrinogen) wildtype and *Nbeal2*<sup>-/-</sup> platelets. Arrows point at residual vWF content in knockout platelets. (B) vWF and fibrinogen content in resting platelets was analyzed using an ELISA. Data is presented as  $\Delta OD_{450} - OD_{620}$  of 4 mice per group normalized to vWF-deficient mice or PBS as control. Values are mean  $\pm$  SD, representative of 3 independent experiments. Published in [34].

In contrast to wildtype mice, proplatelet territories of mature bone marrow MKs from *Nbeal2*<sup>-/-</sup> mice contained no characteristic  $\alpha$ -granules. At the same time, the number of vacuoles and mitochondria were elevated in knockout MKs (see figure 3.12 top). A frequent observation was the presence of leukocytes inside the cytoplasm of *Nbeal2*-deficient MKs, a process called emperipolesis (see figure 3.12 A, bottom left), a finding also seen in samples from human GPS patients [47]. The DMS of *Nbeal2*-deficient MKs showed normal development, with homogeneous distribution of delimiting territories. Proplatelet formation was largely unaltered (see figure 3.12 A, bottom right). Confocal microscopy of *fetal liver cell* (FLC) derived MKs from wildtype and *Nbeal2*-deficient mice revealed unaltered actin cytoskeleton and microtubular structures during proplatelet formation (see figure 3.13 A). Quantification of the percentage of proplatelet-forming MKs in cultures of FLC-derived MKs showed no significant differences between wildtype and *Nbeal2*-deficient mice indicating that deficiency in  $\alpha$ -granular proteins does not cause a general defect in proplatelet formation from bone marrow MKs.

To further test the capacity of *Nbeal2*-deficient megakaryocytes to produce platelets, wildtype and knockout mice were subjected to an *in vivo* assay of antibody-mediated thrombocytopenia. To this end, mice were depleted of platelets by a single injection of 100  $\mu$ g anti-GPIb $\alpha$  antibody

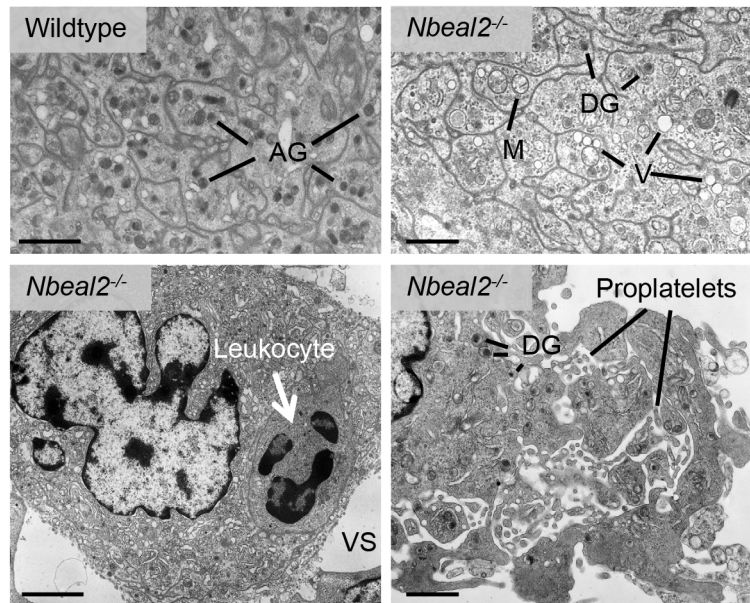


**Figure 3.12: Absence of  $\alpha$ -granules but normal ultrastructure in *Nbeal2*-deficient MKs.** Representative TEM images of mature bone marrow MKs. Normal demarcation membrane system (DMS) in proplatelet territories of wildtype MKs (upper left). Scale bar: 1  $\mu$ m. Normal DMS is present in MKs from *Nbeal2*<sup>-/-</sup> mice (upper right) but  $\alpha$ -granules are completely absent and an increased number of vacuoles is visible. Scale bar: 1  $\mu$ m. Emperipolesis (leukocytes inside the MK cytoplasm) is often observed in knockout bone marrow (lower left, arrow). Scale bar: 3  $\mu$ m. Normal proplatelet development from *Nbeal2*-deficient MKs (lower right). Scale bar: 1  $\mu$ m. AG,  $\alpha$ -granules; DG, dense granules; M, mitochondria; V, vacuoles; VS, vascular sinus. Published in [34].

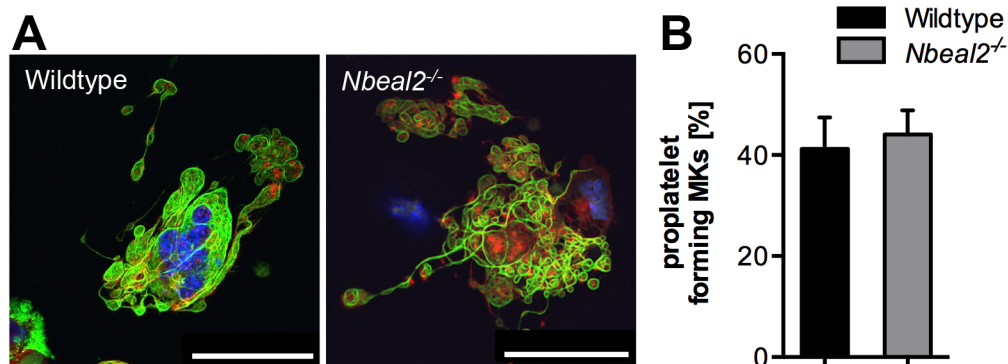


**Figure 3.13: Unaltered proplatelet formation in *Nbeal2*-deficient MKs.** (A) Staining for actin (red) and tubulin (green) structures in MKs from FLCs. Nuclei were stained with DAPI (blue). Scale bar: 50  $\mu$ m. (B) Percentage of proplatelet-forming MKs in cultures of FLC-derived MKs. Values are mean  $\pm$  SD, representative of 3 independent experiments. Published in [34].

and platelet recovery was assessed by evaluating platelet counts over time using flow cytometry. Interestingly, when normalizing the platelet counts to basal levels, *Nbeal2*-deficient mice showed similar kinetics as wildtype mice (see figure 3.14).

Staining of FLC- and bone marrow-derived MKs for vWF revealed a diffuse distribution in wildtype MKs (see figure 3.15 A), while *Nbeal2*-deficient MKs showed two staining patterns: They

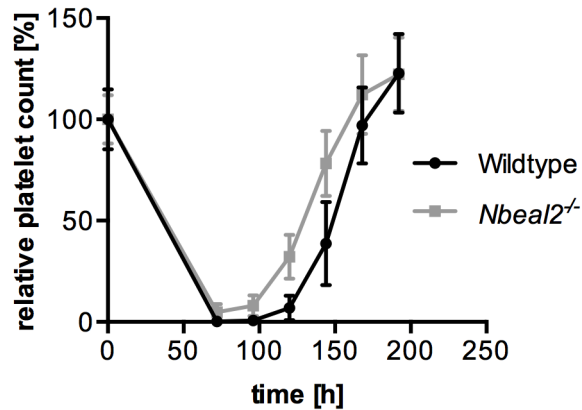


**Figure 3.14: *Nbeal2*<sup>-/-</sup> MKs show unaltered platelet production capacity after antibody-mediated platelet depletion.** Wildtype and *Nbeal2*<sup>-/-</sup> mice were depleted of platelets by single-dose injection of 100  $\mu$ g of anti-GPIb $\alpha$  antibody. Platelet count recovery kinetics were assessed by flow cytometry. Values are mean  $\pm$  SD, n=5 mice per group, representative of 3 independent experiments.

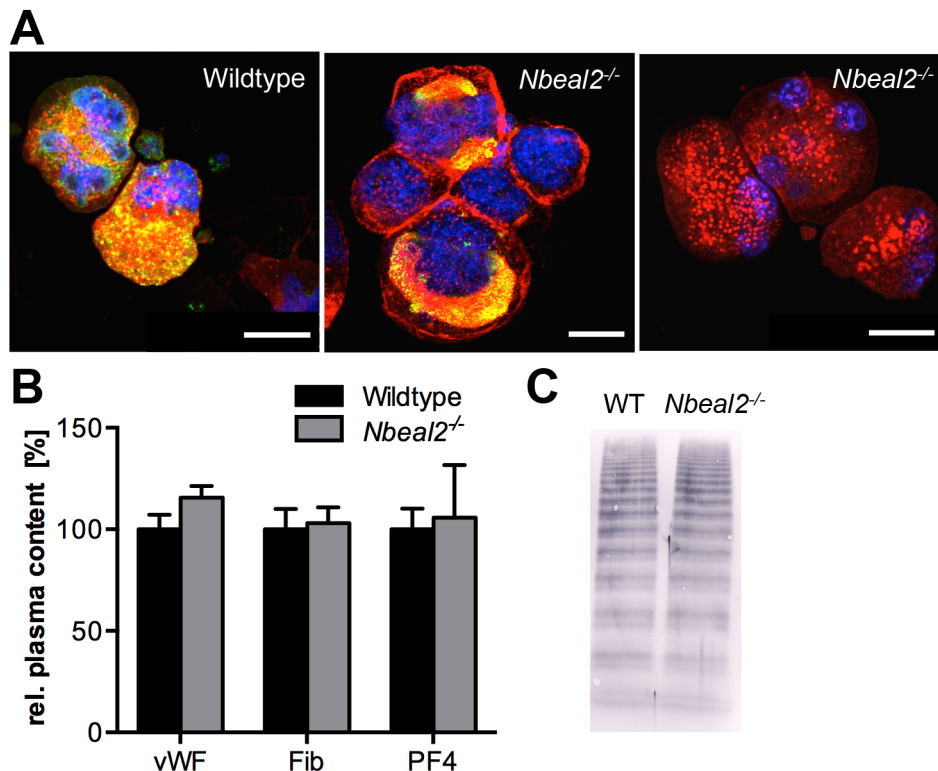


**Figure 3.15: Impaired distribution of  $\alpha$ -granular protein vWF in *Nbeal2*<sup>-/-</sup> MKs.** (A) vWF distribution (green) in bone marrow derived MKs from wildtype and *Nbeal2*<sup>-/-</sup> mice. Actin cytoskeleton was stained using phalloidin (red) and nuclei were stained with DAPI (blue). Scale bar: 25  $\mu$ m. (B) Quantification of vWF, fibrinogen and PF4 levels in plasma of wildtype and *Nbeal2*-deficient mice using ELISAs. Data is presented as  $\Delta$ OD<sub>450</sub> - OD<sub>620</sub>. Values are mean  $\pm$  SD, representative of 3 independent experiments. (C) Analysis of vWF multimer distribution in citrated whole blood of wildtype (WT) and *Nbeal2*-deficient mice. Note unaltered triplet structure, equal distribution and presence of high molecular weight multimers in both samples. Published in [34].

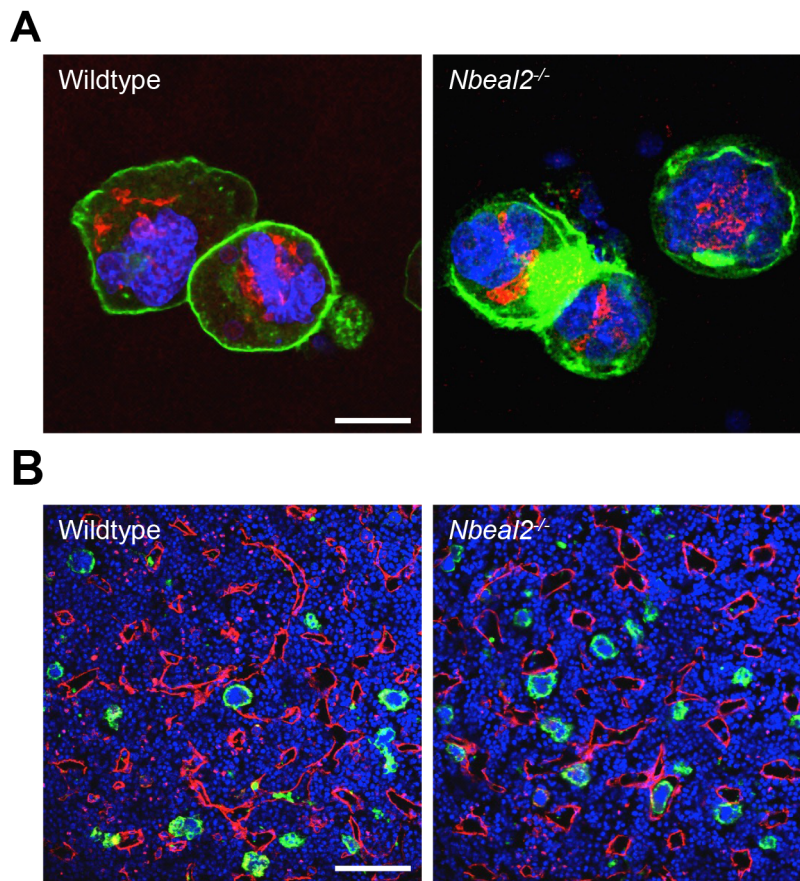


**Figure 3.16: Unaltered Golgi apparatus morphology in *Nbeal2*-deficient MKs and localization of MKs in the bone marrow.** (A) Bone marrow-derived MKs from wildtype and *Nbeal2*<sup>-/-</sup> mice were stained for actin (green), GM130 as a Golgi marker (red) and DAPI as a nuclear marker (blue). Scale bar: 25  $\mu$ m. (B) Bone marrow sections from wildtype and knockout mice were analyzed for GPIb as a MK marker (green), endoglin as an endothelial marker (red) and DAPI as a nuclear marker (blue). Scale bar: 80  $\mu$ m.

either lacked vWF or displayed accumulation of the protein in certain cytoplasmic areas between nucleus and plasma membrane. These areas often also showed additional irregular deposition of actin, which was not seen in *Nbeal2*<sup>-/-</sup> MKs lacking vWF or wildtype MKs. A possible explanation could be that vWF is lost from *Nbeal2*-deficient MKs at an early time point during megakaryopoiesis, resulting in platelets devoid of vWF (see figure 3.15 A). To investigate whether vWF production in endothelial cells was altered, vWF plasma levels and multimer size distribution were analyzed. Both were found to be indistinguishable between wildtype and *Nbeal2*-deficient mice (see figure 3.15 B and C), indicating an unaltered vWF synthesis in endothelial cells. Importantly, fibrinogen and PF4 levels in plasma were also unaltered.

To investigate whether *Nbeal2*-deficiency causes alterations in the morphology of the Golgi apparatus, MKs from wildtype and *Nbeal2*<sup>-/-</sup> mice were analyzed using the Golgi marker GM130. GM130-positive signals were found close to the nucleus in knockout MKs and showed unaltered appearance compared to wildtype cells indicating that overall morphology of the Golgi

apparatus was unaltered.

As MK morphology appeared normal apart from  $\alpha$ -granule deficiency and mislocalization of vWF (see figures 3.12, 3.13 and 3.15), it was interesting to see whether *Nbeal2*-deficient MKs localize normally within the bone marrow. To this end, whole femora from wildtype and knockout mice were sectioned using a cryotome and stained for MKs and vasculature. The analysis showed no alterations in localization of the knockout MKs compared to wildtype with MKs located to the same extent at the vessel, in the space between the vessels and a small fraction even inside the vessel (see figure 3.16 B). This indicates that there is no obvious alteration in MK maturation or migration in *Nbeal2*-deficient animals.

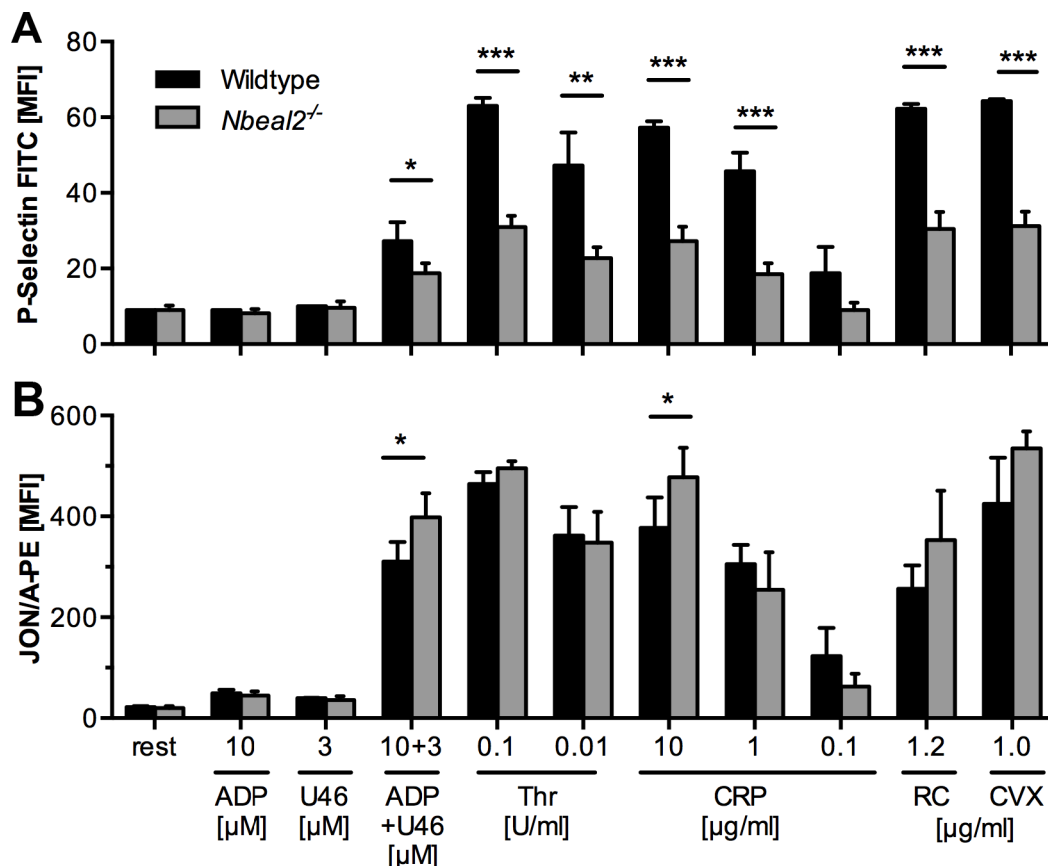


**Figure 3.17: *Nbeal2*<sup>-/-</sup> platelets show reduced P-selectin exposure upon stimulation.** Flow cytometric analysis reveals reduced surface expression of P-selectin (A) but largely unaltered integrin  $\alpha$ IIb $\beta$ 3 activation (JON/A binding, B) in *Nbeal2*-deficient platelets after stimulation with the agonists indicated. Results are presented as MFI  $\pm$  SD. n=5 mice per group, representative of 3 independent experiments. U46, U46619; Thr, thrombin; RC, rhodocytin; CVX, convulxin. \*, p < 0.05; \*\*, p < 0.01; \*\*\*, p < 0.001. Published in [34].

To analyze *Nbeal2*<sup>-/-</sup> platelet activation, flow cytometric analysis of P-selectin surface exposure as a marker of  $\alpha$ -granule release and integrin  $\alpha$ IIb $\beta$ 3 activation was performed using wildtype and knockout platelets. In line with paucity of  $\alpha$ -granules, *Nbeal2*<sup>-/-</sup> platelets showed markedly reduced P-selectin exposure compared with wildtype platelets in response to all agonists tested (see figure 3.17 A), while integrin  $\alpha$ IIb $\beta$ 3 activation was largely unaltered (see figure 3.17 B).

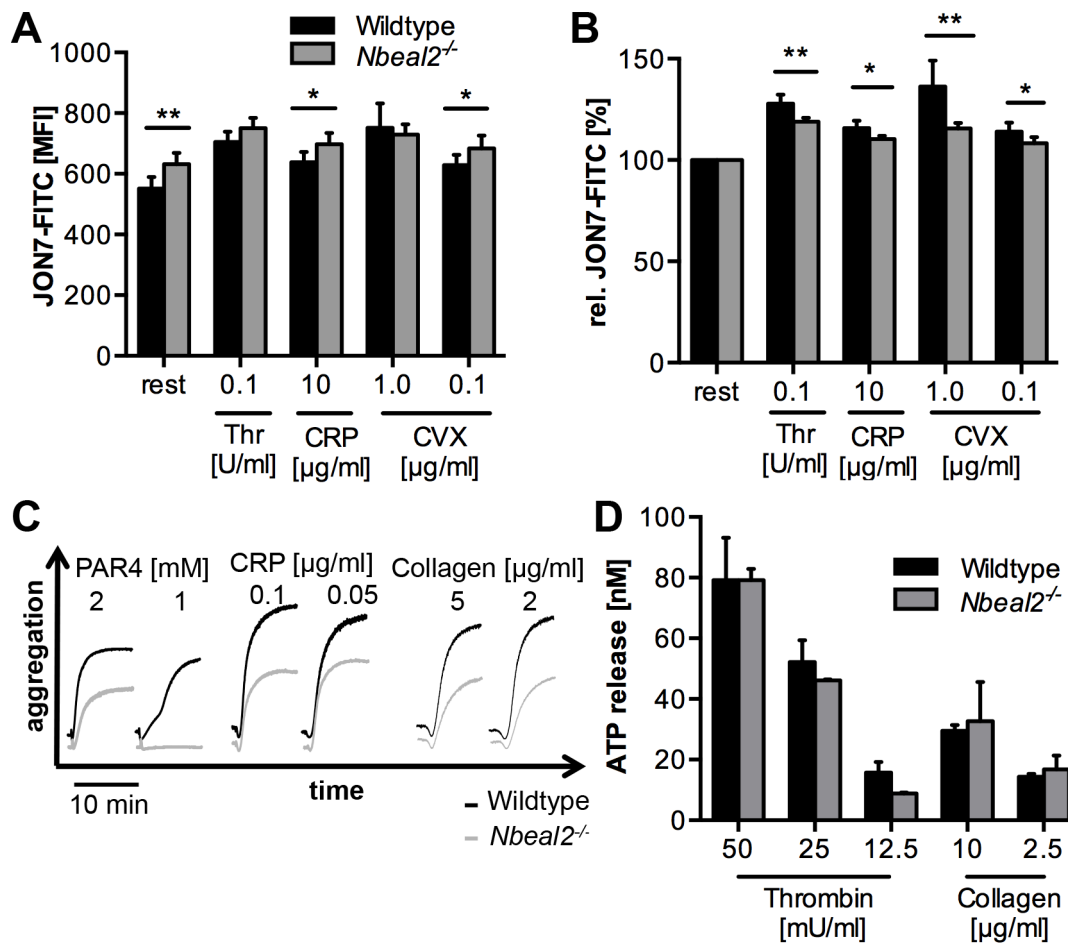


**Figure 3.18: Slightly altered integrin recruitment but impaired aggregation of *Nbeal2*<sup>-/-</sup> platelets.** (A) Binding of the JON7-FITC antibody was used to quantify integrin  $\alpha$ IIb $\beta$ 3 recruitment to the platelet surface upon stimulation with the agonists indicated. Results are presented as MFI  $\pm$  SD.  $n=4$  mice per group, representative of 3 independent experiments. (B) Relative JON7-FITC signal as percentage of resting. (C) Representative aggregation traces (recording time 10 min) show impaired aggregation of *Nbeal2*-deficient platelets upon stimulation with the agonists indicated. (D) ATP release from wildtype and knockout platelets was assessed after stimulation with the indicated agonists using a luciferase assay. Results are presented as mean  $\pm$  SD.  $n=3$  mice per group, representative of 3 independent experiments. \*,  $p<0.05$ ; \*\*,  $p<0.01$ ; \*\*\*,  $p<0.001$ . Published in [34].

Analysis of total integrin  $\alpha$ IIb $\beta$ 3 surface levels further revealed that the activation-dependent recruitment of intracellular  $\alpha$ IIb $\beta$ 3 pools seen in wildtype controls was slightly reduced in *Nbeal2*<sup>-/-</sup> platelets (see figure 3.18 A and B). Surface levels of other glycoproteins on *Nbeal2*<sup>-/-</sup> platelets after stimulation were largely unaltered compared to wildtype platelets (see tables 3.3 and 3.4).

To study the functional consequences of these combined defects, aggregation responses upon stimulation with different agonists were assessed. Consistent with previous results and observations in patients with GPS [139], *Nbeal2*<sup>-/-</sup> platelets showed reduced aggregation upon stimulation with collagen, collagen-related peptide (CRP), or PAR-4 peptide (see figure 3.18 C). Interestingly, ATP release was unaltered upon stimulation with thrombin or collagen (see figure 3.18 D), indicating that dense granule secretion is unaffected in knockout platelets.

MFI	Resting			CVX		
	Wildtype	<i>Nbeal2</i> <sup>-/-</sup>	Sign.	WT	<i>Nbeal2</i> <sup>-/-</sup>	Sign.
GPIb	325 ± 9	365 ± 4	**	274 ± 21	255 ± 29	n.s.
GPV	261 ± 9	268 ± 5	n.s.	266 ± 5	191 ± 16	***
GPIX	362 ± 9	410 ± 11	***	382 ± 20	392 ± 20	n.s.
CD9	1149 ± 18	1226 ± 44	*	1515 ± 96	1595 ± 76	n.s.
GPVI	43 ± 1	42 ± 2	n.s.	36 ± 2	35 ± 3	n.s.
α2	47 ± 3	46 ± 1	n.s.	67 ± 7	65 ± 8	n.s.
β1	140 ± 12	135 ± 4	n.s.	169 ± 11	155 ± 7	*
αIIbβ3	552 ± 38	632 ± 37	**	680 ± 62	596 ± 53	n.s.
CLEC-2	112 ± 8	123 ± 8	n.s.	183 ± 27	166 ± 11	n.s.

**Table 3.3: Glycoprotein expression after stimulation of *Nbeal2*<sup>-/-</sup> platelets with convulxin.** Expression levels of major glycoproteins of resting wildtype and *Nbeal2*-deficient platelets and after stimulation with 0.5 μg/ml convulxin (CVX). Results are expressed as MFI ± SD. n=4 mice per group, representative of 4 independent experiments. \*, p < 0.05; \*\*, p < 0.01; \*\*\*, p < 0.001; n.s., not significant.

### 3.2.2 Defective adhesion and aggregate formation of *Nbeal2*<sup>-/-</sup> platelets under flow

To examine the consequences of platelet α-granule deficiency on thrombus formation under flow, anticoagulated whole blood of *Nbeal2*-deficient and wildtype mice was perfused over immobilized collagen at shear rates of 1,000 s<sup>-1</sup> and 1,700 s<sup>-1</sup>. Wildtype platelets adhered to collagen fibers and formed aggregates within minutes which consistently grew into large thrombi by the end of the perfusion period. In sharp contrast, *Nbeal2*-deficient platelets exhibited reduced adhesion, and three-dimensional growth of thrombi was markedly impaired (see figure 3.19 A). As a consequence, the surface area covered by platelets and the total thrombus volume were reduced by approximately 85% and 88% respectively, at a shear rate of 1,700 s<sup>-1</sup>. Similar results were obtained at an intermediate shear rate of 1,000 s<sup>-1</sup>. These findings indicate that α-granular components are required for efficient platelet adhesion on collagen and stable aggregate formation under flow.

Activated platelets facilitate coagulation by exposing procoagulant *phosphatidylserine* (PS) on their outer surface. To determine a possible role of α-granules in this process, anticoagulated whole blood from wildtype or *Nbeal2*-deficient mice was perfused over collagen at a shear rate of 1,000 s<sup>-1</sup> and PS exposure was determined using Annexin-A5-DyLight488 staining. Remarkably, the procoagulant index, reflecting PS exposure per covered surface area, was dramatically reduced by two orders of magnitude in *Nbeal2*-deficient platelets compared to wildtype controls (see figure 3.20 A and B). This pronounced defect in the coagulant response of *Nbeal2*-deficient platelets was confirmed by flow cytometric analysis of PS exposure upon stimulation with different agonists (see figure 3.20 C). Together, these results revealed that α-granules or components thereof are critical for platelet coagulant activity under shear stress.

MFI	Resting			Thr		
	Wildtype	<i>Nbeal2</i> <sup>-/-</sup>	p	Wildtype	<i>Nbeal2</i> <sup>-/-</sup>	p
GPIIb	325 ± 9	365 ± 4	**	196 ± 8	226 ± 33	n.s.
GPV	261 ± 9	268 ± 5	n.s.	34 ± 3	29 ± 2	*
GPIX	362 ± 9	410 ± 11	***	383 ± 30	389 ± 23	n.s.
CD9	1149 ± 18	1226 ± 44	*	1787 ± 122	1636 ± 66	*
GPVI	43 ± 1	42 ± 2	n.s.	57 ± 3	47 ± 4	**
α2	47 ± 3	46 ± 1	n.s.	75 ± 8	57 ± 10	*
β1	140 ± 12	135 ± 4	n.s.	177 ± 13	158 ± 8	*
αIIbβ3	552 ± 38	632 ± 37	**	801 ± 80	652 ± 61	*
CLEC-2	112 ± 8	123 ± 8	n.s.	211 ± 21	163 ± 13	**

**Table 3.4: Glycoprotein expression after stimulation of *Nbeal2*<sup>-/-</sup> platelets with thrombin.** Expression levels of major glycoproteins of resting wildtype and *Nbeal2*-deficient platelets and after stimulation with 0.1 U/ml thrombin (Thr). Results are expressed as MFI ± SD. n=4 mice per group, representative of 4 independent experiments. \*, p < 0.05; \*\*, p < 0.01; \*\*\*, p < 0.001; n.s., not significant.

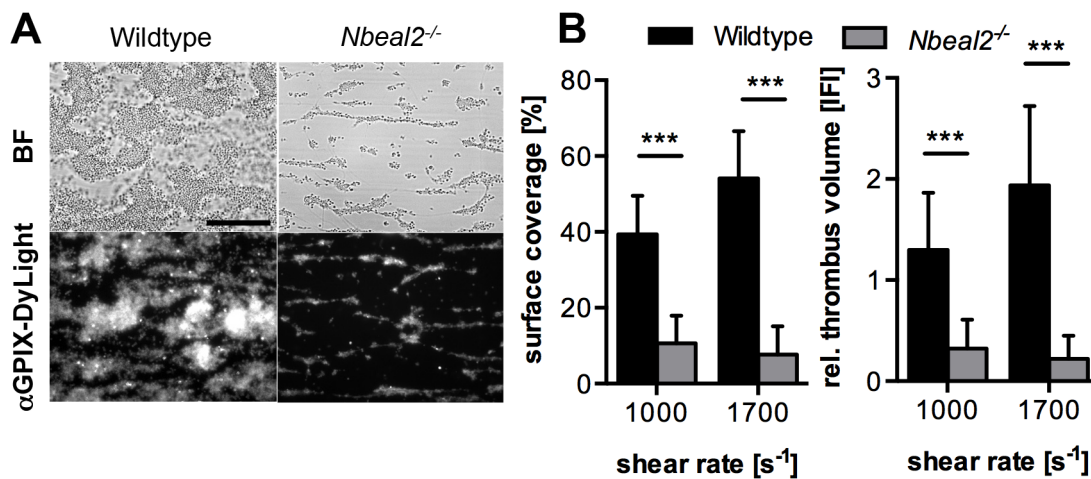


**Figure 3.19: Defective adhesion to collagen under flow of *Nbeal2*<sup>-/-</sup> platelets.** (A) Representative brightfield (BF) and fluorescence images show abrogated platelet adhesion to collagen under flow at a shear rate of 1,700 s<sup>-1</sup>. Platelets were stained using an anti-GPIX-DyLight488 antibody. Scale bar: 50 μm. (B) Surface coverage and relative thrombus volume (measured as integrated fluorescence intensity) at 1,000 s<sup>-1</sup> and 1,700 s<sup>-1</sup>. Results are presented as mean ± SD. n=5 mice per group, representative of 3 independent experiments. \*\*\*, p<0.001. Published in [34].



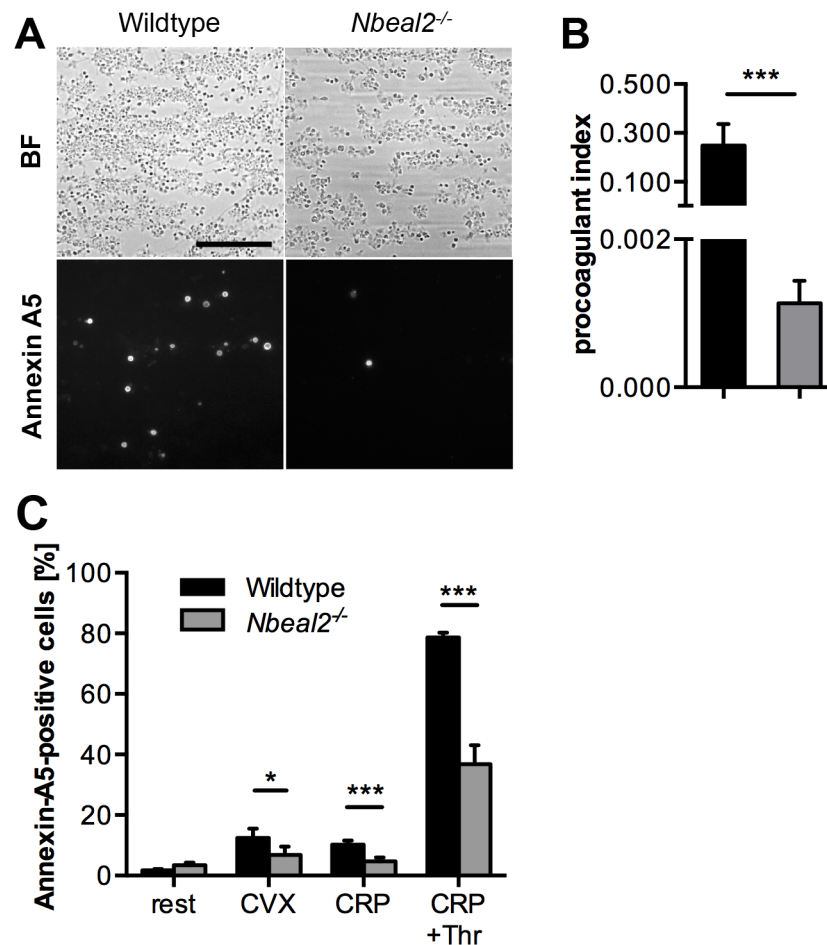


**Figure 3.20: Impaired phosphatidylserine exposure on *Nbeal2*<sup>-/-</sup> platelets under flow.** (A) Representative brightfield (BF) and fluorescence images show impaired *phosphatidylserine* (PS) exposure on platelets perfused over collagen at a shear rate of  $1,000 \text{ s}^{-1}$ . PS was measured using Annexin-A5-DyLight488. Scale bar:  $65 \mu\text{m}$ . (B) Procoagulant index was calculated as the ratio of Annexin-A5-positive cells per surface coverage. (C) Percentage of Annexin-A5-positive cells after stimulation of diluted washed platelets with the agonists indicated was measured using flow cytometry. Results are presented as mean  $\pm$  SD.  $n=5$  mice per group, representative of 3 independent experiments. \*,  $p < 0.05$ ; \*\*\*,  $p < 0.001$ . Published in [34].

### 3.2.3 Severely defective arterial thrombus formation and hemostasis in *Nbeal2*-deficient mice

As platelet aggregation contributes to pathologic occlusive thrombus formation, the effects of *Nbeal2*-deficiency on ischemia and infarction were studied by *in vivo* fluorescence microscopy following ferric chloride-induced mesenteric arteriole injury. *Nbeal2*<sup>-/-</sup> mice showed an unchanged onset of thrombus formation compared to wildtype mice, with appearance of first thrombi of more than  $10 \mu\text{m}$  in diameter approximately 9 min after injury in both groups (see figure 3.21 A and B). However, while thrombus formation rapidly progressed to full occlusion of the vessel in 15 out of 16 wildtype vessels (mean occlusion time:  $18.9 \pm 4.3 \text{ min}$ ), occlusive thrombus formation was markedly impaired in *Nbeal2*<sup>-/-</sup> mice (see figure 3.21 A and C). This defect was caused

by the formation of unstable platelet aggregates, which embolized rapidly. Blood flow was maintained throughout the observation period in 10 out of 16 vessels, indicating a requirement for the content of  $\alpha$ -granules during occlusive thrombus formation.

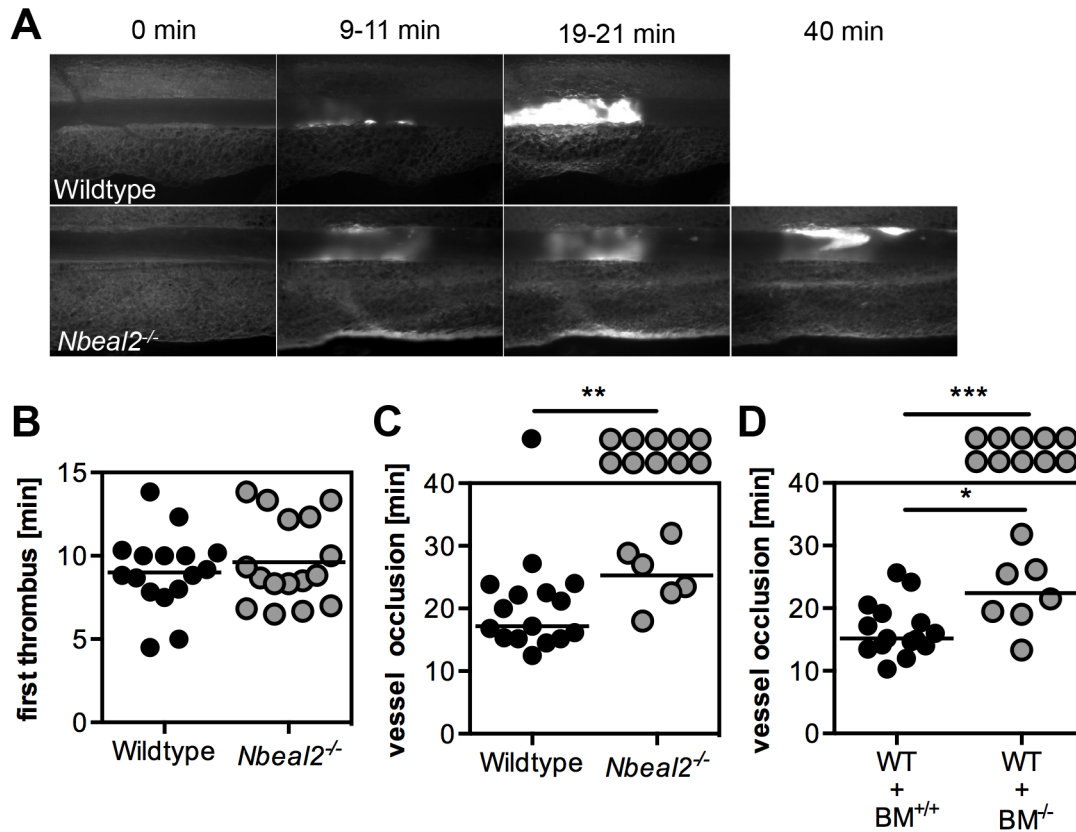


**Figure 3.21: Impaired arterial thrombus formation in *Nbeal2*<sup>-/-</sup> mice.** (A) Representative images of arterioles during injury induced by topical application of 20% FeCl<sub>3</sub>. (B) Time to appearance of first thrombus is depicted. Time to vessel occlusion was analyzed in wildtype and *Nbeal2*-deficient mice (C) as well as in irradiated wildtype mice transplanted with wildtype and *Nbeal2*-deficient bone marrow (D). Each symbol represents one arteriole. Results are presented as mean  $\pm$  SD. n=5 mice per group, representative of 3 independent experiments. \*\*, p<0.01; \*\*\*, p<0.001. Published in [34].

To confirm these findings in a second model of arterial thrombosis, the abdominal aortae of wildtype and *Nbeal2*-deficient mice were mechanically injured and blood flow was monitored with an ultrasonic flow probe. While all wildtype animals formed irreversible occlusions within 10 min (mean occlusion time:  $6.4 \pm 1.7$  minutes), occlusive thrombus formation did not occur in 7 out of 8 *Nbeal2*<sup>-/-</sup> mice during the 30 min observation period (see figure 3.22 A and B). Taken together, these results demonstrate that  $\alpha$ -granules are required for the propagation and stabilization of platelet-rich thrombi in small and large arteries and in response to different types of injury.

We next assessed the impact of *Nbeal2*-deficiency on hemostasis by determining tail bleeding times using a model where 1 mm of the tail tip is cut with a scalpel and bleeding time is assessed by absorbing blood on filter paper without making contact with the wound. While 12 out of 14 wildtype animals arrested bleeding within the observation period of 20 min (mean:  $460 \pm 178$

s), none of the *Nbeal2*-deficient mice investigated was able to arrest bleeding within that time frame (see figure 3.22 D), indicating a strong hemostatic defect.

The results from the *in vivo* thrombosis and hemostasis models were confirmed in irradiated wildtype mice reconstituted with *Nbeal2*-deficient bone marrow, demonstrating the importance of *Nbeal2* in the hematopoietic system for preventing excessive blood loss and for the formation of stable vessel occluding thrombi *in vivo* and excluding that non-hematopoietic cells (e.g. endothelial cells) might play a role (see figure 3.21 D, figure 3.22 C and data not shown).

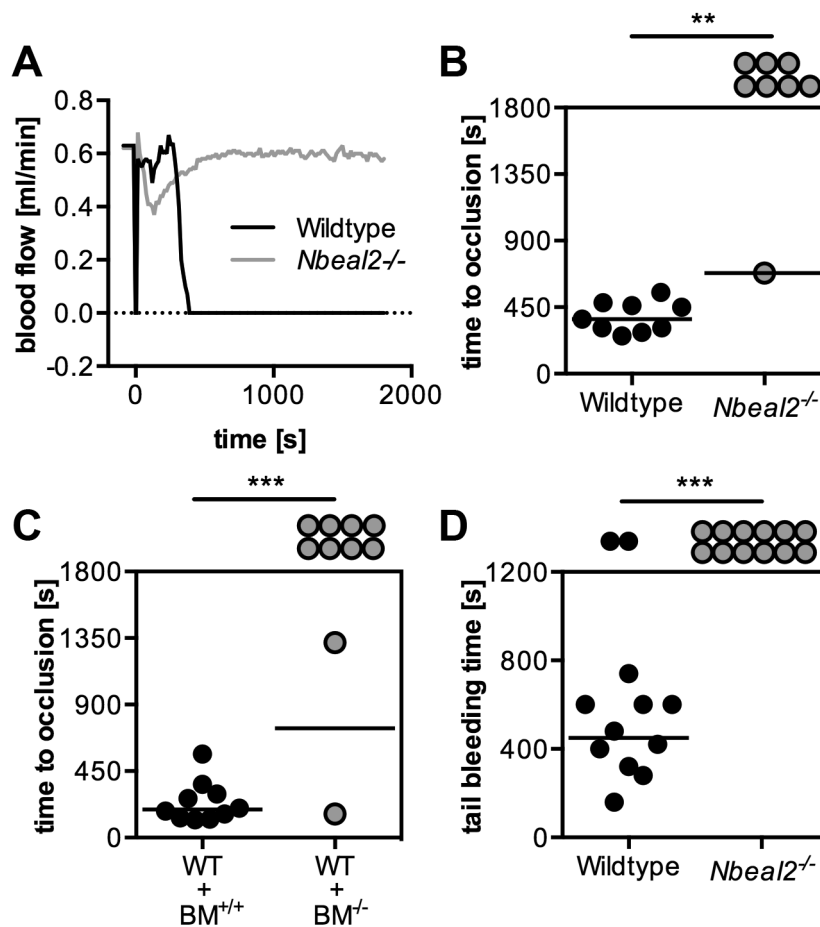


**Figure 3.22: Impaired thrombus formation and hemostasis in *Nbeal2*<sup>-/-</sup> mice.** (A) Representative blood flow curves after aorta injury. Time to vessel occlusion was analyzed in wildtype and *Nbeal2*-deficient mice (B) as well as in irradiated wildtype mice transplanted with wildtype and knockout bone marrow (C). (D) Hemostatic function was assessed using the tail bleeding model. Each symbol represents one mouse. \*\*, p < 0.01; \*\*\*, p < 0.001. Published in [34].

To further exclude the possibility that *Nbeal2*-deficiency leads to defects in endothelial cells, different tissues were stained for vWF, an important Weibel-Palade body marker in endothelial cells of different origin. Endothelial cells in wildtype and knockout samples of lung, liver and intestine showed a punctate distribution of vWF (see figure 3.23), indicating a normal synthesis and storage of proteins in *Nbeal2*-deficient endothelial cells in line with previous results for patients with GPS which showed that endothelial cells were unaffected [57].

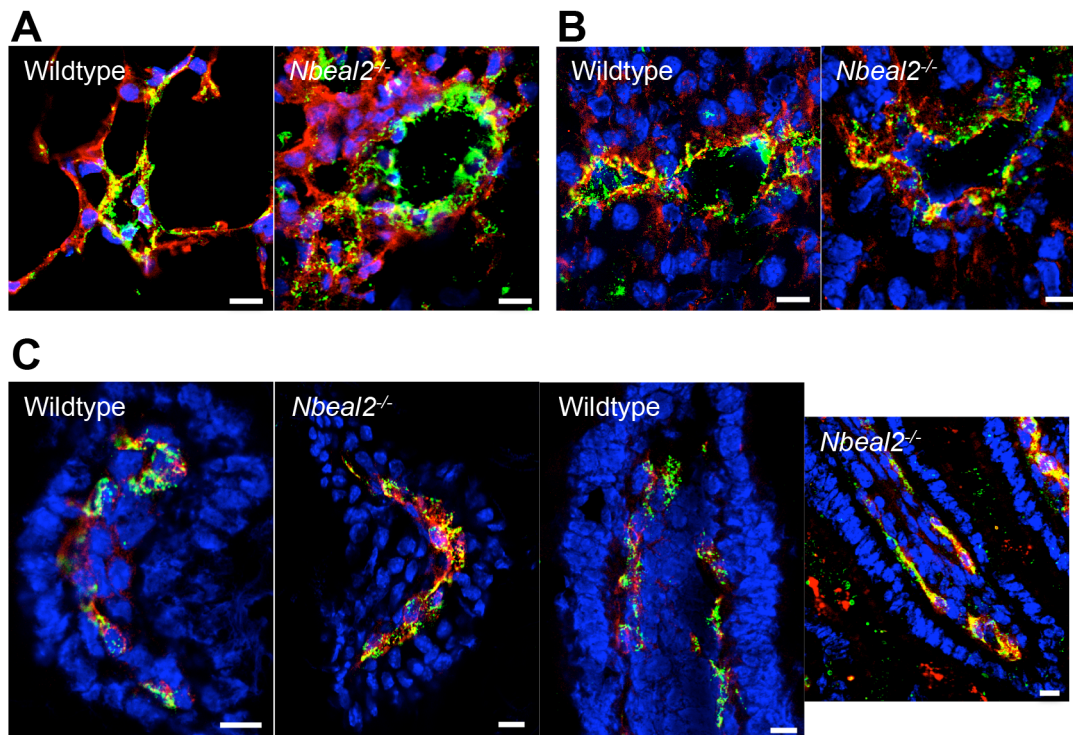


**Figure 3.23: Unaltered vWF distribution in endothelial cells of wildtype and *Nbeal2*-deficient mice.** Cryo-sections of lung (A), liver (B) and intestine (C) were stained for vWF (green). Endoglin (red) was used as an endothelial marker. Cell nuclei were stained using DAPI (blue). Scale bars: 10  $\mu$ m. Parts published in [34].

### 3.2.4 *Nbeal2*<sup>-/-</sup> mice are protected in a model of ischemic stroke

Although it is well established that pathological platelet activation contributes to the disturbance of microvascular integrity during cerebral ischemia through thrombotic and proinflammatory pathways, the underlying mechanisms have not yet been fully elucidated [130]. To determine the importance of platelet  $\alpha$ -granules in this process, we studied the development of neuronal damage following transient cerebral ischemia in *Nbeal2*<sup>-/-</sup> mice using a model that depends on platelet adhesion and activation in microvessels downstream of the MCA [172]. To initiate transient cerebral ischemia, a thread was advanced through the carotid artery into the MCA and allowed to remain for 60 min (tMCAO), reducing regional cerebral flow by >90% [101]. Infarct volumes were assessed by TTC staining 24 h after reperfusion. Infarct size was significantly reduced in *Nbeal2*<sup>-/-</sup> mice compared to wildtype mice ( $40.9 \pm 10.5$  mm<sup>3</sup> versus  $87.29 \pm 9.0$  mm<sup>3</sup>;  $p < 0.01$ ) (see figure 3.24 A and B). The difference in infarct volume was functionally relevant, as the Bederson score assessing global neurological function ( $1.5 \pm 0.2$  versus  $2.9 \pm 0.3$ , respectively;  $p < 0.01$ ) and the grip test, which measures motor function and coordination ( $4.0 \pm 0.3$  versus  $2.4 \pm 0.6$ , respectively;  $p < 0.05$ ), were significantly better in *Nbeal2*<sup>-/-</sup> mice compared to wildtype controls (see figure 3.24 C and D).

Irradiated wildtype mice reconstituted with *Nbeal2*<sup>-/-</sup> bone marrow developed small infarcts comparable to those of *Nbeal2*<sup>-/-</sup> mice, whereas wildtype mice transplanted with wildtype bone mar-

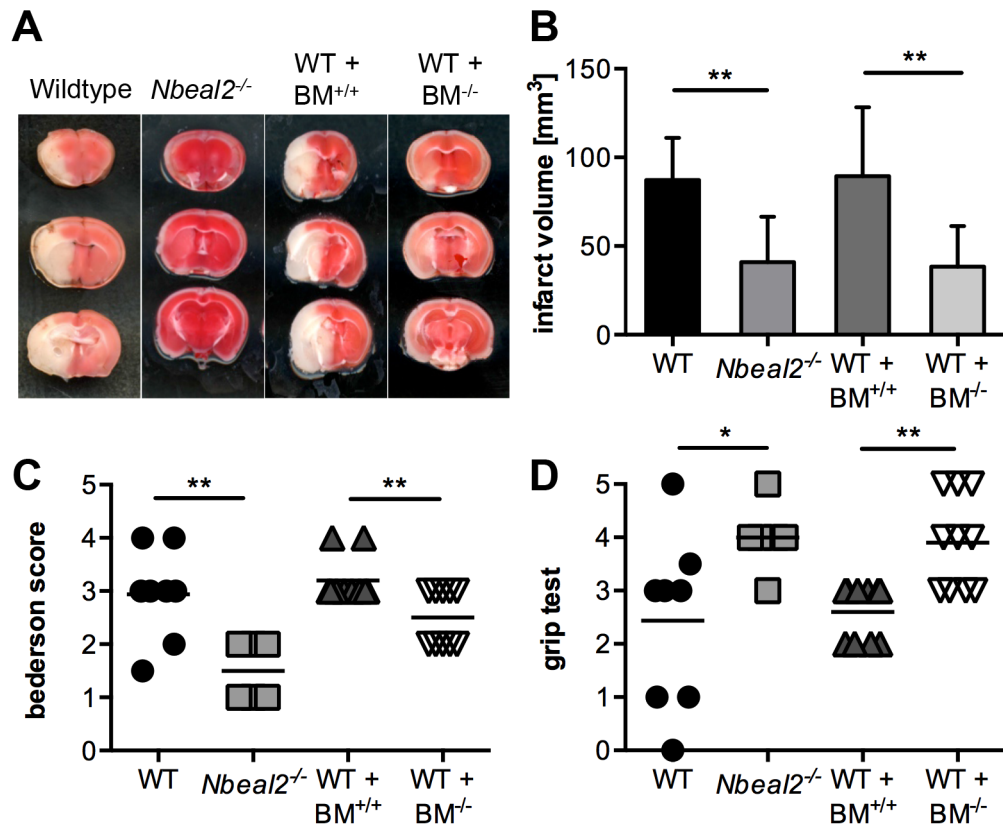


**Figure 3.24: *Nbeal2*-deficient mice are protected in a model of cerebral ischemia.** Mice were subjected to 60 min of tMCAO. (A) Representative images of coronal sections stained with TTC 24 h after tMCAO of wildtype and knockout mice as well as irradiated wildtype mice reconstituted with wildtype and knockout bone marrow. Infarcted areas are shown in white. (B) Planimetric analysis was used to quantify the infarct volume. Results are presented as mean  $\pm$  SD.  $n \geq 10$  mice per group, representative of 3 independent experiments. Bederson score (C) and grip test (D) were used to analyze neurological outcome 24 h after tMCAO. Each symbol represents one mouse. \*,  $p < 0.05$ ; \*\*,  $p < 0.01$ . Published in [34].

row developed infarcts comparable to those of control wildtype mice (see figure 3.24 B). Mice reconstituted with knockout bone marrow also performed significantly better in both the Bederson score and the grip test (see figure 3.24 C and D). Notably, there was no evidence of intracranial hemorrhage in any of the animals analyzed. These results indicated that platelet  $\alpha$ -granules are critical to drive thrombo-inflammatory neuronal damage in the acutely ischemic brain.

### 3.2.5 *Nbeal2*<sup>-/-</sup> mice show impaired dermal healing due to reduced TGF- $\beta$ release from mutant platelets

Platelets are among the first cell types infiltrating sites of injury and contribute to wound hemostasis. In addition, platelets provide essential mediators, which attract neutrophils, macrophages, endothelial cells, and fibroblasts to the wound site [41, 192]. Platelet  $\alpha$ -granules contain TGF- $\beta$ , which is one of the most abundant mediators that limits immune cell proliferation [104] and is

required for the differentiation of myofibroblasts, which produce the majority of extracellular matrix components forming the temporary granulation tissue [182] and ultimately the scar. While the importance of TGF- $\beta$  for a successful healing process is well established, the relative contribution of the platelet-derived pool of this and other growth factors or  $\alpha$ -granule component released during platelet activation is unknown.

To assess the functional significance of  $\alpha$ -granule-derived mediators for efficient tissue repair, full-thickness wounds comprising epidermis, dermis, and subcutaneous fat were inflicted on the backs of *Nbeal2*<sup>-/-</sup> mice and wildtype control animals. Seven days post injury, the amount of granulation tissue filling the wound and the presence of myofibroblasts in this tissue were assessed (see figure 3.25). Routine histological analysis (H&E) revealed that wounds in mice from both genotypes were fully reepithelialized (see figure 3.25 A). However, the area of the underlying granulation tissue was severely reduced in wounds from *Nbeal2*<sup>-/-</sup> mice compared to control animals (see figure 3.25 A and B). In particular, the collagenous tissue, visualized by picrosirius red stain (see figure 3.25 A, middle), was much less developed in mutants, while the extent of neovasculature, detected by CD31 staining, was not altered (data not shown). This suggests either reduced abundance or impaired function of myofibroblasts, the key effector cells elaborating the new dermal matrix. In fact, wounds from mutant animals contained significantly fewer myofibroblasts than controls, as shown by staining for  $\alpha$ SMA, a marker of the myofibroblast contractile microfilament apparatus, indicating impaired myofibroblast differentiation (see figure 3.25 A, bottom and C).

As the differentiation of myofibroblasts relies on TGF- $\beta$ , we speculated that *Nbeal2*-deficient platelets might not provide sufficient amounts of this mediator. Immunoblotting of control and *Nbeal2*-deficient platelet lysates confirmed dramatically diminished amounts of free, mature TGF- $\beta$  (12 kDa) as well as of its precursor pro-TGF- $\beta$  (approx. 50 kDa; see figure 3.25 D and E). These results demonstrate for the first time that biologically active proteins released from platelet  $\alpha$ -granules are crucial for myofibroblast differentiation and production of matrix proteins (e.g. collagens) reconstituting dermal integrity after injury.

#### 3.2.6 Comparison of *Nbeal2*<sup>-/-</sup> and human GPS platelets and MKs

As apparent from the data presented in the sections before, *Nbeal2*<sup>-/-</sup> mice phenocopy several major characteristics of the GPS. For direct comparison, platelets and MKs from GPS patients as well as *Nbeal2*<sup>-/-</sup> platelets were analyzed. Electron microscopy revealed that platelets from GPS patients and *Nbeal2*-deficient mice display similar morphological properties including the presence of vacuole-like structures with no electron-dense material inside, as well as an increase in platelet size, while dense granule numbers were unaltered (see figure 3.26).

As shown before,  $\alpha$ -granular protein vWF accumulates in *Nbeal2*<sup>-/-</sup> MKs indicating dysregulated protein targeting (see figure 3.15). To compare these findings to the GPS phenotype, CD34<sup>+</sup> cells from a GPS patient were isolated and cultured. vWF staining of MKs at different maturation stages showed that vWF is present in early stage MKs but is not transported into proplatelets

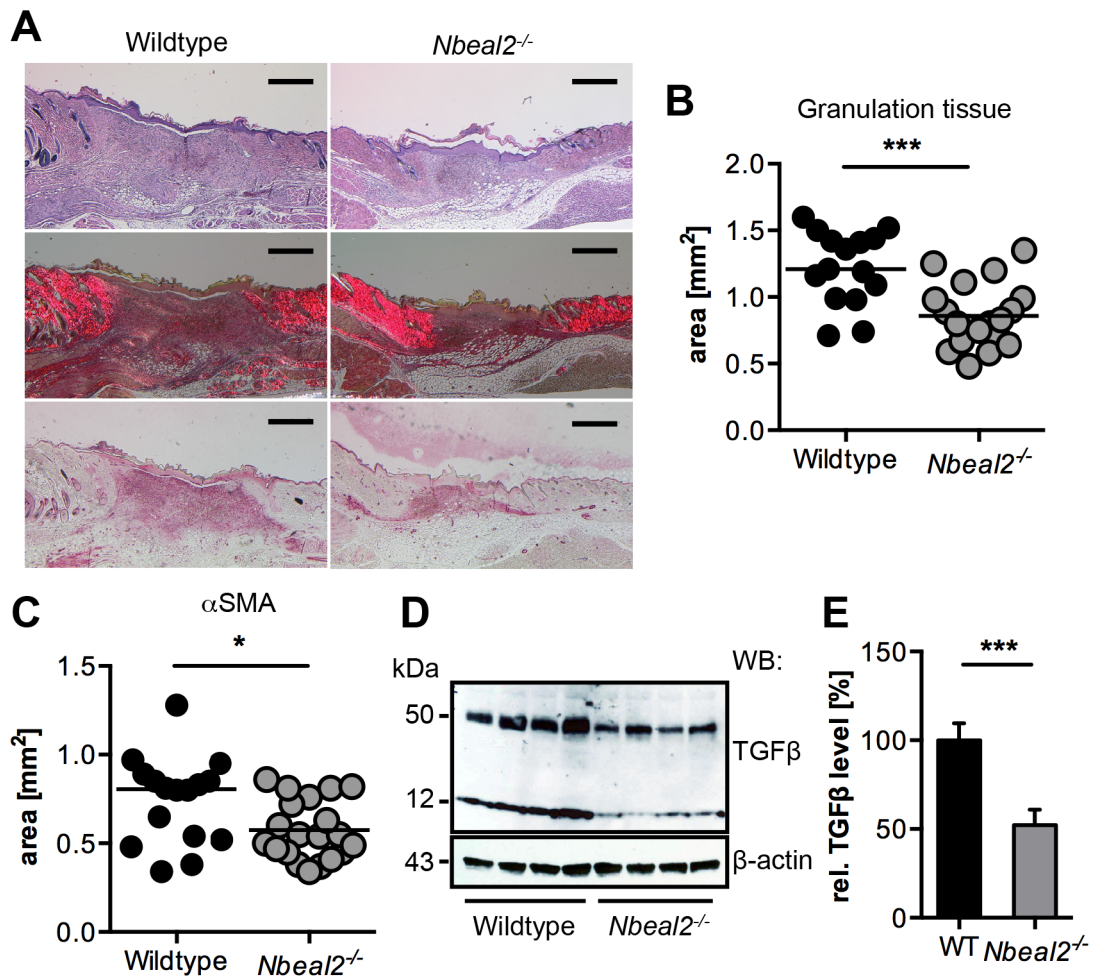


**Figure 3.25: *Nbeal2*-deficiency interferes with healing of dermal wounds.** (A) Representative images of wounds on day 7 after injury. Wounds of *Nbeal2*<sup>-/-</sup> mice show less granulation tissue but unaltered wound closure (H&E staining, top), reduced collagenous granulation tissue (dark red in picrosirius red staining, middle) and abrogated myofibroblast numbers (bottom). Scale bars: 500 μm. (B) Quantification of granulation tissue (n≥15). (C) Analysis of αSMA positive area indicative of myofibroblasts (n≥16). (D) Western blot analysis of the mature TGF-β monomer (12 kDa) and of the pro-TGF-β monomer (50 kDa) in lysates from *Nbeal2*<sup>-/-</sup> and wildtype platelets. (E) Densitometric quantification of TGF-β signals (12+50 kDa), normalized to β-actin signals (n=4). \*, p<0.05; \*\*\*, p<0.001. Published in [34].

during MK maturation (see figure 3.27).

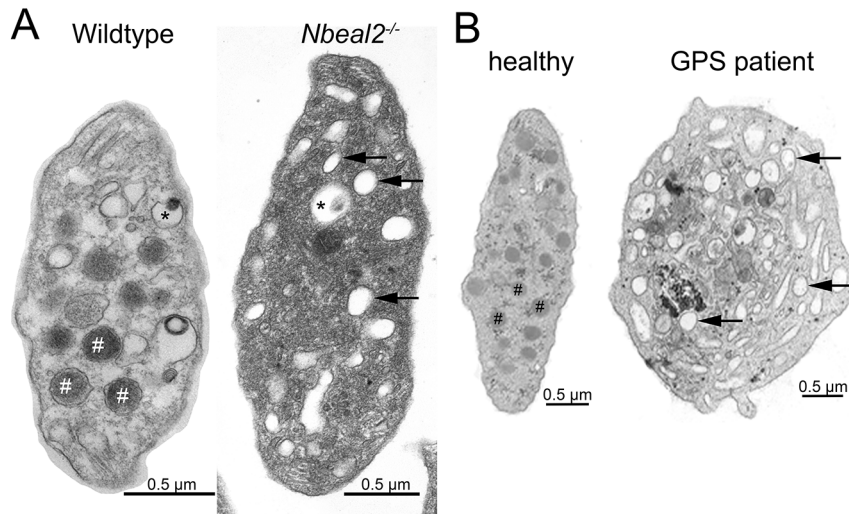


**Figure 3.26: Ultrastructure of platelets from *Nbeal2*-deficient mice and human GPS patients.** Representative TEM images of resting wildtype and *Nbeal2*<sup>-/-</sup> platelets (A) and from a healthy human subject as well as a characterized GPS patient with a homozygous L388P mutation. Platelets deficient in NBEAL2 both show lack of  $\alpha$ -granules (#) and an increased number of vacuoles (arrows) while platelet size was increased and dense granule (\*) content was unaltered. Published in [35].

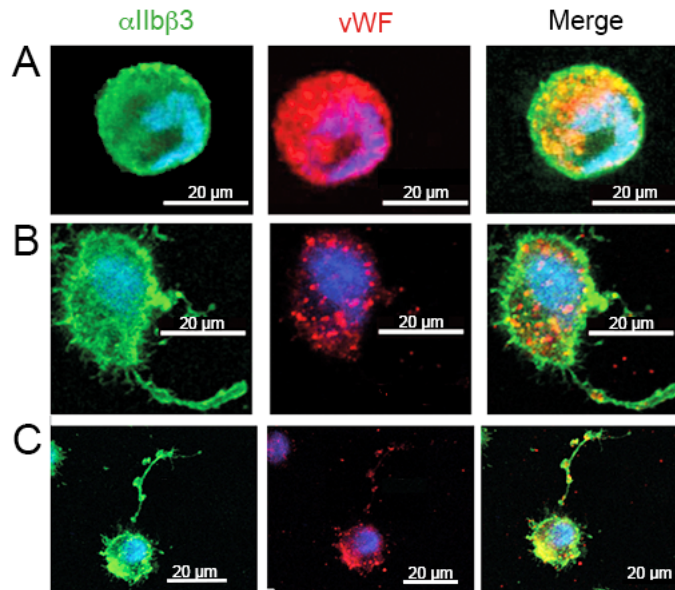


**Figure 3.27: vWF distribution in cultured MKs from a GPS patient.** Confocal microscopy of MKs cultured *in vitro* from CD34<sup>+</sup> cells from the peripheral blood of a GPS patient with a homozygous L388P mutation in *NBEAL2*. (A) A round immature MK shows abundant labeling for vWF. (B) A MK shows vWF staining along the proplatelet extension, the vWF labeling is decreased compared to control and is absent from the proplatelet tip. (C) A very mature MK with a long proplatelet string exhibits typical swellings along its length while the vWF labeling is minimal. This suggests that vWF is not maintained in the MK during maturation. Published in [35].



### 3.3 Analysis of *Munc13-4/Nbeal2*-deficient mice

#### 3.3.1 Macrothrombocytopenia but unaltered platelet glycoprotein expression in *Unc13d<sup>-/-</sup>/Nbeal2<sup>-/-</sup>* mice

To analyze the effect of combined deficiency in secretion from  $\alpha$ - and dense granules, *Unc13d<sup>-/-</sup>* and *Nbeal2<sup>-/-</sup>* mice were intercrossed to generate animals deficient in both *Munc13-4* and *Nbeal2*. *Unc13d<sup>-/-</sup>/Nbeal2<sup>-/-</sup>* mice were born in the expected Mendelian ratios, developed normally and did not show spontaneous bleeding (data not shown).

Double-deficient mice showed a platelet count of approximately 50% of control mice which was slightly below that of *Nbeal2<sup>-/-</sup>* mice (see figure 3.28) and an increase in platelet size by about 15%. This indicates that additional dense granule deficiency most likely does not cause further defects in platelet biogenesis.

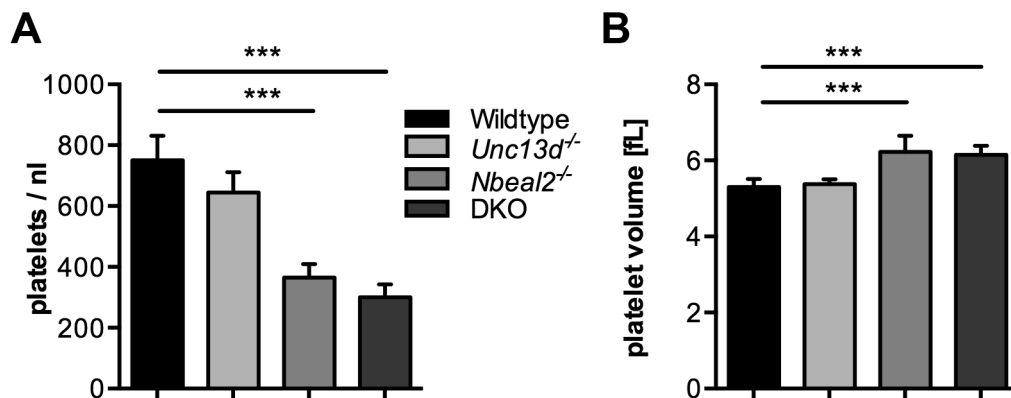


**Figure 3.28: Macrothrombocytopenia in *Unc13d<sup>-/-</sup>/Nbeal2<sup>-/-</sup>* mice.** Platelet count (A) and platelet volume (B) of wildtype, *Unc13d<sup>-/-</sup>*, *Nbeal2<sup>-/-</sup>* and *Unc13d<sup>-/-</sup>/Nbeal2<sup>-/-</sup>* (DKO) mice were analyzed using a Sysmex hematology analyzer. Values are mean  $\pm$  SD. n=4 mice per group; representative of 3 independent experiments. \*\*\*,  $p < 0.001$ .

*Unc13d<sup>-/-</sup>/Nbeal2<sup>-/-</sup>* mice displayed unaltered basic blood parameters like RBC and WBC count, HGB concentration, HCT and surface expression of important platelet glycoproteins like GPIb, GPVI or CLEC-2, while there were slight alterations in integrin  $\alpha 2$  and  $\alpha \text{IIb}\beta 3$  levels (see table 3.5). ATP release measurements from double-deficient platelets using lumi-aggregometry confirmed complete absence of dense granule secretion (see figure 3.29).

#### 3.3.2 Abrogated P-selectin exposure and reduced integrin activation upon stimulation of *Munc13-4/Nbeal2*-deficient platelets

To assess the impact of defective  $\alpha$ - and dense granule secretion on platelet reactivity, platelets from *Unc13d<sup>-/-</sup>*, *Nbeal2<sup>-/-</sup>*, double-deficient and wildtype mice were stimulated with different agonists and P-selectin surface expression as well as integrin  $\alpha \text{IIb}\beta 3$  activation were measured using a flow cytometer. Double-deficient platelets showed an additional reduction in P-selectin exposure at the platelet surface compared to *Nbeal2*-deficient platelets upon stimulation with

	Wildtype	<i>Unc13d</i> <sup>-/-</sup> / <i>Nbeal2</i> <sup>-/-</sup>	Significance
WBC [ $\times 10^3/\mu\text{l}$ ]	6.4 $\pm$ 1.67	8.4 $\pm$ 0.9	n.s.
RBC [ $\times 10^6/\mu\text{l}$ ]	6.44 $\pm$ 1.45	5.68 $\pm$ 0.78	n.s.
HGB [g/dl]	9.6 $\pm$ 1.67	8.4 $\pm$ 0.89	n.s.
HCT [%]	33.6 $\pm$ 7.13	29.6 $\pm$ 3.29	n.s.
GPIb [MFI]	393 $\pm$ 4	395 $\pm$ 50	n.s.
GPV [MFI]	255 $\pm$ 18	241 $\pm$ 34	n.s.
GPIX [MFI]	447 $\pm$ 18	447 $\pm$ 31	n.s.
CD9 [MFI]	991 $\pm$ 30	990 $\pm$ 48	n.s.
GPVI [MFI]	51 $\pm$ 4	48 $\pm$ 5	n.s.
$\alpha 2$ [MFI]	63 $\pm$ 5	79 $\pm$ 4	**
$\beta 1$ [MFI]	179 $\pm$ 5	174 $\pm$ 13	n.s.
$\alpha \text{IIb}\beta 3$ [MFI]	511 $\pm$ 30	441 $\pm$ 11	*
CLEC-2 [MFI]	162 $\pm$ 8	169 $\pm$ 14	n.s.

**Table 3.5: Basic blood parameters of *Unc13d*<sup>-/-</sup>/*Nbeal2*<sup>-/-</sup> mice.** Basic blood parameters were assessed in diluted whole blood using a Sysmex hematology analyzer. To quantify surface expression of major platelet glycoproteins, diluted whole blood was analyzed by flow cytometry. Results are expressed as mean  $\pm$  SD. n=4 mice per group, representative of 3 independent experiments. \*, p < 0.05; \*\*, p < 0.01; n.s., not significant.

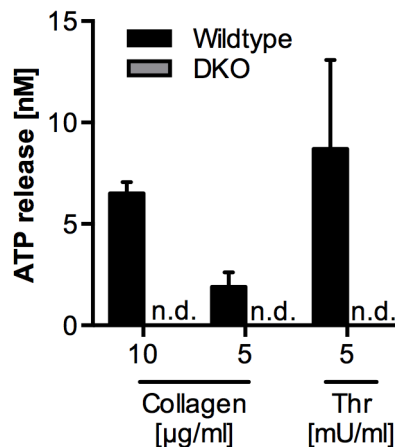


**Figure 3.29: Abrogated ATP secretion from *Unc13d*<sup>-/-</sup>/*Nbeal2*<sup>-/-</sup> platelets upon stimulation.** ATP release from wildtype and *Unc13d*<sup>-/-</sup>/*Nbeal2*<sup>-/-</sup> (DKO) platelets after collagen or thrombin (Thr) stimulation was assessed using a luciferase assay. Values are mean  $\pm$  SD. n=4 mice per group; representative of 3 independent experiments. n.d., not detectable

all thrombin and CRP concentrations tested (see figure 3.30 A). It is noteworthy that despite the combined secretion deficiency of both granule types still 25-30% of wildtype P-selectin levels could be recruited to the surface upon stimulation. Integrin activation of double-deficient platelets displayed an additional reduction compared to *Unc13d*<sup>-/-</sup> platelets after stimulation with all thrombin and CRP concentrations tested (see figure 3.30 B).

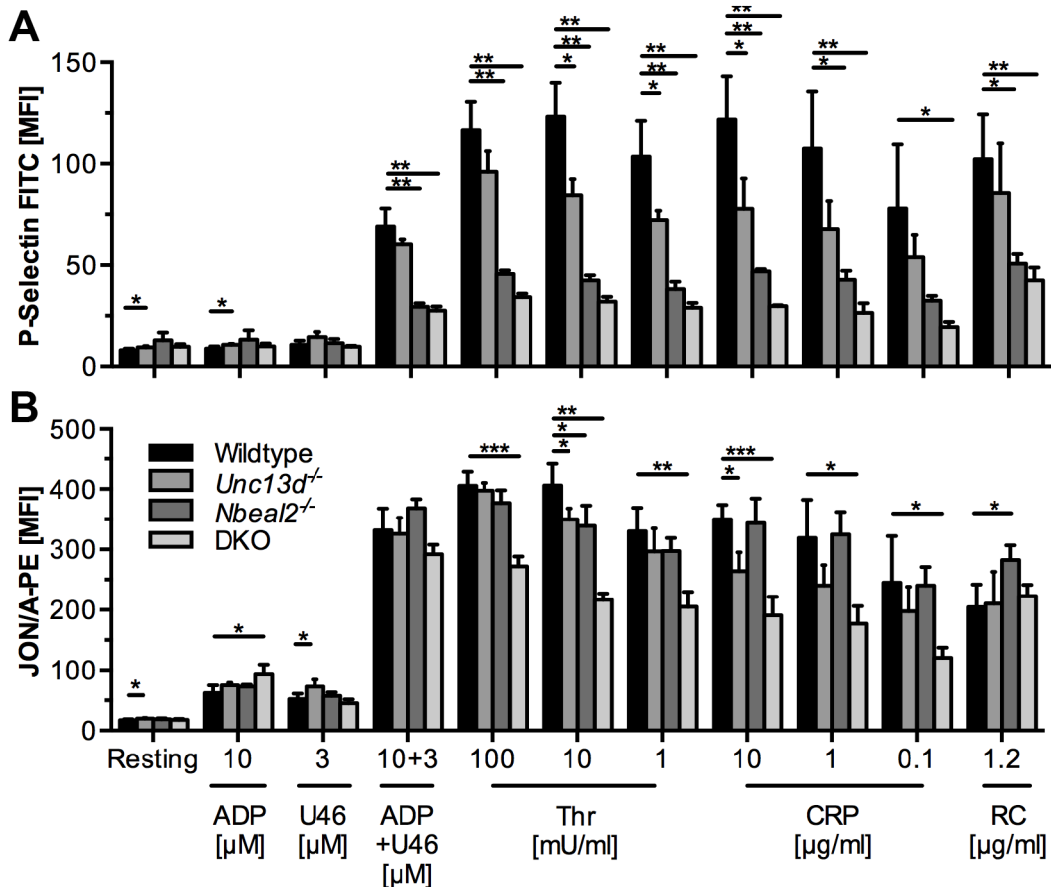


**Figure 3.30: Impaired activation of *Munc13-4/Nbeal2*-deficient platelets in suspension.** Flow-cytometric analysis revealed reduced surface expression of P-selectin (A) and integrin  $\alpha$ IIb $\beta$ 3 activation (JON/A binding, B) in *Unc13d<sup>-/-</sup>/Nbeal2<sup>-/-</sup>* (DKO) platelets after stimulation with the agonists indicated. Results are presented as MFI  $\pm$  SD.  $n=4$  mice per group, representative of 3 independent experiments. U46, U46619; Thr, thrombin; CRP, collagen-related peptide; RC, rhodocytin. \*,  $p<0.05$ ; \*\*,  $p<0.01$ ; \*\*\*,  $p<0.001$ .

### 3.3.3 *Unc13d<sup>-/-</sup>/Nbeal2<sup>-/-</sup>* platelets show defective aggregation, adhesion to collagen under flow and PS exposure

In line with the markedly reduced activation responses in the flow cytometry assay, double-deficient platelets were unable to form stable aggregates in suspension (see figure 3.31) or under flow (see figure 3.32). The defect in platelet aggregation was more severe than that observed for *Unc13d<sup>-/-</sup>* or *Nbeal2<sup>-/-</sup>* platelets and was most pronounced upon stimulation with CRP, collagen and low-dose thrombin (see figure 3.31). Stimulation with high-dose thrombin led to aggregation responses that were comparable to those of single-deficient platelets, indicating that strong stimulation might partially overcome the defect observed.

To investigate the effect of a combined deficiency of both  $\alpha$ - and dense granule secretion on platelet adhesion to ECM components under flow, diluted whole blood from double-deficient and wildtype animals was perfused over collagen-coated glass slides at a shear rate of  $1,000\text{s}^{-1}$ . Wildtype platelets rapidly adhered and formed three-dimensional thrombi resulting in a surface

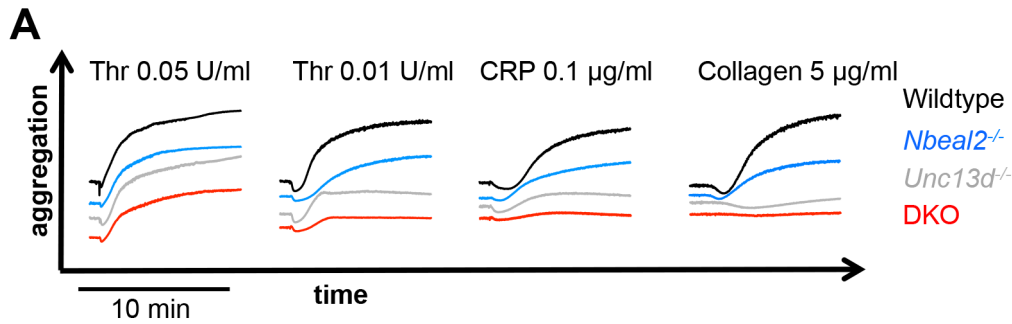


**Figure 3.31: Impaired aggregation of Munc13-4/Nbeal2-deficient platelets.** (A) Representative aggregation traces (recording time 10 min) of wildtype, *Unc13d<sup>-/-</sup>*, *Nbeal2<sup>-/-</sup>* and *Unc13d<sup>-/-</sup>/Nbeal2<sup>-/-</sup>* (DKO) platelets upon stimulation with the indicated agonists. Note almost abrogated aggregation of DKO platelets upon stimulation with CRP or collagen. Thr, thrombin; CRP, collagen-related peptide.

coverage of about 40%. In contrast, Munc13-4/Nbeal2-deficient platelets were virtually unable to adhere, resulting in a strongly reduced surface coverage and thrombus volume (see figure 3.32).

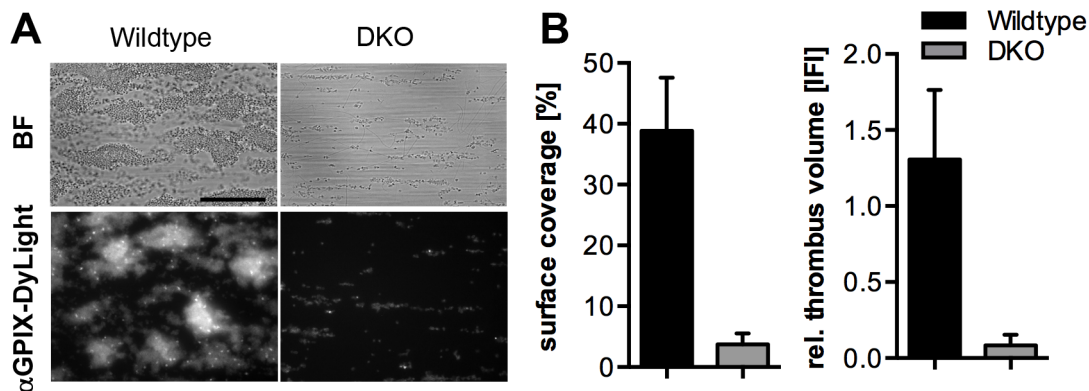


**Figure 3.32: Impaired adhesion of Munc13-4/Nbeal2-deficient platelets to collagen under flow.** (A) Representative brightfield (BF, top) and fluorescence (bottom) images show virtually abrogated adhesion of *Unc13d<sup>-/-</sup>/Nbeal2<sup>-/-</sup>* (DKO) platelets to collagen under flow at a shear rate of  $1,000 \text{ s}^{-1}$ . Platelets were stained using an anti-GPIX-DyLight488 antibody. Scale bar:  $50 \mu\text{m}$ . (B) Surface coverage and relative thrombus volume (integrated fluorescence intensity, IFI) at a shear rate of  $1,000 \text{ s}^{-1}$  were quantified. Results are presented as mean  $\pm$  SD.  $n=5$  mice per group, representative of 3 independent experiments. \*\*\*,  $p<0.001$ .

Munc13-4/Nbeal2-deficient platelets exhibited markedly decreased PS exposure upon stimulation with a combination of CRP and thrombin or convulxin as assessed by flow cytometric analysis of Annexin-A5-positive cells. Total PS content, which was quantified by incubation with the ionophore A23187, was largely preserved in double-deficient compared to wildtype platelets (see figure 3.33).

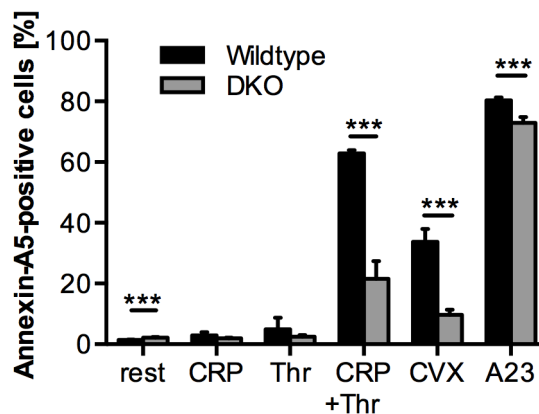


**Figure 3.33: Defective phosphatidylserine exposure on *Unc13d*<sup>-/-</sup>/*Nbeal2*<sup>-/-</sup> platelets.** Percentage of Annexin-A5-positive cells after stimulation of diluted washed wildtype and *Unc13d*<sup>-/-</sup>/*Nbeal2*<sup>-/-</sup> (DKO) platelets with the agonists indicated was measured using flow cytometry. Results are presented as mean  $\pm$  SD. n=5 mice per group, representative of 3 independent experiments. CRP, collagen-related peptide; Thr, thrombin; CVX, convulxin; A23, A23187. \*\*\*, p<0.001.

### 3.3.4 *Munc13-4/Nbeal2*-deficient mice display impaired thrombosis and hemostasis *in vivo*

To investigate the effect of combined deficiency of platelet  $\alpha$ - and dense granule secretion on thrombus formation *in vivo*, double-deficient and wildtype mice were subjected to an aorta injury model. In this model, mechanical injury using forceps causes denudation of the underlying ECM and thereby triggers platelet adhesion and aggregation. While in wildtype animals full vessel occlusion occurred approximately 300 s after injury, only very small or no thrombi formed at the site of injury in double-deficient mice. None of the 9 animals investigated were able to fully occlude the vessel during the observation period (see figure 3.34 A). When subjected to an *in vivo* tail bleeding time model, *Munc13-4/Nbeal2*-deficient mice were unable to arrest bleeding, while wildtype animals stopped bleeding after approximately 400 s (see figure 3.34 B). Taken together, this confirms that platelet  $\alpha$ - and dense granule secretion are crucial for both *in vivo* thrombosis and hemostasis.

### 3.3.5 *Unc13d*<sup>-/-</sup>/*Nbeal2*<sup>-/-</sup> mice maintain vascular integrity at sites of local inflammation but not ischemic stroke

Recently, it was reported that platelets are required to maintain vascular integrity during local inflammation of the skin, lung and in the brain in the course of ischemic stroke [59]. Signaling through platelet (hem)ITAM receptors has been identified as a key step in the initiation of this process, but the downstream effects remained unknown [18]. To investigate whether platelet granule secretion is involved, animals deficient for both  $\alpha$ - and dense granule secretion were subjected to models of skin and lung inflammation as well as ischemic stroke and the occurrence of hemorrhage was assessed.

The *reverse passive Arthus reaction* (rpA) triggers local inflammation by intradermal injection

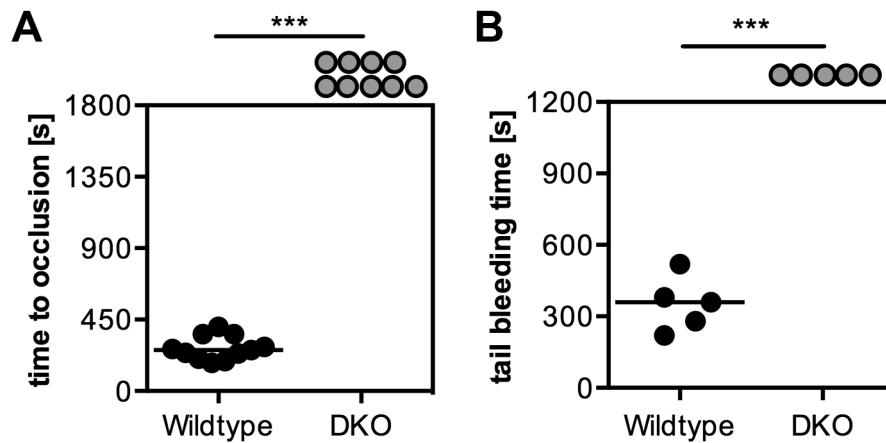


**Figure 3.34: Abrogated *in vivo* thrombus formation and hemostasis in *Unc13d*<sup>-/-</sup>/*Nbeal2*<sup>-/-</sup> mice.** (A) Time to vessel occlusion in an aorta injury model was analyzed in wildtype and *Unc13d*<sup>-/-</sup>/*Nbeal2*<sup>-/-</sup> (DKO) mice. (B) Tail bleeding times were assessed in wildtype and DKO mice using the filter paper model. Each symbol represents one mouse. \*\*\*, p<0.001.

of an antibody (e.g. anti-BSA) followed by intravenous injection of the respective antigen (e.g. BSA). In agreement with previous studies [59], wildtype mice showed only edema formation at the site of antibody injection, while platelet-depleted mice displayed massive intradermal hemorrhage (see figure 3.35 A). Double-deficient mice exhibited no or minimal intradermal bleeding in this assay, which originated from needle injury. Quantification of the hemoglobin content in tissue punch biopsies revealed a strong increase in samples from platelet-depleted but not wildtype control or *Unc13d*<sup>-/-</sup>/*Nbeal2*<sup>-/-</sup> mice (see figure 3.35 B).

Intranasal application of LPS leads to severe lung inflammation in mice, which causes massive pulmonary hemorrhage in the absence of platelets [59]. Following LPS-induced lung inflammation, the *bronchoalveolar lavage* (BAL) of thrombocytopenic mice showed a high content of RBCs while there were much less RBCs in the BAL of wildtype and *Unc13d*<sup>-/-</sup>/*Nbeal2*<sup>-/-</sup> mice (see figure 3.35 C). Quantification of the hemoglobin content revealed an eightfold increase in the BAL from platelet-depleted compared to wildtype mice, while double-deficient mice showed only a slight elevation (see figure 3.35 D). Taken together, these results indicate that  $\alpha$ - and dense granule contents are most likely dispensable for maintaining vascular integrity during local inflammation.

To investigate whether the observations made regarding the vascular integrity during inflammation of the skin and lung also hold true during ischemic stroke, mice deficient for both *Munc13-4* and *Nbeal2* were subjected to the tMCAO model of cerebral ischemia. Infarct volumes, as assessed by TTC staining 24 h after reperfusion, were significantly reduced by approximately 50% in *Unc13d*<sup>-/-</sup>/*Nbeal2*<sup>-/-</sup> compared to wildtype mice (see figure 3.36 A and B). The decrease in infarct volume was functionally relevant, as both the Bederson score which assesses global neurological function and the grip test that measures motor function and coordination were significantly improved in double-deficient compared to wildtype control animals (see figure 3.36 C

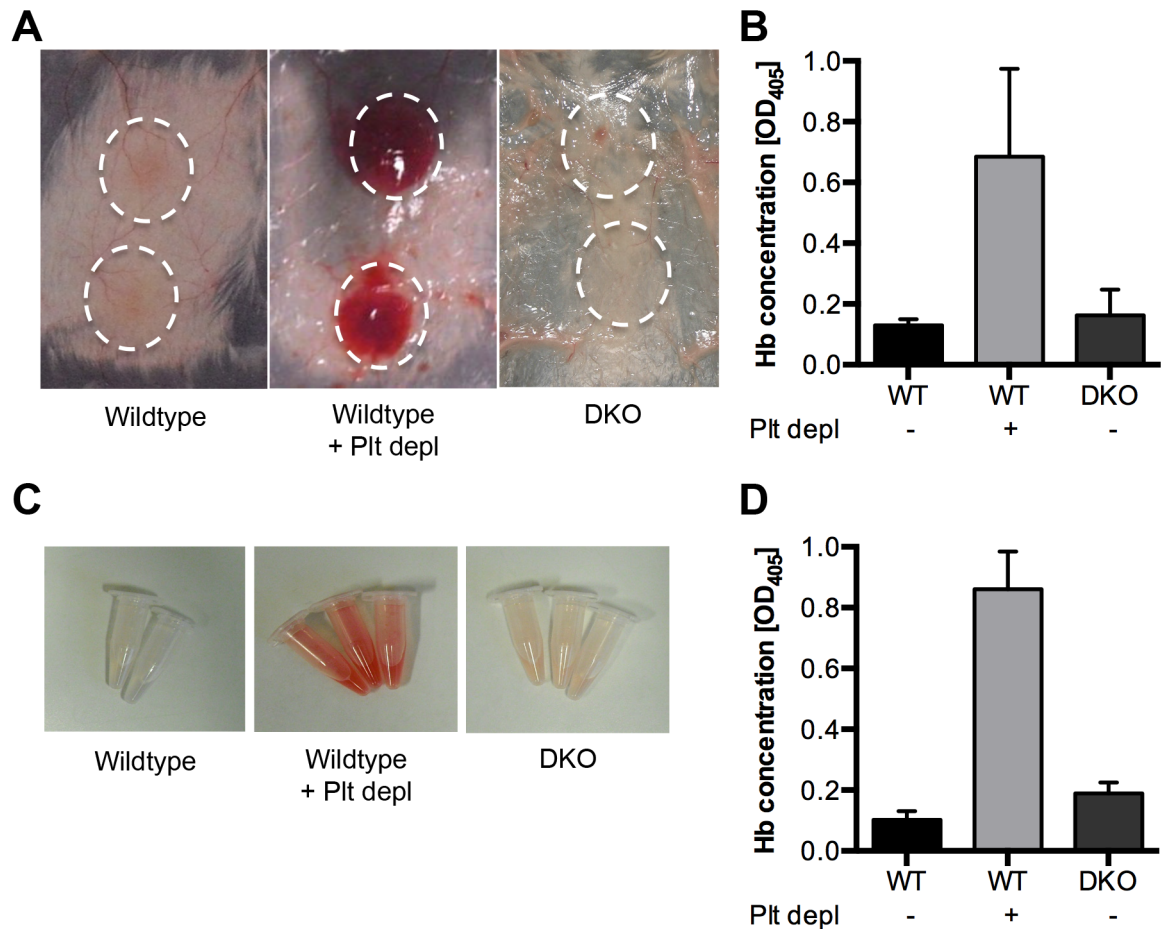


**Figure 3.35: *Munc13-4/Nbeal2*-deficient platelets maintain vascular integrity during local inflammation of the skin and lung.** Wildtype (WT), platelet-depleted WT and *Unc13d*<sup>-/-</sup>/*Nbeal2*<sup>-/-</sup> (DKO) mice were subjected to the rpA reaction to induce local skin inflammation (A+B) or to a model of LPS-induced lung inflammation (C+D). (A) Representative images. Inflammatory spots are highlighted. (B) Quantification of the hemoglobin content in tissue punch biopsies. (C) Representative images of BAL 4 h after LPS application. (D) Quantification of the hemoglobin content in BAL liquid 4 h after LPS application. Results are presented as mean  $\pm$  SD. n=4 mice per group, representative of 3 independent experiments.

and D). Importantly, however, double-deficient mice showed an increased mortality rate within 24 h after tMCAO of 40% versus 0% in wildtype animals. Further investigation revealed that the mice died from intracranial hemorrhage and that surviving mice showed microbleedings, intraparenchymal and subarachnoid hemorrhage in the infarcted area (see figure 3.36 B and E). This indicates that vascular integrity during local inflammation of the skin or lung and thromboinflammation in the brain is maintained by two different processes and that the latter requires platelet granule secretion. Of note, no intracranial hemorrhage was observed in the brains from *Unc13d*<sup>-/-</sup> or *Nbeal2*<sup>-/-</sup> single-deficient mice after tMCAO indicating that intact release from either  $\alpha$ - or dense granules is sufficient to maintain vascular integrity during ischemic stroke while combined deficiency causes loss of vascular integrity during thromboinflammation.

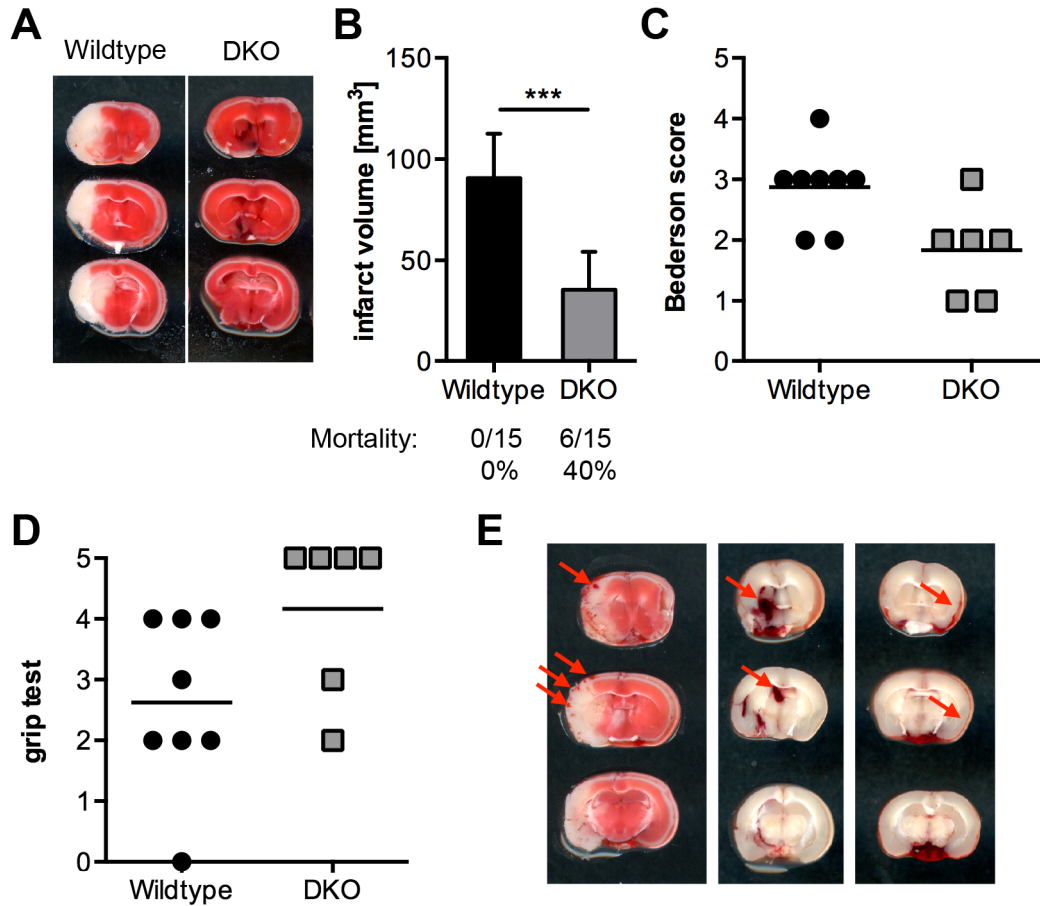


**Figure 3.36: Increased rate of hemorrhage and mortality after ischemic stroke in *Unc13d*<sup>-/-</sup>/*Nbeal2*<sup>-/-</sup> mice** (A) Representative images of coronal sections stained with TTC 24 h after tMCAO of wildtype and knockout mice. Infarcted areas are shown in white. (B) Planimetric analysis was used to quantify the infarct volume. Mortality rates 24 h after tMCAO are indicated. Results are presented as mean ± SD. n=15 mice per group, representative of 3 independent experiments. Bederson score (C) and grip test (D) were used to analyze neurological outcome 24 h after tMCAO. Each symbol represents one mouse. (E) Representative images show microbleedings in TTC-stained brain sections (left) or intraparenchymal (middle) and subarachnoid (right) bleedings (arrows) in native brain sections of double-deficient mice after stroke. \*\*\*, p<0.001.



## 4 Discussion

In this thesis, the role of platelet  $\alpha$ - and dense granule secretion was investigated using mice deficient in Munc13-4, Nbeal2, or both. The results presented reveal important functions for platelet granule content in thrombosis, hemostasis, stroke and the maintenance of vascular integrity during inflammation. Furthermore, it could be shown that knockout of *Nbeal2* reproduces the GPS phenotype, thereby establishing the *Nbeal2*<sup>-/-</sup> mouse as a model for this disease and as a tool to study the role of platelet  $\alpha$ -granules in physiology and pathology.

### 4.1 Platelet dense granules in thrombosis, hemostasis and stroke

The results obtained with *Unc13d*<sup>-/-</sup> mice confirm the essential role of Munc13-4 in dense granule secretion and its contribution to  $\alpha$ -granule secretion (see figure 3.2 and 3.3), confirming results of a previous study which used *Unc13d*<sup>Jinx/Jinx</sup> mice [151]. In this study, *Unc13d*<sup>-/-</sup> mice were used to investigate the relevance of dense granule secretion for arterial thrombosis and ischemic stroke. As expected from studies with ADP receptor blockers [54] or mice lacking the corresponding receptors P2Y<sub>1</sub> [107] or P2Y<sub>12</sub> [6] ablated dense granule secretion resulted in abolished thrombus formation *in vitro* and *in vivo* and in severely compromised hemostasis (see figure 3.5). However, so far it has not been clear whether ADP secreted from platelets is essential for thrombus formation, since vessel injury also results in ADP release from endothelial cells or erythrocytes. The results obtained with *Unc13d*<sup>-/-</sup> mice argue for platelets as the major source of ADP during arterial thrombosis.

Further, despite the widespread use of ADP receptor antagonists for the prevention of recurrent stroke [1, 72, 89], the multifaceted role of platelets in acute stroke development is unclear, especially the mechanisms by which antiplatelet agents prevent thrombus growth within the brain microvasculature [172]. One early study using clopidogrel in a photo-induced model of ischemic stroke indicated a beneficial role of ADP blockade for the prevention of arterial thrombosis and ischemic stroke [183]. However, there is only limited data available on the efficacy of ADP receptor antagonist during ischemia-reperfusion injury. The results obtained in this study using the *Unc13d*<sup>-/-</sup> mice argue for a central role of dense granule secretion for the progression of ischemic stroke during the reperfusion phase (see figure 3.6). Importantly, abolished thrombus formation and reduced infarct progression was not associated with increased incidence of intracerebral hemorrhages (see figure 3.7) despite severely prolonged tail bleeding times (see figure 3.5 E). This is in line with studies using vWF-deficient mice [100] or GPIIb-blocking antibodies [101] which in both cases resulted in reduced infarct sizes but no intracranial bleedings despite infinite bleeding times in the tail clip assay.

Interestingly, interference with initial platelet adhesion [30, 53, 100, 101, 202], important activation pathways like GPVI [101] or platelet activation amplificatory mediators (e.g. granule release) like in the present study (see figure 3.6) all prevent the progression of ischemic stroke without increasing the incidence of intracranial bleedings (see figure 3.7). In sharp contrast, blocking GPIIb/IIIa and thereby prevention of the final step of platelet aggregation does not protect from ischemic stroke due to increased intracranial hemorrhages (see figure 3.7).

Given the fact that dense granule secretion is completely abolished in *Munc13-4*-deficient mice (see figure 3.2 A and [151]) it is worth noting that also other components of dense granules, namely polyphosphates [125, 168, 167], serotonin [28, 37] and  $\text{Ca}^{2+}$  [19, 185] play roles in thrombosis and inflammation and that these two processes are of major importance for the pathogenesis of ischemic stroke [130]. Interestingly, it could be shown that ADP supplementation can partially restore the thrombotic defects observed in *Unc13d*<sup>-/-</sup> mice *in vitro* and *in vivo* [159]. However, there might still be other factors involved. Thus, further studies are required to identify the components of dense granules which are responsible for infarct progression during ischemic stroke.

### 4.2 Platelet $\alpha$ -granules in thrombosis, hemostasis and stroke

Although the first description of a patient with GPS was reported in 1971 [149], it took until 2011 for *NBEAL2* to be identified as the mutated gene causing the disease, a finding which thereby provided the molecular basis for detailed studies on the function and (patho-)physiological significance of  $\alpha$ -granules, the most abundant organelles in platelets [5, 68, 91]. This study now provides compelling complementary evidence that *NBEAL2* is essential for platelet  $\alpha$ -granule biogenesis and establishes the *Nbeal2*<sup>-/-</sup> mouse as a valuable animal model of GPS that recapitulates many of the symptoms found in patients with GPS. The mice show a moderate thrombocytopenia and a relatively modest increase in platelet size in line with the human phenotype. While earlier studies reported that GPS is a progressive disorder, with platelet counts decreasing with age, no such correlation was seen over the short study period in the mouse model. Platelet aggregation upon stimulation with PAR-4 peptide, collagen, and CRP was reduced with *Nbeal2*-deficient platelets, which is in accordance with data from patients with GPS that show diversity with respect both to genotype and phenotype [17]. *Nbeal2*<sup>-/-</sup> mice as a model for GPS allow for the first time to study the *in vivo* role of  $\alpha$ -granule proteins in both normal hemostasis and thrombo-inflammatory disease states.

In addition, *Nbeal2*<sup>-/-</sup> mice will serve as a valuable model to study  $\alpha$ -granule biogenesis, which is still poorly understood. MK-synthesized  $\alpha$ -granule proteins share a three-dimensional granule-targeting motif that is required to properly target them to  $\alpha$ -granules [39]. The studies presented here show the accumulation of  $\alpha$ -granule proteins at distinct sites inside the MKs, indicating aberrant protein sorting rather than defective protein synthesis, which is in line with observations in GPS patients [139]. It should be emphasized that the *Nbeal2*<sup>-/-</sup> mice, like human GPS patients, show deficiency of all platelet  $\alpha$ -granule proteins independent of whether the proteins

are sequestered by endocytosis (e.g., fibrinogen) or, as for the most part, synthesized by MKs. The deficiency was also independent of the proposed distinct packaging of certain proteins within different granule subpopulations or within the  $\alpha$ -granule itself [86, 94]. Further studies will be required to determine how NBEAL2, which encodes a BEACH/ARM/WD40 domain protein, regulates  $\alpha$ -granule biogenesis.

Interestingly, the studies on FLC-derived MKs revealed no marked abnormality in proplatelet formation, suggesting that the reduced platelet numbers in the mutant mice are caused by a defect in the terminal steps of platelet production. This is in line with the unaltered platelet lifespan observed in *Nbeal2*<sup>-/-</sup> mice. Although platelets from GPS patients allowed studies on the role of  $\alpha$ -granules in platelet function tests *in vitro*, the sometimes severe thrombocytopenia in the human subjects often makes the assessment difficult [69, 139]. As a consequence, the contribution of secreted adhesive proteins to platelet-mediated processes *in vivo* has remained poorly understood since early reports pointing to roles of fibrinogen and thrombospondin in secretion-dependent platelet aggregation [166, 78]. These studies unambiguously show a role of secreted proteins both in platelet aggregation *in vitro* and in thrombus formation under flow. There is also considerable clinical heterogeneity in human GPS with mild to moderate bleeding tendencies as well as severe life-threatening hemorrhages in rare cases [69, 62, 139]. We found severely prolonged tail bleeding times in *Nbeal2*<sup>-/-</sup> mice but no signs of spontaneous hemorrhage. This confirms that there is no direct correlation between bleeding time and bleeding risk [155] and reveals an essential function of  $\alpha$ -granules in the arrest of posttraumatic bleeding, whereas they appear not to be required for the maintenance of vascular integrity in the absence of injury.

Significantly, the platelet aggregation defect of *Nbeal2*<sup>-/-</sup> platelets translated into a severely defective formation of stable thrombi under conditions of medium and high shear stress (see figure 3.19). A similar albeit less pronounced phenotype has been reported previously in different mouse lines, including those lacking CD40 ligand (CD40-L) [7] or the calcium sensor molecule STIM1 [185], with marked defects in thrombus stability under flow *in vitro* and *in vivo* despite only mild defects in activation/aggregation in the absence of flow. This suggests that  $\alpha$ -granule-derived mediators and/or adhesion molecules are particularly important to build shear-resistant thrombi under conditions in which agonist potency becomes limiting due to rapid dilution and various receptor-ligand interactions have to be integrated to produce appropriate cell-cell interactions.

Interestingly, we found a markedly reduced coagulant activity of *Nbeal2*<sup>-/-</sup> platelets, which was not based on impaired agonist receptor function, as indicated by the normal integrin  $\alpha$ IIb $\beta$ 3 activation and unaltered dense granule release responses of the mutant platelets upon stimulation with all agonists tested (see figures 3.20, 3.17 B and 3.18 A, B and D). This suggests that  $\alpha$ -granule-derived factors are required for the efficient collapse of the membrane asymmetry and exposure of coagulant PS in platelets activated under flow [76]. This Ca<sup>2+</sup>-dependent process involves the activity of the TMEM16F ion channel [176, 197] and is mediated by lipid transporters (scramblases) whose identity and subcellular localization have remained elusive.

While a role for some  $\alpha$ -granule proteins in hemostasis and thrombosis has been demonstrated, most of them are also present in other vascular compartments, making conclusions on the relative importance of their  $\alpha$ -granule pool difficult [87, 157]. One prominent example is vWF, which is also present at high concentrations in Weibel-Palade bodies of endothelial cells and in plasma. Nbeal2-deficient mice, which lacked vWF in platelets but not in plasma or endothelium (see figure 3.11, 3.15 and 3.23), displayed severely defective platelet adhesion and aggregate formation on collagen under high shear flow conditions, a process known to depend on GPIb-vWF interactions [158]. This indicates that  $\alpha$ -granular vWF is of central importance for the formation of shear-resistant thrombi under these experimental conditions but also that multiple other  $\alpha$ -granule proteins, including fibrinogen and thrombospondin and possibly also vitronectin and fibronectin [198], probably contribute to this process. In line with this, the thrombus formation defect observed in Nbeal2-deficient mice *in vivo* appeared to be more severe than that seen in mice lacking vWF [33], P-selectin [46], or CD40-L [7]. It is unlikely that the reduced platelet count in Nbeal2-deficient mice was responsible for their hemostatic and thrombotic defect, as it was recently shown that thrombotic occlusion of the injured aorta and the carotid artery was only partially impaired when platelet counts were reduced by 70% or 80%, respectively. Furthermore, tail bleeding times and thrombus formation in small arterioles were largely unaffected by reductions of platelet count up to 97.5% [123].

Significantly, Nbeal2-deficient mice or chimeric mice lacking Nbeal2 in the hematopoietic system were profoundly protected from tMCAO-induced brain infarction (see figure 3.24), indicating that platelet  $\alpha$ -granule components are critical pathogenic factors in this setting. The lack of platelet vWF may not be critical here, as plasma vWF has been shown to be sufficient to promote infarct growth in this model [100]. This reveals that different vWF pools contribute to very distinct (patho-)physiological processes and indicates that other  $\alpha$ -granule components are critical to promote thrombo-inflammation in the ischemic brain. On the other hand, despite markedly prolonged bleeding times, we did not observe intracranial bleeding in Nbeal2-deficient mice after tMCAO, suggesting that the  $\alpha$ -granule storage pool of adhesion molecules is not required to maintain vascular integrity under conditions of acute brain infarction. This is especially interesting as it has been shown before that platelets are crucial to safeguard vessel wall integrity during inflammation and stroke [59].

The relevance of platelets and their products for successful tissue reconstitution is reflected by the use of PRP to promote wound healing [3, 45, 138]. However, rendering mice thrombocytopenic leads to increased wound inflammation without affecting the reparative aspects of wound repair [179]. A recent study demonstrated better healing responses in diabetic mice injected with nonactivated versus thrombin-activated platelets. From this the authors concluded that platelets may be used as cell therapy rather than using only their growth factor content [160].

The approach that we have taken preserved the cells and ablated the defined spectrum of growth factors specifically contained in platelet  $\alpha$ -granules. Our results clearly demonstrate for the first time the crucial importance of platelet-derived proteins, released during the first hours

after injury, for myofibroblast differentiation, which peaks at 7 days after wounding. This result implies that TGF- $\beta$  released by macrophages, which are abundantly present throughout the inflammatory and reparative phases of healing [40], does not compensate for early deficiency due to platelet dysfunction. At 7 days after wounding we did not detect differences in wound macrophage numbers. Detailed characterization of the early inflammatory infiltrate will show whether their numbers differ at earlier time points in the healing process. However, large differences might have resulted in vascular abnormalities [110], which we did not detect. To investigate whether *Nbeal2*-deficiency affects other hematopoietic cells, *Nbeal2* expression was analyzed in lymphocytes, splenocytes, and CD4<sup>+</sup> T cells by qPCR (see figure 4.1). Indeed, these cells showed very low expression levels when compared with MKs, thereby confirming results from previous studies [5]. However, further conclusions on the possible role of *Nbeal2* in other cells in the healing process will require the generation of conditional mouse models. Likewise, defining the roles of TGF- $\beta$  relative to other secreted proteins will require extensive studies on multiple mouse models.

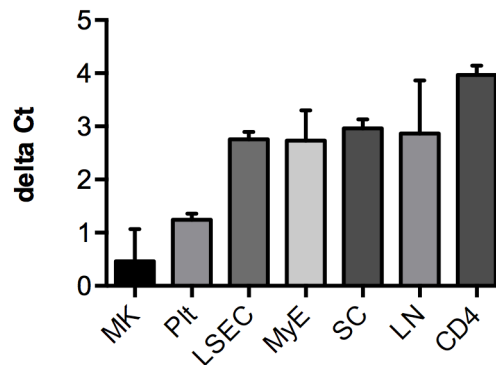


**Figure 4.1: Expression of *Nbeal2* in different cell types.** qRT-PCR was used to quantify *Nbeal2* mRNA in several cell types. Results are presented as delta Ct versus reference mRNA. MK, megakaryocyte; Plt, platelet; LSEC, liver sinusoidal endothelial cells; MyE, MyEnd endothelial cells; SC, splenocytes; LN, lymph node cells; CD4, CD4<sup>+</sup> T cells.

#### 4.2.1 The *Nbeal2*<sup>-/-</sup> mouse as a model for the gray platelet syndrome

Using a reverse genetic approach it could be shown that *Nbeal2*-deficient mice mimic most of the important hallmarks of GPS thereby establishing this mouse as a model of the disease, a finding that was confirmed by a second group [92]. As in human GPS, *Nbeal2*-deficient mice exhibit thrombocytopenia with enlarged platelets, a mild splenomegaly and absence of  $\alpha$ -granules in platelets. While taking into account the smaller size of mouse platelets, *Nbeal2*<sup>-/-</sup> platelets show the same morphological characteristics as human GPS including a high number of vacuoles, which mostly appear empty (see figure 3.26). The content of  $\alpha$ -granule proteins synthesized by MKs, such as vWF, PF4 and thrombospondin-1 was strongly reduced in the knockout platelets [92]. The platelet fibrinogen content was also decreased, indicating that endocytosed proteins also fail to be stored in *Nbeal2*-deficient platelets, as seen in the human

disease.

On the other hand, P-selectin, which serves widely as a marker for  $\alpha$ -granule secretion and is a component of the  $\alpha$ -granule membrane, was still present, albeit at lower levels. Its surface exposure upon activation reached approximately 50% of wildtype levels. For human GPS, P-selectin levels have been shown to be either reduced or normal [141]. In line with observations for GPS patients [139], dense granule secretion was not affected in *Nbeal2*-deficient platelets [92].

*Nbeal2*<sup>-/-</sup> mice recapitulate the hallmarks of GPS patients with the absence of  $\alpha$ -granules and their content. Nevertheless, a few differences exist. We did not observe the heterogeneity of the platelet aggregation responses seen in GPS patients upon stimulation with different agonists [69, 139]. This could be explained by the different mutations that were found in the *NBEAL2* gene, which in contrast to the full knockout in the mouse model, may not necessarily lead to a complete loss of protein function or expression [5, 17, 68, 91]. Furthermore, *Nbeal2*<sup>-/-</sup> mice all have a common genetic background while in human disease the phenotype will be influenced by the whole range of single-nucleotide polymorphisms that define the hemostatic response. Similarly, the platelet count is highly variable in GPS patients and thrombocytopenia can be severe, which almost certainly contributes to bleeding. Another frequent characteristic of GPS patients is myelofibrosis probably caused by  $\alpha$ -granule proteins being released from MKs into the marrow leading to dysregulated cell proliferation and differentiation. In *Nbeal2*-deficient mice, signs of myelofibrosis were not observed in young as well as in 4- and 6-month-old animals and this finding was confirmed by another group [92]. Whether onset of myelofibrosis will occur later in these animals needs to be investigated.

### 4.2.2 The role of NBEAL2 in $\alpha$ -granule biogenesis

Beyond the functional analyses, the question of the mechanism by which NBEAL2 regulates protein sorting during  $\alpha$ -granule biogenesis, remains to be addressed. NBEAL2 is a large, multi-domain protein that consists of 2754 amino acids and contains ARM, ConA-like, PH, BEACH and WD40 domains. Of note, GPS-causing point mutations are not limited to one particular domain but are distributed throughout the entire protein [5, 17, 68, 91]. While it is thought that ConA-like lectin domains could be involved in protein sorting and secretion [22], it is known that WD40 domains enable protein-protein interactions and PH domains facilitate membrane association. BEACH domain containing proteins are of emerging clinical importance, as more members of this family become associated with human disease [27]. However, they act in different cellular processes including vesicular transport, apoptosis, membrane dynamics and receptor signaling.

A role for NBEAL2 in membrane dynamics and vesicular transport is consistent with the finding that *Nbeal2*-deficiency causes a dramatically increased number of empty vacuoles and mis-targeting of  $\alpha$ -granule proteins that leads to loss or accumulation of the protein. This has also been shown for human GPS, where MKs cultured *in vitro* from peripheral blood CD34<sup>+</sup> cells from a typical GPS patient with a homozygous L388P mutation [5], clearly show synthesis of

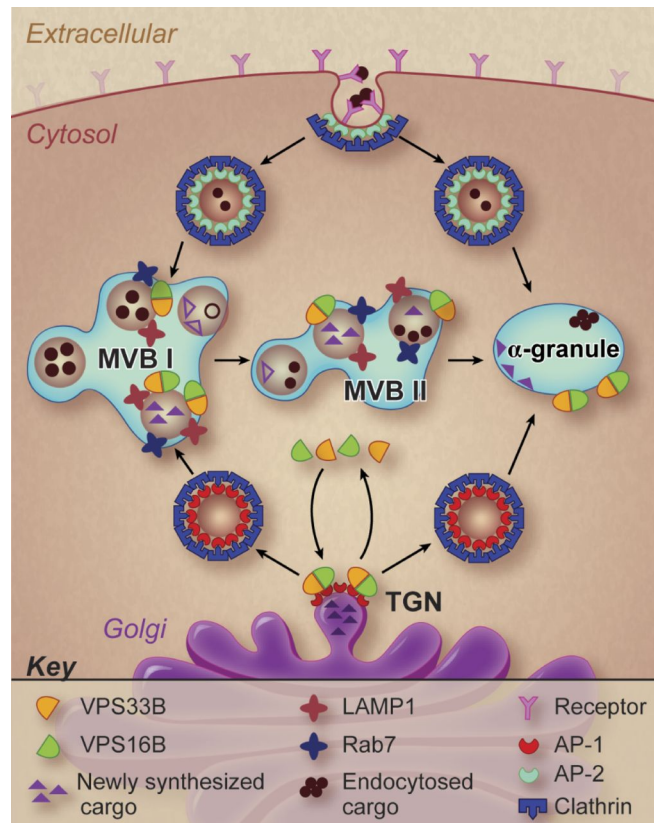


**Figure 4.2: Working model of  $\alpha$ -granule biogenesis.** This artwork illustrates the localization and interaction of proteins involved in  $\alpha$ -granule biogenesis in MKs, that have been identified recently. Image taken from [50].

vWF. However, the protein is lost prior to proplatelet formation and vWF trafficking along proplatelets in mature cells is lacking (see figure 3.27). Recently, VPS33B and VPS16B have been shown to be involved in  $\alpha$ -granule biogenesis [184]. Significantly, protein levels of VPS16B and VPS33B were unchanged in *Nbeal2*<sup>-/-</sup> platelets [92]. The fact that platelets from ARC syndrome patients, which harbour a mutation in *VPS33B* completely lack  $\alpha$ -granules, while platelets from *Nbeal2*-deficient mice and GPS patients contain vacuole-like  $\alpha$ -granule remnants implies that VPS33B and its binding partner VPS16B act at an earlier stage during  $\alpha$ -granule biogenesis than NBEAL2 (see figure 4.2) [50, 184].

### 4.3 Combined deficiency of platelet $\alpha$ - and dense granule secretion

To study the effect of combined deficiency of  $\alpha$ - and dense granule secretion, *Unc13d*<sup>-/-</sup>/*Nbeal2*<sup>-/-</sup> mice were generated. Platelets from these mice were unable to secrete their dense granule content and lacked  $\alpha$ -granules. Double-deficient mice displayed platelet count and size similar to those of *Nbeal2*-deficient platelets (see figure 3.28) indicating that combined deficiency does not further impair platelet production.

Upon stimulation with different agonists, double-deficient platelets displayed P-selectin surface expression below that of *Nbeal2*<sup>-/-</sup> platelets (see figure 3.30). This supports the notion that P-selectin is also stored in dense granules, however, to a limited extent [153]. Interestingly, upon stimulation, double-deficient platelets were still capable of recruiting 25-30% of wildtype P-selectin levels to the surface, indicating that there might be P-selectin stores besides  $\alpha$ - and dense granules, for example the OCS.

Double-deficient platelets showed a strong reduction in aggregation upon stimulation with CRP or collagen (see figure 3.31) which was more pronounced than the defects observed in *Nbeal2*<sup>-/-</sup> or *Unc13d*<sup>-/-</sup> platelets. This underlines the importance of secondary mediators released from both  $\alpha$ - and dense granules during collagen-induced aggregation [134].

In agreement with the severely impaired platelet adhesion to collagen under flow (see figure 3.32), double-deficient mice displayed abolished arterial thrombus formation which is in line with previous reports showing that the thrombus formation in the aorta injury model largely depends on GPVI activation by collagen [11]. In addition, the single-deficient mice already demonstrated a strong protection from *in vivo* thrombus formation as well as an impaired hemostasis (see figures 3.5 and 3.21).

Interestingly, double-deficient platelets showed a severe reduction of PS-exposure after stimulation while the total level of PS in the cells appeared largely unaltered (see figure 3.33). This confirms the importance of mediators released from  $\alpha$ - and dense granules in PS-exposure and coagulation [16].

Platelets and the (hem)ITAM signaling in particular have recently been recognized as key players for the maintenance of the vascular integrity during (thrombo)inflammation [18, 59]. However, the downstream mediators remained elusive and it was speculated that platelet granule content might play a role [64, 79]. To investigate the role of platelet granule content in inflammatory bleeding, *Munc13-4/Nbeal2*-deficient mice were subjected to the rpA reaction of the skin, LPS-induced lung inflammation and the tMCAO model of ischemic stroke. While platelet-depleted animals showed massive hemorrhage upon skin or lung inflammation, this was not the case in *Unc13d*<sup>-/-</sup>/*Nbeal2*<sup>-/-</sup> mice (see figure 3.35). These results indicate that platelet granule content is likely not involved in maintaining vascular integrity during local inflammation. However, contrary results were obtained when subjecting *Unc13d*<sup>-/-</sup>/*Nbeal2*<sup>-/-</sup> mice to the tMCAO model of ischemic stroke: 40% of the animals died from intracranial hemorrhage within 24 h after infarction (see figure 3.36 B and E). This shows that while defective dense granule secretion or the absence of  $\alpha$ -granules alone have no effect on vascular integrity during stroke, the combination of both defects causes vascular damage and an increase in mortality to a similar degree as observed after GPIIb/IIIa blockade (see figure 4.3 and [101]). This correlation is relevant since a clinical trial that investigated the impact of abolishing platelet aggregation with abciximab (an antibody directed against GPIIb/IIIa) on stroke progression failed due to excess intracranial hemorrhages and inefficacy [2]. Therefore, blocking secretion from both major platelet granule types is most likely not an optimal and safe target for stroke therapy.



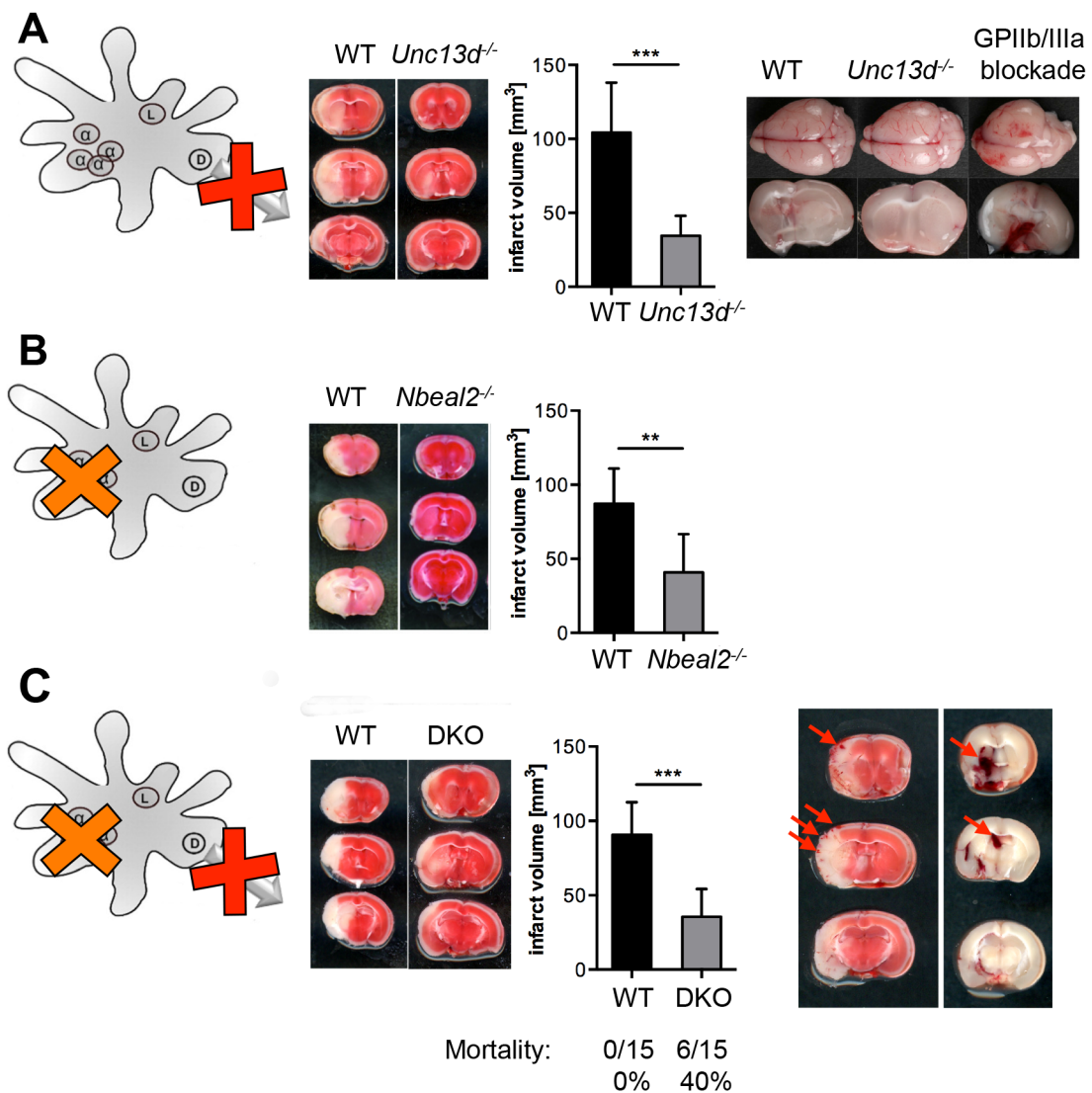


**Figure 4.3: The role of platelet granule release in maintaining vascular integrity during stroke.** Overview of the impact of defective dense granule secretion (A), absence of  $\alpha$ -granules (B) or the combination of both (C) on infarct volumes and vascular integrity after tMCAO. Representative images of coronal sections stained with TTC 24 h after tMCAO. Infarcted areas are shown in white (left column). Planimetric analysis was used to quantify the infarct volume (center column). Representative images show native whole brains, native brain sections and TTC-stained brain sections to illustrate the degree of hemorrhage. Parts taken from [34, 170].

Taken together, there seem to be different mechanisms by which platelets maintain vascular integrity during acute inflammation (*immune complex* (IC)-mediated inflammation of the skin or LPS-induced lung inflammation) or during thromboinflammation (following tMCAO). Additionally, in a recent study, thioglycollate-induced peritonitis, which is a model for macrophage-driven sterile inflammation, did not cause bleeding in thrombocytopenic mice [146]. Clearly, further research is needed to clarify, whether inflammatory bleeding during thrombocytopenia depends on the organ affected or the cause and severity of inflammation. A very recent publication showed that during IC-mediated inflammation, single platelets prevent neutrophil-induced vas-

cular damage in a GPVI-dependent manner [65]. Whether the same mechanism also prevents hemorrhage in other pathophysiological situations (e.g. in the brain during stroke) remains to be shown.

### 4.4 Concluding remarks and outlook

The work presented here provides new insights into the role of platelet  $\alpha$ - and dense granule secretion in platelet biogenesis and function as well as in thrombosis, hemostasis, stroke, wound healing and maintaining vascular integrity during inflammation and stroke using genetically modified mice deficient for Munc13-4, Nbeal2, or both. The results may have important implications for the development of strategies to modulate platelet reactivity and to prevent excessive platelet activation and adhesion in pathological settings such as thrombosis and ischemic stroke. Although caution is required when translating results from mouse studies into clinical practice, findings presented in this thesis suggest that restricting platelet granule secretion might be useful for the prevention of thrombosis or thrombo-inflammation, e.g. following stroke. However, the abrogated hemostatic function that was observed in all knockout strains analyzed has to be considered carefully. Therefore, it would not be advisable to aim at full but rather partial granule secretion blockade. Certainly, further studies are necessary for a more detailed characterization of the anti-thrombotic potential of  $\alpha$ - and dense granule secretion inhibition and the accompanying loss in hemostatic function. Furthermore, to inhibit platelet granule secretion, it would be necessary to first identify suitable target proteins that could be blocked, e.g. using small molecule inhibitors. Ideal targets would be signaling molecules that regulate secretion (e.g. PKC $\alpha$ ) or proteins directly involved in the secretion process like the SNARE proteins (e.g. VAMP-3 and 8, Syntaxin-2 and 4 and SNAP-23). For several SNARE proteins blocking peptides or inhibitory antibodies have been identified and were shown to efficiently inhibit platelet granule secretion [49]. For example, *recombinant VAMP-3* (rVAMP-3) was shown to potently inhibit both  $\alpha$ - and dense granule secretion [148]. To minimize side effects, it would be important to analyze the effect of the potential inhibitors on other cells (e.g. T-cells and mast cells).

Open questions that remain from the studies presented in this thesis include those regarding the morphology of MKs in *Nbeal2*<sup>-/-</sup> mice, which besides lack of  $\alpha$ -granular proteins appeared largely unaltered in this study (see figures 3.12, 3.13 and 3.15) although platelet count was reduced by 40% and platelet lifespan was unaltered. However, recent reports showed both altered and unaltered morphology of MKs in *Nbeal2*-deficient mice [67, 93]. To further examine MK morphology in the intact bone marrow, whole femora could be analyzed, e.g. using *light sheet fluorescence microscopy* (LSFM). This would also enable 3D reconstruction and analysis of MKs in their native environment.

Further studies would also be needed to reveal whether the constitutive full knockout approaches that were used in the studies presented here had an impact on cells other than platelets. While in case of the *Nbeal2* knockout this question was partially addressed by the

analysis of bone marrow chimeric mice, all hematopoietic cells (including immune cells) remained deficient for *Nbeal2* in these animals. One way to address this issue would be to generate tissue-specific knockout animals by using the Cre/loxP system and Pf4-Cre transgenic mice to achieve MK-specific deletion of the gene of interest. Using the Pf4-Cre system for a conditional *Nbeal2* knockout could be challenging since *Nbeal2* might be expressed at earlier stages of MK maturation than PF4. Another option would be to perform platelet transfusion experiments. However, finding the correct antibody dosage (e.g. of an anti-GPIb antibody) that reliably depletes all platelets but leaves no free circulating antibody remaining that would capture the transfused platelets, is challenging. Therefore, using the h-IL4R/GPIb transgenic mouse as a recipient for transfused platelets would be the best choice since it enables platelet depletion with an anti-h-IL4R antibody that does not recognize transfused wildtype platelets [18, 95].

In this thesis, it could also be shown that *Nbeal2*-deficient mice phenocopy most of the characteristics of GPS with macrothrombocytopenia, splenomegaly and absence of  $\alpha$ -granules in platelets and MKs. This confirms that mutations in *Nbeal2* cause GPS and establishes the *Nbeal2*<sup>-/-</sup> mouse as a model of the disease, contributing to risk evaluation of GPS patients in various disease settings. Moreover, potential treatment options could be tested in these mice.

Besides, *Nbeal2*<sup>-/-</sup>, *Unc13d*<sup>-/-</sup> and double-deficient mice have recently been used as tools to study the role of platelet granules in other pathological settings such as metastasis [67, 162] or maintaining the integrity of developing cerebral blood vessels [109]. Moreover, the three knockout mouse lines presented here in combination with talin-deficient mice could be used to decipher whether platelet granule release or platelet aggregation is the key function needed in pathological settings where platelets recently have been shown to be involved, e.g. *multiple sclerosis* (MS) or sepsis.

It has been reported that platelets are present in human MS lesions as well as in the *central nervous system* (CNS) of mice subjected to a mouse model of *experimental autoimmune encephalomyelitis* (EAE). Platelet depletion in mice resulted in significantly ameliorated disease development and progression and was associated with reduced recruitment of leukocytes to the inflamed CNS [105].

In a recent study it was shown that platelets protect from septic shock by inhibiting macrophage-dependent inflammation via the COX-1 signaling pathway [196]. Furthermore, intravascular NETs capture bacteria from the bloodstream during sepsis and NET production requires platelet-neutrophil interactions [119].

EAE as a mouse model for MS and sepsis are two examples of diseases for which safe and efficient treatment options are needed and where only recently platelets have been identified to play an important role. Hence investigating the relevant platelet functions using the mouse models described in this thesis will provide further insights into the role of platelets beyond thrombosis and hemostasis.

## Bibliography

- [1] H. P. Adams, G. del Zoppo, M. J. Alberts, D. L. Bhatt, L. Brass, A. Furlan, R. L. Grubb, R. T. Higashida, E. C. Jauch, C. Kidwell, P. D. Lyden, L. B. Morgenstern, A. I. Qureshi, R. H. Rosenwasser, P. A. Scott, and E. F. M. Wijndicks. Guidelines for the Early Management of Adults With Ischemic Stroke. *Circulation*, 115(20):e478–e534, 2007.
- [2] H. P. Adams, M. B. Effron, J. Torner, A. Dávalos, J. Frayne, P. Teal, J. Leclerc, B. Oemar, L. Padgett, E. S. Barnathan, and W. Hacke. Emergency administration of abciximab for treatment of patients with acute ischemic stroke: results of an international phase III trial: Abciximab in Emergency Treatment of Stroke Trial (AbESTT-II). *Stroke*, 39(1):87–99, 2008.
- [3] A. Akingboye, S. Giddins, P. Gamston, A. Tucker, H. Navsaria, and C. Kyriakides. Application of autologous derived-platelet rich plasma gel in the treatment of chronic wound ulcer: diabetic foot ulcer. *J. Extracorpor. Technol.*, 42(1):20–9, 2010.
- [4] R. Al Hawas, Q. Ren, S. Ye, Z. A. Karim, A. H. Filipovich, and S. W. Whiteheart. Munc18b/STXBP2 is required for platelet secretion. *Blood*, 120(12):2493–500, 2012.
- [5] C. A. Albers, A. Cvejic, R. Favier, E. E. Bouwmans, M.-C. Alessi, P. Bertone, G. Jordan, R. N. W. Kettleborough, G. Kiddle, M. Kostadima, R. J. Read, B. Sipos, S. Sivapalaratnam, P. A. Smethurst, J. Stephens, K. Voss, A. T. Nurden, A. Rendon, P. Nurden, and W. H. Ouwehand. Exome sequencing identifies NBEAL2 as the causative gene for gray platelet syndrome. *Nat. Genet.*, 43(8):735–737, 2011.
- [6] P. André, S. M. Delaney, T. LaRocca, D. Vincent, F. DeGuzman, M. Jurek, B. Koller, D. R. Phillips, and P. B. Conley. P2Y<sub>12</sub> regulates platelet adhesion/activation, thrombus growth, and thrombus stability in injured arteries. *J. Clin. Invest.*, 112(3):398–406, 2003.
- [7] P. André, K. S. S. Prasad, C. V. Denis, M. He, J. M. Papalia, R. O. Hynes, D. R. Phillips, and D. D. Wagner. CD40L stabilizes arterial thrombi by a beta<sub>3</sub> integrin–dependent mechanism. *Nat. Med.*, 8(3):247–52, 2002.
- [8] M. Arman, K. Krauel, D. O. Tilley, C. Weber, D. Cox, A. Greinacher, S. W. Kerrigan, and S. P. Watson. Amplification of bacteria-induced platelet activation is triggered by Fc $\gamma$ R1IA, integrin  $\alpha$ IIb $\beta$ 3 and platelet factor 4. *Blood*, 123(20):3166–74, Mar. 2014.
- [9] E. M. Battinelli, J. H. Hartwig, and J. E. Italiano. Delivering new insight into the biology of megakaryopoiesis and thrombopoiesis. *Curr. Opin. Hematol.*, 14(5):419–26, 2007.

- [10] J. B. Bederson, L. H. Pitts, M. Tsuji, M. C. Nishimura, R. L. Davis, and H. Bartkowski. Rat middle cerebral artery occlusion: evaluation of the model and development of a neurologic examination. *Stroke*, 17(3):472–476, 1986.
- [11] M. Bender, I. Hagedorn, and B. Nieswandt. Genetic and antibody-induced glycoprotein VI deficiency equally protects mice from mechanically and FeCl<sub>3</sub>-induced thrombosis. *J. Thromb. Haemost.*, 9(7):1423–1426, 2011.
- [12] J. S. Bennett. Structure and function of the platelet integrin  $\alpha$ IIb $\beta$ 3. *J. Clin. Invest.*, 115(12):3363–3369, 2005.
- [13] M. E. Bentfeld and D. F. Bainton. Cytochemical Localization of Lysosomal Enzymes in Rat Megakaryocytes and Platelets. *J. Clin. Invest.*, 56(6):1635–1649, 1975.
- [14] W. Bergmeier, V. Schulte, G. Brockhoff, U. Bier, H. Zirngibl, and B. Nieswandt. Flow cytometric detection of activated mouse integrin  $\alpha$ IIb $\beta$ 3 with a novel monoclonal antibody. *Cytometry*, 48:80–86, 2002.
- [15] M. J. Berridge, M. D. Bootman, and H. L. Roderick. Calcium signalling: dynamics, homeostasis and remodelling. *Nat. Rev. Mol. Cell Biol.*, 4(7):517–529, 2003.
- [16] P. Blair and R. Flaumenhaft. Platelet  $\alpha$ -granules: basic biology and clinical correlates. *Blood Rev.*, 23(4):177–189, 2009.
- [17] R. Bottega, A. Pecci, E. De Candia, N. Pujol-Moix, P. G. Heller, P. Noris, D. De Rocco, G. M. Podda, A. C. Glembotsky, M. Cattaneo, C. L. Balduini, and A. Savoia. Correlation between platelet phenotype and NBEAL2 genotype in patients with congenital thrombocytopenia and  $\alpha$ -granule deficiency. *Haematologica*, 98(6):868–874, 2013.
- [18] Y. Boulaftali, P. R. Hess, T. M. Getz, A. Cholka, M. Stolla, N. Mackman, A. P. Owens, J. Ware, M. L. Kahn, and W. Bergmeier. Platelet ITAM signaling is critical for vascular integrity in inflammation. *J. Clin. Invest.*, 123(2):908–916, 2013.
- [19] A. Braun, D. Varga-Szabo, C. Kleinschnitz, I. Pleines, M. Bender, M. Austinat, M. Bösl, G. Stoll, and B. Nieswandt. Orai1 (CRACM1) is the platelet SOC channel and essential for pathological thrombus formation. *Blood*, 113(9):2056–2063, 2009.
- [20] A. Brill, H. Elinav, and D. Varon. Differential role of platelet granular mediators in angiogenesis. *Cardiovasc. Res.*, 63(2):226–235, 2004.
- [21] S. Bunting, R. Widmer, T. Lipari, L. Rangell, H. Steinmetz, K. Carver-Moore, M. W. Moore, G.-A. Keller, and F. J. de Sauvage. Normal platelets and megakaryocytes are produced in vivo in the absence of thrombopoietin. *Blood*, 90(9):3423–3429, 1997.
- [22] A. Burgess, J.-P. Mornon, G. de Saint-Basile, and I. Callebaut. A concanavalin A-like lectin domain in the CHS1/LYST protein, shared by members of the BEACH family. *Bioinformatics*, 25(10):1219–22, 2009.

- [23] Y. Chang, F. Aurade, F. Larbret, Y. Zhang, J. P. Le Couedic, L. Momeux, J. Larghero, J. Bertoglio, F. Louache, E. Cramer, W. Vainchenker, and N. Debili. Proplatelet formation is regulated by the Rho / ROCK pathway. *Blood*, 109(10):4229–4236, 2007.
- [24] D. Chen, P. P. Lemons, T. Schraw, and S. W. Whiteheart. Molecular mechanisms of platelet exocytosis: role of SNAP-23 and syntaxin 2 and 4 in lysosome release. *Blood*, 96(5):1782–1788, 2000.
- [25] W. Clark, N. Lessov, M. Dixon, and F. Eckenstein. Monofilament intraluminal middle cerebral artery occlusion in the mouse. *Neurol. Res.*, 19(6):641–8, 1997.
- [26] E. M. Cramer, F. Norol, J. Guichard, J. Breton-Gorius, W. Vainchenker, J. M. Massé, and N. Debili. Ultrastructure of platelet formation by human megakaryocytes cultured with the Mpl ligand. *Blood*, 89(7):2336–2346, 1997.
- [27] A. R. Cullinane, A. a. Schäffer, and M. Huizing. The BEACH is hot: A LYST of emerging roles for BEACH-domain containing proteins in human disease. *Traffic*, 14:749–66, 2013.
- [28] G. L. Dale, P. Friese, P. Batar, S. F. Hamilton, G. L. Reed, K. W. Jackson, K. J. Clemetson, and L. Alberio. Stimulated platelets use serotonin to enhance their retention of procoagulant proteins on the cell surface. *Nature*, 415(6868):175–179, 2002.
- [29] M. E. Daly. Determinants of platelet count in humans. *Haematologica*, 96(1):10–13, 2011.
- [30] S. F. De Meyer, T. Schwarz, H. Deckmyn, C. V. Denis, B. Nieswandt, G. Stoll, K. Vanhoorelbeke, and C. Kleinschnitz. Binding of von Willebrand factor to collagen and glycoprotein Iba, but not to glycoprotein IIb/IIIa, contributes to ischemic stroke in mice—brief report. *Arterioscler. Thromb. Vasc. Biol.*, 30(10):1949–1951, 2010.
- [31] G. de Saint Basile, G. Ménasché, and S. Latour. Inherited defects causing hemophagocytic lymphohistiocytic syndrome. *Ann. N. Y. Acad. Sci.*, 1246(1):64–76, 2011.
- [32] S. M. de Witt, R. Verdoold, J. M. E. M. Cosemans, and J. W. M. Heemskerk. Insights into platelet-based control of coagulation. *Thromb. Res.*, 133 S2:S139–48, May 2014.
- [33] C. Denis, N. Methia, P. S. Frenette, H. Rayburn, M. Ullman-Culleré, R. O. Hynes, and D. D. Wagner. A mouse model of severe von Willebrand disease: defects in hemostasis and thrombosis. *Proc. Natl. Acad. Sci. U. S. A.*, 95(16):9524–9, 1998.
- [34] C. Deppermann, D. Cherpokova, P. Nurden, J.-N. Schulz, I. Thielmann, P. Kraft, T. Vögtle, C. Kleinschnitz, S. Dütting, G. Krohne, S. A. Eming, A. T. Nurden, B. Eckes, G. Stoll, D. Stegner, and B. Nieswandt. Gray platelet syndrome and defective thromboinflammation in Nbeal2-deficient mice. *J. Clin. Invest.*, 123(8):3331–42, 2013.
- [35] C. Deppermann, P. Nurden, A. T. Nurden, B. Nieswandt, and D. Stegner. The Nbeal2-/- mouse as a model for the gray platelet syndrome. *Rare Dis.*, 1(1):e26561, 2013.

- [36] U. Dirnagl. Bench to bedside: the quest for quality in experimental stroke research. *J. Cereb. Blood Flow Metab.*, 26:1465–1478, 2006.
- [37] D. Duerschmied, G. L. Suidan, M. Demers, N. Herr, C. Carbo, A. Brill, S. M. Cifuni, M. Mauler, S. Cicko, M. Bader, M. Idzko, C. Bode, and D. D. Wagner. Platelet serotonin promotes the recruitment of neutrophils to sites of acute inflammation in mice. *Blood*, 121(6):1008–1015, 2013.
- [38] S. Dütting, M. Bender, and B. Nieswandt. Platelet GPVI: a target for antithrombotic therapy?! *Trends Pharmacol. Sci.*, 33(11):583–90, 2012.
- [39] N. El Golli, O. Issertial, J.-P. Rosa, and V. Briquet-Laugier. Evidence for a granule targeting sequence within platelet factor 4. *J. Biol. Chem.*, 280(34):30329–35, 2005.
- [40] S. A. Eming, M. Hammerschmidt, T. Krieg, and A. Roers. Interrelation of immunity and tissue repair or regeneration. *Semin. Cell Dev. Biol.*, 20(5):517–27, 2009.
- [41] S. A. Eming and T. Krieg. Molecular Mechanisms of VEGF-A Action during Tissue Repair. *J. Investig. Dermatology Symp. Proc.*, 11(1):79–86, 2006.
- [42] S. A. Eming, T. Krieg, and J. M. Davidson. Inflammation in wound repair: molecular and cellular mechanisms. *J. Invest. Dermatol.*, 127(3):514–525, 2007.
- [43] B. I. Eriksson, D. J. Quinlan, and J. W. Eikelboom. Novel oral factor Xa and thrombin inhibitors in the management of thromboembolism. *Annu. Rev. Med.*, 62:41–57, 2011.
- [44] L. Erpenbeck and M. P. Schön. Deadly allies: the fatal interplay between platelets and metastasizing cancer cells. *Blood*, 115(17):3427–36, 2010.
- [45] P. Everts, M. Hoogbergen, T. Weber, R. Devilee, G. von Monfort, and I. de Hingh. Is the use of autologous platelet-rich plasma gels in gynecologic, cardiac, and general reconstructive surgery beneficial? *Curr. Pharm. Biotechnol.*, 13(7):1163–1172, 2012.
- [46] S. Falati, Q. Liu, P. Gross, G. Merrill-Skoloff, J. Chou, E. Vandendries, A. Celi, K. Croce, B. C. Furie, and B. Furie. Accumulation of tissue factor into developing thrombi in vivo is dependent upon microparticle P-selectin glycoprotein ligand 1 and platelet P-selectin. *J. Exp. Med.*, 197(11):1585–98, 2003.
- [47] T. C. Falik-Zaccari, Y. Anikster, C. E. Rivera, M. K. Horne, L. Schliamser, C. Phornphutkul, D. Attias, T. Hyman, J. G. White, and W. A. Gahl. A new genetic isolate of gray platelet syndrome (GPS): clinical, cellular, and hematologic characteristics. *Mol. Genet. Metab.*, 74(3):303–13, 2001.
- [48] J. Feldmann, I. Callebaut, G. Raposo, S. Certain, D. Bacq, C. Dumont, N. Lambert, M. Ouachée-Chardin, G. Chedeville, H. Tamary, V. Minard-Colin, E. Vilmer, S. Blanche,

- F. Le Deist, A. Fischer, and G. De Saint Basile. Munc13-4 Is Essential for Cytolytic Granules Fusion and Is Mutated in a Form of Familial Hemophagocytic Lymphohistiocytosis (FHL3). *Cell*, 115(4):461–473, 2003.
- [49] R. Flaumenhaft. Molecular basis of platelet granule secretion. *Arterioscler. Thromb. Vasc. Biol.*, 23(7):1152–60, 2003.
- [50] R. Flaumenhaft. Alpha-Granules: a Story in the Making. *Blood*, 120(25):4908–4909, 2012.
- [51] J. G. Fox, S. W. Barthold, M. T. Davisson, C. E. Newcomer, F. W. Quimby, and A. L. Smith. *The Mouse in Biomedical Research*. Academic Press, 2007.
- [52] M. M. Frojmovic and J. G. Milton. Human platelet size, shape, and related functions in health and disease. *Physiol. Rev.*, 62(1):185–261, 1982.
- [53] M. Fujioka, K. Hayakawa, K. Mishima, A. Kunizawa, K. Irie, S. Higuchi, T. Nakano, C. Muroi, H. Fukushima, M. Sugimoto, F. Banno, K. Kokame, T. Miyata, M. Fujiwara, K. Okuchi, and K. Nishio. ADAMTS13 gene deletion aggravates ischemic brain damage: A possible neuroprotective role of ADAMTS13 by ameliorating postischemic hypoperfusion. *Blood*, 115(8):1650–1653, 2010.
- [54] C. Gachet. P2 receptors, platelet function and pharmacological implications. *Thromb. Haemost.*, 99:466–472, 2008.
- [55] G. J. Gasic, T. B. Gasic, and C. C. Stewart. Antimetastatic effects associated with platelet reduction. *Proc. Natl. Acad. Sci. U. S. A.*, 61(1):46–52, 1968.
- [56] L. J. Gay and B. Felding-Habermann. Contribution of platelets to tumour metastasis. *Nat. Rev. Cancer*, 11(2):123–34, 2011.
- [57] J. Gebrane-Younès, E. M. Cramer, L. Orcel, and J. P. Caen. Gray Platelet Syndrome - Dissociation between Abnormal Sorting in Megakaryocyte  $\alpha$ -Granules and Normal Sorting in Weibel-Palade Bodies in Endothelial Cells. *J. Clin. Invest.*, 92(6):3023–3028, 1993.
- [58] C. A. Gleissner, P. Von Hundelshausen, and K. Ley. Platelet chemokines in vascular disease. *Arterioscler. Thromb. Vasc. Biol.*, 28(11):1920–1927, 2008.
- [59] T. Goerge, B. Ho-Tin-Noe, C. Carbo, C. Benarafa, E. Remold-O'Donnell, B. Zhao, S. Cifuni, and D. Wagner. Inflammation induces hemorrhage in thrombocytopenia. *Blood*, 111(10):4958–64, 2008.
- [60] E. M. Golebiewska and A. W. Poole. Secrets of platelet exocytosis - what do we really know about platelet secretion mechanisms? *Br. J. Haematol.*, 165(2):204–216, 2014.
- [61] E. M. Golebiewska and A. W. Poole. Platelet secretion: From haemostasis to wound healing and beyond. *Blood Rev.*, 29(3):153–162, 2015.



- [62] J. Gootenberg and G. Buchanan. Severe hemorrhage in a patient with gray platelet syndrome. *J. Pediatr.*, 109(6):1017–9, 1986.
- [63] G. J. Graham, Q. Ren, J. R. Dilks, P. Blair, S. W. Whiteheart, and R. Flaumenhaft. Endobrevin/VAMP-8-dependent dense granule release mediates thrombus formation in vivo. *Blood*, 114(5):1083–1090, 2009.
- [64] A. Gros, V. Ollivier, and B. Ho-Tin-Noe. Platelets in Inflammation: Regulation of Leukocyte Activities and Vascular Repair. *Front. Immunol.*, 5(678), 2015.
- [65] A. Gros, V. Syvannarath, L. Lamrani, V. Ollivier, S. Loyau, T. Goerge, B. Nieswandt, M. Jandrot-Perrus, and B. Ho-Tin-Noe. Single platelets seal neutrophil-induced vascular breaches via GPVI during immune complex-mediated inflammation in mice. *Blood First Ed.*, 2015.
- [66] S. Grüner, M. Prostedna, V. Schulte, T. Krieg, B. Eckes, C. Brakebusch, and B. Nieswandt. Multiple integrin-ligand interactions synergize in shear-resistant platelet adhesion at sites of arterial injury in vivo. *Blood*, 102(12):4021–4027, 2003.
- [67] J. A. Guerrero, C. Bennett, L. van der Weyden, H. McKinney, M. Chin, P. Nurden, Z. McIntyre, E. L. Cambridge, J. Estabel, H. Wardle-Jones, A. O. Speak, W. N. Erber, A. Rendon, W. H. Ouwehand, and C. Ghevaert. Gray Platelet Syndrome: Pro-inflammatory megakaryocytes and  $\alpha$ -granule loss cause myelofibrosis and confer resistance to cancer metastasis in mice. *Blood*, 124(24):3624–3635, Sept. 2014.
- [68] M. Gunay-Aygun, T. C. Falik-Zaccai, T. Vilboux, Y. Zivony-Elboun, F. Gumruk, M. Cetin, M. Khayat, C. F. Boerkoel, N. Kfir, Y. Huang, D. Maynard, H. Dorward, K. Berger, R. Kleta, Y. Anikster, M. Arat, A. S. Freiberg, B. E. Kehrel, K. Jurk, P. Cruz, J. C. Mullikin, J. G. White, M. Huizing, and W. A. Gahl. NBEAL2 is mutated in gray platelet syndrome and is required for biogenesis of platelet  $\alpha$ -granules. *Nat. Genet.*, 43(8):732–734, 2011.
- [69] M. Gunay-Aygun, Y. Zivony-Elboun, F. Gumruk, D. Geiger, M. Cetin, M. Khayat, R. Kleta, N. Kfir, Y. Anikster, J. Chezar, M. Arcos-Burgos, A. Shalata, H. Stanescu, J. Manaster, M. Arat, H. Edwards, A. S. Freiberg, P. S. Hart, L. C. Riney, K. Patzel, P. Tanpaiboon, T. Markello, M. Huizing, I. Maric, M. Horne, B. E. Kehrel, K. Jurk, N. F. Hansen, P. F. Cherukuri, M. Jones, P. Cruz, J. C. Mullikin, A. Nurden, J. G. White, W. A. Gahl, and T. Falik-Zaccai. Gray platelet syndrome: natural history of a large patient cohort and locus assignment to chromosome 3p. *Blood*, 116(23):4990–5001, 2010.
- [70] A. L. Gurney, K. Carver-Moore, F. J. D. Sauvage, and M. W. Moore. Thrombocytopenia in c-mpl-Deficient Mice. *Science*, 265:1445–1447, 1994.
- [71] W. Hacke, M. Kaste, E. Bluhmki, M. Brozman, A. Dávalos, D. Guidetti, V. Larrue, K. Lees, Z. Medeghri, T. Machnig, D. Schneider, R. von Kummer, N. Wahlgren, and D. Toni. Thrombolysis with Alteplase 3 to 4.5 Hours after Acute Ischemic Stroke. *N. Engl. J. Med.*, 359(13):1317–1329, 2008.

- [72] G. J. Hankey and J. W. Eikelboom. Antithrombotic drugs for patients with ischaemic stroke and transient ischaemic attack to prevent recurrent major vascular events. *Lancet Neurol.*, 9(3):273–284, 2010.
- [73] G. K. Hansson and A. Hermansson. The immune system in atherosclerosis. *Nat. Immunol.*, 12(3):204–212, 2011.
- [74] L. A. Harker, L. K. Roskos, U. M. Marzec, R. A. Carter, J. K. Cherry, B. Sundell, E. N. Cheung, D. Terry, and W. Sheridan. Effects of megakaryocyte growth and development factor on platelet production, platelet life span, and platelet function in healthy human volunteers. *Blood*, 95(8):2514–2522, 2000.
- [75] J. H. Hartwig. Mechanisms of actin rearrangements mediating platelet activation. *J. Cell Biol.*, 118(6):1421–1441, 1992.
- [76] J. W. M. Heemskerk, N. J. A. Mattheij, and J. M. E. M. Cosemans. Platelet-based coagulation: different populations, different functions. *J. Thromb. Haemost.*, 11(1):2–16, 2013.
- [77] H. F. Heijnen, N. Debili, W. Vainchencker, J. Breton-Gorius, H. J. Geuze, and J. J. Sixma. Multivesicular bodies are an intermediate stage in the formation of platelet alpha-granules. *Blood*, 91(7):2313–2325, 1998.
- [78] E. Heilmann, P. Hourdille, A. Pruvost, A. Paponneau, and A. T. Nurden. Thrombin-induced platelet aggregates have a dynamic structure. Time-dependent redistribution of glycoprotein IIb-IIIa complexes and secreted adhesive proteins. *Arterioscler. Thromb. Vasc. Biol.*, 11(3):704–718, 1991.
- [79] B. Ho-Tin-Noé, M. Demers, and D. D. Wagner. How platelets safeguard vascular integrity. *J. Thromb. Haemost.*, 9(S1):56–65, 2011.
- [80] B. Ho-Tin-Noé, T. Goerge, and S. Cifuni. Platelet granule secretion continuously prevents intratumor hemorrhage. *Cancer Res.*, 68(16):6851–6858, 2008.
- [81] W. Hong. SNAREs and traffic. *Biochim. Biophys. Acta*, 1744(2):120–144, 2005.
- [82] M. Huizing, A. Helip-Wooley, W. Westbroek, M. Gunay-Aygun, and W. A. Gahl. Disorders of lysosome-related organelle biogenesis: clinical and molecular genetics. *Annu. Rev. Genomics Hum. Genet.*, 9:359–386, 2008.
- [83] Y. Huo, A. Schober, S. B. Forlow, D. F. Smith, M. C. Hyman, S. Jung, D. R. Littman, C. Weber, and K. Ley. Circulating activated platelets exacerbate atherosclerosis in mice deficient in apolipoprotein E. *Nat. Med.*, 9(1):61–67, 2003.
- [84] R. R. Isberg and G. Tran Van Nhieu. Binding and internalization of microorganisms by integrin receptors. *Trends Microbiol.*, 2(1):10–14, 1994.

- [85] J. E. Italiano and E. M. Battinelli. Selective sorting of alpha-granule proteins. *J. Thromb. Haemost.*, 7(S1):173–6, 2009.
- [86] J. E. Italiano, J. L. Richardson, S. Patel-Hett, E. Battinelli, A. Zaslavsky, S. Short, S. Ryeom, J. Folkman, and G. L. Klement. Angiogenesis is regulated by a novel mechanism: pro- and antiangiogenic proteins are organized into separate platelet alpha granules and differentially released. *Blood*, 111(3):1227–33, 2008.
- [87] S. P. Jackson. Arterial thrombosis—insidious, unpredictable and deadly. *Nat. Med.*, 17(11):1423–36, 2011.
- [88] S. Jain, M. Zuka, J. Liu, S. Russell, J. Dent, J. a. Guerrero, J. Forsyth, B. Maruszak, T. K. Gartner, B. Felding-Habermann, and J. Ware. Platelet glycoprotein Ib alpha supports experimental lung metastasis. *Proc. Natl. Acad. Sci. U. S. A.*, 104(21):9024–9028, 2007.
- [89] S. K. James, R. F. Storey, N. S. Khurmi, S. Husted, M. Keltai, K. W. Mahaffey, J. Maya, J. Morais, R. D. Lopes, J. C. Nicolau, P. Pais, D. Raev, J. L. Lopez-Sendon, S. R. Stevens, and R. C. Becker. Ticagrelor versus clopidogrel in patients with acute coronary syndromes and a history of stroke or transient ischemic attack. *Circulation*, 125(23):2914–2921, 2012.
- [90] T. Junt, H. Schulze, Z. Chen, S. Massberg, T. Goerge, A. Krueger, D. D. Wagner, T. Graf, J. E. Italiano, R. A. Shivdasani, and U. H. von Andrian. Dynamic visualization of thrombopoiesis within bone marrow. *Science*, 317(5845):1767–1770, 2007.
- [91] W. H. A. Kahr, J. Hinckley, L. Li, H. Schwertz, H. Christensen, J. W. Rowley, F. G. Pluthero, D. Urban, S. Fabbro, B. Nixon, R. Gadzinski, M. Storck, K. Wang, G.-Y. Ryu, S. M. Jobe, B. C. Schutte, J. Moseley, N. B. Loughran, J. Parkinson, A. S. Weyrich, and J. Di Paola. Mutations in NBEAL2, encoding a BEACH protein, cause gray platelet syndrome. *Nat. Genet.*, 43(8):738–740, 2011.
- [92] W. H. A. Kahr, R. W. Lo, L. Li, F. G. Pluthero, H. Christensen, R. Ni, N. Vaezzadeh, C. E. Hawkins, a. S. Weyrich, J. Di Paola, C. Landolt-Marticorena, and P. L. Gross. Abnormal megakaryocyte development and platelet function in Nbeal2<sup>-/-</sup> mice. *Blood*, 122(19):3349–58, 2013.
- [93] W. H. A. Kahr, R. W. Lo, L. Li, F. G. Pluthero, H. Christensen, R. Ni, N. Vaezzadeh, C. E. Hawkins, A. S. Weyrich, J. Di Paola, C. Landolt-Marticorena, and P. L. Gross. Abnormal megakaryocyte development and platelet function in Nbeal2<sup>-/-</sup> mice. *Blood*, 122(19):3349–58, 2013.
- [94] J. Kamykowski, P. Carlton, S. Sehgal, and B. Storrie. Quantitative immunofluorescence mapping reveals little functional coclustering of proteins within platelet  $\alpha$ -granules. *Blood*, 118(5):1370–3, 2011.

- [95] T. Kanaji, S. Russell, and J. Ware. Amelioration of the macrothrombocytopenia associated with the murine Bernard-Soulier syndrome. *Blood*, 100(6):2102–2107, 2002.
- [96] S. Karpatkin, E. Pearlstein, C. Ambrogio, and B. S. Coller. Role of adhesive proteins in platelet tumor interaction in vitro and metastasis formation in vivo. *J. Clin. Invest.*, 81(4):1012–1019, 1988.
- [97] E. Karshovska, C. Weber, and P. von Hundelshausen. Platelet chemokines in health and disease. *Thromb. Haemost.*, 110(3):1–9, 2013.
- [98] R. M. Kaufman, R. Airo, S. Pollack, and W. H. Crosby. Circulating Megakaryocytes and Platelet Release in the Lung. *Blood*, 26(6):720–731, 1965.
- [99] S. King and G. Reed. Development of platelet secretory granules. *Semin. Cell Dev. Biol.*, 13(4):293–302, 2002.
- [100] C. Kleinschnitz, S. F. De Meyer, T. Schwarz, M. Austinat, K. Vanhoorelbeke, B. Nieswandt, H. Deckmyn, and G. Stoll. Deficiency of von Willebrand factor protects mice from ischemic stroke. *Blood*, 113(15):3600–3, 2009.
- [101] C. Kleinschnitz, M. Pozgajova, M. Pham, M. Bendszus, B. Nieswandt, and G. Stoll. Targeting platelets in acute experimental stroke: impact of glycoprotein Ib, VI, and IIb/IIIa blockade on infarct size, functional outcome, and intracranial bleeding. *Circulation*, 115(17):2323–30, 2007.
- [102] M. H. F. Klinger and W. Jelkmann. Role of blood platelets in infection and inflammation. *J. Interf. Cytokine Res.*, 22(9):913–922, 2002.
- [103] G. Kosaki. Platelet production by megakaryocytes: Protoplatelet theory justifies cytoplasmic fragmentation model. *Int. J. Hematol.*, 88(3):255–267, 2008.
- [104] A. Kulkarni, C. Huh, D. Becker, A. Geiser, M. Lyght, K. Flanders, A. Roberts, M. Sporn, J. Ward, and S. Karlsson. Transforming growth factor beta 1 null mutation in mice causes excessive inflammatory response and early death. *Proc. Natl. Acad. Sci. U. S. A.*, 90(2):770–4, 1993.
- [105] H. F. Langer, E. Y. Choi, H. Zhou, R. Schleicher, K. J. Chung, Z. Tang, K. Göbel, K. Bdeir, A. Chatzigeorgiou, C. Wong, S. Bhatia, M. J. Kruhlak, J. W. Rose, J. B. Burns, K. E. Hill, H. Qu, Y. Zhang, E. Lehrmann, K. G. Becker, Y. Wang, D. I. Simon, B. Nieswandt, J. D. Lambris, X. Li, S. G. Meuth, P. Kubes, and T. Chavakis. Platelets contribute to the pathogenesis of experimental autoimmune encephalomyelitis. *Circ. Res.*, 110(9):1202–1210, 2012.
- [106] P. P. Lemons, D. Chen, a. M. Bernstein, M. K. Bennett, and S. W. Whiteheart. Regulated secretion in platelets: identification of elements of the platelet exocytosis machinery. *Blood*, 90(4):1490–1500, 1997.

- [107] C. Léon, B. Hechler, M. Freund, A. Eckly, C. Vial, P. Ohlmann, A. Dierich, M. LeMeur, J. P. Cazenave, and C. Gachet. Defective platelet aggregation and increased resistance to thrombosis in purinergic P2Y1 receptor-null mice. *J. Clin. Invest.*, 104(12):1731–1737, 1999.
- [108] W. Li, M. E. Rusiniak, S. Chintala, R. Gautam, E. K. Novak, and R. T. Swank. Murine Hermansky-Pudlak syndrome genes: Regulators of lysosome-related organelles. *BioEssays*, 26(6):616–628, 2004.
- [109] K. L. Lowe, B. A. Finney, C. Deppermann, R. Hagerling, S. L. Gazit, J. Frampton, C. D. Buckley, E. Camerer, B. Nieswandt, F. Kiefer, and S. P. Watson. Podoplanin and CLEC-2 drive cerebrovascular patterning and integrity during development. *Blood*, 125(24):3769–3777, 2015.
- [110] T. Lucas, A. Waisman, R. Ranjan, J. Roes, T. Krieg, W. Müller, A. Roers, and S. A. Eming. Differential roles of macrophages in diverse phases of skin repair. *J. Immunol.*, 184(7):3964–77, 2010.
- [111] K. R. Machlus and J. E. Italiano. The incredible journey: From megakaryocyte development to platelet formation. *J. Cell Biol.*, 201(6):785–796, 2013.
- [112] M. S. Marks. A Munc in the platelet granule works. *Blood*, 116(6):864–5, 2010.
- [113] M. S. Marks. SNARing platelet granule secretion. *Blood*, 120(12):2355–2357, 2012.
- [114] L. Martorell, J. Martínez-González, C. Rodríguez, M. Gentile, O. Calvayrac, and L. Badimon. Thrombin and protease-activated receptors (PARs) in atherothrombosis. *Thromb. Haemost.*, 99(2):305–315, 2008.
- [115] J. Masliah-Planchon, L. Darnige, and S. Bellucci. Molecular determinants of platelet delta storage pool deficiencies: An update. *Br. J. Haematol.*, 160(1):5–11, 2013.
- [116] S. Massberg, M. Gawaz, S. Grüner, V. Schulte, I. Konrad, D. Zohlnhöfer, U. Heinzmann, and B. Nieswandt. A crucial role of glycoprotein VI for platelet recruitment to the injured arterial wall in vivo. *J. Exp. Med.*, 197(1):41–49, 2003.
- [117] F. May, I. Hagedorn, I. Pleines, M. Bender, T. Vogtle, J. Eble, M. Elvers, and B. Nieswandt. CLEC-2 is an essential platelet activating receptor in hemostasis and thrombosis. *Blood*, 114(16):3464–3473, 2009.
- [118] D. M. Maynard, H. F. G. Heijnen, W. A. Gahl, and M. Gunay-Aygun. The  $\alpha$ -granule proteome: novel proteins in normal and ghost granules in gray platelet syndrome. *J. Thromb. Haemost.*, 8(8):1786–96, Aug. 2010.
- [119] B. McDonald, R. Urrutia, B. G. Yipp, C. N. Jenne, and P. Kubes. Intravascular neutrophil extracellular traps capture bacteria from the bloodstream during sepsis. *Cell Host Microbe*, 12(3):324–333, 2012.

- [120] B. J. McMorran, V. M. Marshall, C. D. Graaf, K. E. Drysdale, M. Shabbar, G. K. Smyth, J. E. Corbin, W. S. Alexander, and S. J. Foote. Platelets Kill Intraerythrocytic Malarial Parasites and Mediate Survival to Infection. *Science*, 323(5915):797–800, 2009.
- [121] M. M. Ménager, G. Ménasché, M. Romao, P. Knapnougel, C.-H. Ho, M. Garfa, G. Raposo, J. Feldmann, A. Fischer, and G. de Saint Basile. Secretory cytotoxic granule maturation and exocytosis require the effector protein hMunc13-4. *Nat. Immunol.*, 8(3):257–267, 2007.
- [122] P. M. Moran, L. S. Higgins, B. Cordell, and P. C. Moser. Age-related learning deficits in transgenic mice expressing the 751-amino acid isoform of human beta-amyloid precursor protein. *Proc. Natl. Acad. Sci. U. S. A.*, 92(12):5341–5345, 1995.
- [123] M. Morowski, T. Vögtle, P. Kraft, C. Kleinschnitz, G. Stoll, and B. Nieswandt. Only severe thrombocytopenia results in bleeding and defective thrombus formation in mice. *Blood*, 121(24):4938–47, 2013.
- [124] M. Moser, B. Nieswandt, S. Ussar, M. Pozgajova, and R. Fässler. Kindlin-3 is essential for integrin activation and platelet aggregation. *Nat. Med.*, 14(3):325–330, 2008.
- [125] F. Müller, N. J. Mutch, W. a. Schenk, S. a. Smith, L. Esterl, H. M. Spronk, S. Schmidbauer, W. a. Gahl, J. H. Morrissey, and T. Renné. Platelet Polyphosphates Are Proinflammatory and Procoagulant Mediators In Vivo. *Cell*, 139(6):1143–1156, 2009.
- [126] M. Naghavi, H. Wang, ..., A. D. Lopez, and C. J. L. Murray. Global, regional, and national age–sex specific all-cause and cause-specific mortality for 240 causes of death , 1990–2013: a systematic analysis for the Global Burden of Disease Study 2013. *Lancet*, 385(9963):117–171, 2015.
- [127] A. P. Ng, M. Kauppi, D. Metcalf, C. D. Hyland, E. C. Josefsson, M. Lebois, J.-G. Zhang, T. M. Baldwin, L. Di Rago, D. J. Hilton, and W. S. Alexander. Mpl expression on megakaryocytes and platelets is dispensable for thrombopoiesis but essential to prevent myeloproliferation. *Proc. Natl. Acad. Sci. U. S. A.*, 111(16):5884–9, 2014.
- [128] B. Nieswandt, W. Bergmeier, K. Rackebrandt, J. E. Gessner, and H. Zirngibl. Identification of critical antigen-specific mechanisms in the development of immune thrombocytopenic purpura in mice. *Blood*, 96(7):2520–2527, 2000.
- [129] B. Nieswandt, C. Brakebusch, W. Bergmeier, V. Schulte, D. Bouvard, R. Mokhtari-Nejad, T. Lindhout, J. W. Heemskerk, H. Zirngibl, and R. Fässler. Glycoprotein VI but not alpha2beta1 integrin is essential for platelet interaction with collagen. *EMBO J.*, 20(9):2120–30, 2001.
- [130] B. Nieswandt, C. Kleinschnitz, and G. Stoll. Ischaemic stroke: a thrombo-inflammatory disease? *J. Physiol.*, 589(17):4115–23, 2011.

- [131] B. Nieswandt, I. Pleines, and M. Bender. Platelet adhesion and activation mechanisms in arterial thrombosis and ischaemic stroke. *J. Thromb. Haemost.*, 9(S1):92–104, 2011.
- [132] B. Nieswandt, V. Schulte, W. Bergmeier, R. Mokhtari-Nejad, K. Rackebrandt, J. P. Cazenave, P. Ohlmann, C. Gachet, and H. Zirngibl. Long-term antithrombotic protection by in vivo depletion of platelet glycoprotein VI in mice. *J. Exp. Med.*, 193(4):459–469, 2001.
- [133] B. Nieswandt and S. Stritt. Megakaryocyte rupture for acute platelet needs. *J. Cell Biol.*, 209(3):327–328, 2015.
- [134] B. Nieswandt and S. P. Watson. Platelet-collagen interaction: Is GPVI the central receptor? *Blood*, 102(2):449–461, 2003.
- [135] S. Nishimura, M. Nagasaki, S. Kunishima, A. Sawaguchi, A. Sakata, H. Sakaguchi, T. Ohmori, I. Manabe, J. E. Italiano, T. Ryu, N. Takayama, I. Komuro, T. Kadowaki, K. Eto, and R. Nagai. IL-1alpha induces thrombopoiesis through megakaryocyte rupture in response to acute platelet needs. *J. Cell Biol.*, 209(3):453–466, 2015.
- [136] A. Nurden. Platelets, inflammation and tissue regeneration. *Thromb. Haemost.*, 105(S6):S13–33, 2011.
- [137] A. Nurden and P. Nurden. Advances in our understanding of the molecular basis of disorders of platelet function. *J. Thromb. Haemost.*, 9(S1):76–91, 2011.
- [138] A. Nurden, P. Nurden, M. Sanchez, I. Andia, and E. Anitua. Platelets and wound healing. *Front. Biosci.*, 13:3532–3548, 2008.
- [139] A. T. Nurden and P. Nurden. The gray platelet syndrome: clinical spectrum of the disease. *Blood Rev.*, 21(1):21–36, 2007.
- [140] A. T. Nurden and P. Nurden. Congenital platelet disorders and understanding of platelet function. *Br. J. Haematol.*, 165(2):165–178, 2014.
- [141] A. T. Nurden, P. Nurden, E. Bermejo, R. Combrié, D. W. McVicar, and a. V. Washington. Phenotypic heterogeneity in the Gray platelet syndrome extends to the expression of TREM family member, TLT-1. *Thromb. Haemost.*, 100(1):45–51, 2008.
- [142] S. Offermanns. Activation of platelet function through G protein-coupled receptors. *Circ. Res.*, 99(12):1293–1304, 2006.
- [143] L. Pang, M. J. Weiss, and M. Poncz. Megakaryocyte biology and related disorders. *J. Clin. Invest.*, 115(12):3332–3338, 2005.
- [144] S. R. Patel, J. H. Hartwig, and J. E. Italiano. The biogenesis of platelets from megakaryocyte proplatelets. *J. Clin. Invest.*, 115(12):3348–3354, 2005.

- [145] C. G. Peters, A. D. Michelson, and R. Flaumenhaft. Granule exocytosis is required for platelet spreading: differential sorting of  $\alpha$ -granules expressing VAMP-7. *Blood*, 120(1):199–206, 2012.
- [146] B. Petri, A. Broermann, H. Li, A. G. Khandoga, A. Zarbock, F. Krombach, T. Goerge, S. W. Schneider, C. Jones, B. Nieswandt, M. K. Wild, and D. Vestweber. von Willebrand factor promotes leukocyte extravasation. *Blood*, 116(22):4712–4719, 2010.
- [147] I. Pleines, I. Hagedorn, S. Gupta, F. May, L. Chakarova, J. van Hengel, S. Offermanns, G. Krohne, C. Kleinschnitz, C. Brakebusch, and B. Nieswandt. Megakaryocyte-specific RhoA deficiency causes macrothrombocytopenia and defective platelet activation in hemostasis and thrombosis. *Blood*, 119(4):1054–63, Jan. 2012.
- [148] J. Polgár, S. H. Chung, and G. L. Reed. Vesicle-associated membrane protein 3 (VAMP-3) and VAMP-8 are present in human platelets and are required for granule secretion. *Blood*, 100(3):1081–1083, 2002.
- [149] G. Raccuglia. Gray platelet syndrome. *Am. J. Med.*, 51(12):818–828, 1971.
- [150] Q. Ren, H. K. Barber, G. L. Crawford, Z. A. Karim, C. Zhao, W. Choi, C.-C. Wang, W. Hong, and S. W. Whiteheart. Endobrevin/VAMP-8 is the primary v-SNARE for the platelet release reaction. *Mol. Biol. Cell*, 18(1):24–33, 2007.
- [151] Q. Ren, C. Wimmer, M. C. Chicka, S. Ye, Y. Ren, F. M. Hughson, and S. W. Whiteheart. Munc13-4 is a limiting factor in the pathway required for platelet granule release and hemostasis. *Blood*, 116(6):869–77, 2010.
- [152] Q. Ren, S. Ye, and S. Whiteheart. The platelet release reaction: just when you thought platelet secretion was simple. *Curr. Opin. Hematol.*, 15(5):537, 2008.
- [153] F. Rendu and B. Brohard-Bohn. The platelet release reaction: granules' constituents, secretion and functions. *Platelets*, 12(5):261–73, 2001.
- [154] J. L. Richardson, R. A. Shivdasani, C. Boers, J. H. Hartwig, and J. E. Italiano. Mechanisms of organelle transport and capture along proplatelets during platelet production. *Blood*, 106(13):4066–4075, 2005.
- [155] R. P. Rodgers and J. Levin. A critical reappraisal of the bleeding time. *Semin. Thromb. Hemost.*, 16(1):1–20, 1990.
- [156] B. Roscic-Mrkic, M. Fischer, C. Leemann, A. Manrique, C. J. Gordon, J. P. Moore, A. E. I. Proudfoot, and A. Trkola. RANTES (CCL5) uses the proteoglycan CD44 as an auxiliary receptor to mediate cellular activation signals and HIV-1 enhancement. *Blood*, 102(4):1169–1177, 2003.
- [157] U. J. H. Sachs and B. Nieswandt. In vivo thrombus formation in murine models. *Circ. Res.*, 100(7):979–91, 2007.



- [158] B. Savage, F. Almus-Jacobs, and Z. M. Ruggeri. Specific synergy of multiple substrate-receptor interactions in platelet thrombus formation under flow. *Cell*, 94(5):657–66, 1998.
- [159] J. S. Savage, C. M. Williams, O. Konopatskaya, I. Hers, M. T. Harper, and A. W. Poole. Munc13-4 is critical for thrombosis through regulating release of ADP from platelets. *J. Thromb. Haemost.*, 11(4):771–5, 2013.
- [160] S. S. Scherer, M. Tobalem, E. Vigato, Y. Heit, A. Modarressi, B. Hinz, B. Pittet, and G. Pietramaggiore. Nonactivated versus thrombin-activated platelets on wound healing and fibroblast-to-myofibroblast differentiation in vivo and in vitro. *Plast. Reconstr. Surg.*, 129(1):46e–54e, 2012.
- [161] H. Schulze, M. Korpai, J. Hurov, S. W. Kim, J. Zhang, L. C. Cantley, T. Graf, and R. A. Shivdasani. Characterization of the megakaryocyte demarcation membrane system and its role in thrombopoiesis. *Blood*, 107(10):3868–3875, 2006.
- [162] D. Schumacher, B. Strilic, K. K. Sivaraj, N. Wettschureck, and S. Offermanns. Platelet-Derived Nucleotides Promote Tumor-Cell Transendothelial Migration and Metastasis via P2Y2 Receptor. *Cancer Cell*, 24(1):130–137, 2013.
- [163] J. W. Semple, J. E. Italiano, and J. Freedman. Platelets and the immune continuum. *Nat. Rev. Immunol.*, 11(4):264–74, 2011.
- [164] H. Seppa, G. Grotendorst, S. Seppa, E. Schiffmann, and G. R. Martin. Platelet-derived Growth Factor Is Chemotactic for Fibroblasts Sources of Growth Factors Synthesis in Fibroblast Cultures. *J Cell Biol.*, 92(2):584–588, 1982.
- [165] S. J. Shattil, C. Kim, and M. H. Ginsberg. The final steps of integrin activation: the end game. *Nat. Rev. Mol. Cell Biol.*, 11(4):288–300, 2010.
- [166] R. L. Silverstein, L. L. Leung, and R. L. Nachman. Thrombospondin: a versatile multifunctional glycoprotein. *Arterioscler. Thromb. Vasc. Biol.*, 6(3):245–253, 1986.
- [167] S. A. Smith, S. H. Choi, J. N. R. Collins, R. J. Travers, B. C. Cooley, and J. H. Morrissey. Inhibition of polyphosphate as a novel strategy for preventing thrombosis and inflammation. *Blood*, 120(26):5103–5110, 2012.
- [168] S. A. Smith, N. J. Mutch, D. Baskar, P. Rohloff, R. Docampo, and J. H. Morrissey. Polyphosphate modulates blood coagulation and fibrinolysis. *Proc. Natl. Acad. Sci. U. S. A.*, 103(4):903–908, 2006.
- [169] T. Söllner, S. W. Whiteheart, M. Brunner, H. Erdjument-Bromage, S. Geromanos, P. Tempst, and J. E. Rothman. SNAP receptors implicated in vesicle targeting and fusion. *Nature*, 362(6418):318–324, 1993.

- [170] D. Stegner, C. Deppermann, P. Kraft, M. Morowski, C. Kleinschnitz, G. Stoll, and B. Nieswandt. Munc13-4 mediated secretion is essential for infarct progression but not intracranial haemostasis in acute stroke. *J. Thromb. Haemost.*, 11(7):1430–33, 2013.
- [171] D. Stegner, S. Dütting, and B. Nieswandt. Mechanistic explanation for platelet contribution to cancer metastasis. *Thromb. Res.*, 133(S2):S149–57, 2014.
- [172] G. Stoll, C. Kleinschnitz, and B. Nieswandt. Molecular mechanisms of thrombus formation in ischemic stroke: novel insights and targets for treatment. *Blood*, 112(9):3555–62, 2008.
- [173] S. Stritt, K. Wolf, V. Lorenz, V. Timo, S. Gupta, R. B. Michael, and B. Nieswandt. Rap1-GTP – interacting adaptor molecule (RIAM) is dispensable for platelet integrin activation and function in mice. *Blood*, 125(2):219–223, 2015.
- [174] T. C. Südhof and J. E. Rothman. Membrane fusion: grappling with SNARE and SM proteins. *Science*, 323(5913):474–477, 2009.
- [175] A. Suzuki, J. W. Shin, Y. Wang, S. H. Min, M. Poncz, J. K. Choi, D. E. Discher, C. L. Carpenter, L. Lian, L. Zhao, Y. Wang, and C. S. Abrams. RhoA Is Essential for Maintaining Normal Megakaryocyte Ploidy and Platelet Generation. *PLoS One*, 8(7), 2013.
- [176] J. Suzuki, M. Umeda, P. J. Sims, and S. Nagata. Calcium-dependent phospholipid scrambling by TMEM16F. *Nature*, 468(7325):834–8, 2010.
- [177] K. Suzuki-Inoue, G. L. J. Fuller, A. García, J. A. Eble, S. Pöhlmann, O. Inoue, T. K. Gartner, S. C. Hughan, A. C. Pearce, G. D. Laing, R. D. G. Theakston, E. Schweighoffer, N. Zitzmann, T. Morita, V. L. J. Tybulewicz, Y. Ozaki, and S. P. Watson. A novel Syk-dependent mechanism of platelet activation by the C-type lectin receptor CLEC-2. *Blood*, 107(2):542–549, 2006.
- [178] R. Swanson, M. Morton, G. Tsao-Wu, R. Savalos, C. Davidson, and F. Sharp. A semi-automated method for measuring brain infarct volume. *J. Cereb. Blood Flow Metab.*, 10:290–293, 1990.
- [179] A. Szpaderska, E. Egozi, R. Gamelli, and L. DiPietro. The effect of thrombocytopenia on dermal wound healing. *J. Investig. Dermatology Symp. Proc.*, 120(6):1130–7, 2003.
- [180] J. N. Thon, A. Montalvo, S. Patel-Hett, M. T. Devine, J. L. Richardson, A. Ehrlicher, M. K. Larson, K. Hoffmeister, J. H. Hartwig, and J. E. Italiano. Cytoskeletal mechanics of pro-platelet maturation and platelet release. *J. Cell Biol.*, 191(4):861–74, Nov. 2010.
- [181] M. R. Tijssen and C. Ghevaert. Transcription factors in late megakaryopoiesis and related platelet disorders. *J. Thromb. Haemost.*, 11(4):593–604, 2013.
- [182] J. J. Tomasek, G. Gabbiani, B. Hinz, C. Chaponnier, and R. A. Brown. Myofibroblasts and mechano-regulation of connective tissue remodelling. *Nat. Rev. Mol. Cell Biol.*, 3(5):349–63, 2002.

- [183] K. Umemura, H. Ishihara, and M. Nakashima. Anti-platelet effects of clopidogrel in rat middle cerebral artery thrombosis model. *Thromb. Res.*, 80(3):209–216, 1995.
- [184] D. Urban, N. Li, H. Christensen, F. G. Pluthero, S. Z. Chen, M. Puhacz, P. M. Garg, K. K. Lanka, J. J. Cummings, H. Kramer, J. D. Wasmuth, J. Parkinson, and W. H. A. Kahr. The VPS33B-binding protein VPS16B is required in megakaryocyte and platelet  $\alpha$ -granule biogenesis. *Blood*, 120(25):5032–5040, 2012.
- [185] D. Varga-Szabo, A. Braun, C. Kleinschnitz, M. Bender, I. Pleines, M. Pham, T. Renné, G. Stoll, and B. Nieswandt. The calcium sensor STIM1 is an essential mediator of arterial thrombosis and ischemic brain infarction. *J. Exp. Med.*, 205(7):1583–1591, 2008.
- [186] D. Varga-Szabo, a. Braun, and B. Nieswandt. Calcium signaling in platelets. *J. Thromb. Haemost.*, 7(7):1057–1066, 2009.
- [187] D. Varga-Szabo, I. Pleines, and B. Nieswandt. Cell adhesion mechanisms in platelets. *Arterioscler. Thromb. Vasc. Biol.*, 28(3):403–12, 2008.
- [188] N. Vitrat, K. Cohen-Solal, C. Pique, J. P. Le Couedic, F. Norol, A. K. Larsen, A. Katz, W. Vainchenker, and N. Debili. Endomitosis of human megakaryocytes are due to abortive mitosis. *Blood*, 91(10):3711–3723, 1998.
- [189] T. Vögtle, D. Cherpokova, M. Bender, and B. Nieswandt. Targeting platelet receptors in thrombotic and thrombo-inflammatory disorders. *Haemostaseologie*, 35(2), 2015.
- [190] Y. Wang, V. Hayes, D. Jarocha, X. Sim, D. C. Harper, R. Fuentes, S. K. Sullivan, P. Gadue, S. T. Chou, B. J. Torok-storb, M. S. Marks, D. L. French, and M. Poncz. Comparative analysis of human ex vivo – generated platelets vs megakaryocyte-generated platelets in mice : a cautionary tale. *Blood*, 125(23):3627–3637, 2015.
- [191] S. P. Watson, J. M. Auger, O. J. T. McCarty, and a. C. Pearce. GPVI and integrin  $\alpha$ IIb  $\beta$ 3 signaling in platelets. *J. Thromb. Haemost.*, 3(8):1752–1762, 2005.
- [192] S. Werner and R. Grose. Regulation of Wound Healing by Growth Factors and Cytokines. *Physiol. Rev.*, 83:835–870, 2003.
- [193] T. A. Wilgus, A. M. Matthies, K. A. Radek, J. V. Dovi, A. L. Burns, R. Shankar, and L. A. DiPietro. Novel function for vascular endothelial growth factor receptor-1 on epidermal keratinocytes. *Am. J. Pathol.*, 167(5):1257–66, 2005.
- [194] C. H. Y. Wong, C. N. Jenne, B. Petri, N. L. Chrobok, and P. Kubes. Nucleation of platelets with blood-borne pathogens on Kupffer cells precedes other innate immunity and contributes to bacterial clearance. *Nat. Immunol.*, 14(8):785–92, 2013.
- [195] D. S. Woulfe, J. K. Lilliendahl, S. August, L. Rauova, M. A. Kowalska, M. Abrink, G. Pejler, J. G. White, and B. P. Schick. Serglycin proteoglycan deletion induces defects in platelet aggregation and thrombus formation in mice. *Blood*, 111(7):3458–3467, 2008.

- [196] B. Xiang, G. Zhang, L. Stefanini, W. Bergmeier, T. K. Gartner, S. W. Whiteheart, and Z. Li. The Src family kinases and protein kinase C synergize to mediate Gq-dependent platelet activation. *J. Biol. Chem.*, 287(49):41277–87, 2012.
- [197] H. Yang, A. Kim, T. David, D. Palmer, T. Jin, J. Tien, F. Huang, T. Cheng, S. R. Coughlin, Y. N. Jan, and L. Y. Jan. TMEM16F Forms a Ca(2+)-Activated Cation Channel Required for Lipid Scrambling in Platelets during Blood Coagulation. *Cell*, 151(1):111–22, 2012.
- [198] H. Yang, A. Reheman, P. Chen, G. Zhu, R. O. Hynes, J. Freedman, D. D. Wagner, and H. Ni. Fibrinogen and von Willebrand factor-independent platelet aggregation in vitro and in vivo. *J. Thromb. Haemost.*, 4(10):2230–7, 2006.
- [199] S. Ye, Z. A. Karim, R. Al Hawas, J. E. Pessin, A. H. Filipovich, and S. W. Whiteheart. Syntaxin-11, but not syntaxin-2 or syntaxin-4, is required for platelet secretion. *Blood*, 120(12):2484–2492, 2012.
- [200] A. Zarbock, R. K. Polanowska-Grabowska, and K. Ley. Platelet-neutrophil-interactions: Linking hemostasis and inflammation. *Blood Rev.*, 21(2):99–111, 2007.
- [201] L. Zhang, M. Orban, M. Lorenz, V. Barocke, D. Braun, N. Urtz, C. Schulz, M.-L. von Brühl, A. Tirniceriu, F. Gaertner, R. L. Proia, T. Graf, S.-S. Bolz, E. Montanez, M. Prinz, A. Müller, L. von Baumgarten, A. Billich, M. Sixt, R. Fässler, U. H. von Andrian, T. Junt, and S. Massberg. A novel role of sphingosine 1-phosphate receptor S1pr1 in mouse thrombopoiesis. *J. Exp. Med.*, 209(12):2165–81, 2012.
- [202] B.-Q. Zhao, A. K. Chauhan, M. Canault, I. S. Patten, J. J. Yang, M. Dockal, F. Scheiflinger, and D. D. Wagner. von Willebrand factor – cleaving protease ADAMTS13 reduces ischemic brain injury in experimental stroke. *Blood*, 114(15):3329–3334, 2009.
- [203] L. Zhen, S. Jiang, L. Feng, N. A. Bright, A. A. Peden, A. B. Seymour, E. K. Novak, R. Elliott, M. B. Gorin, M. S. Robinson, and R. T. Swank. Abnormal expression and subcellular distribution of subunit proteins of the AP-3 adaptor complex lead to platelet storage pool deficiency in the pearl mouse. *Blood*, 94(1):146–155, 1999.
- [204] D. Zucker-Franklin. Endocytosis by human platelets: Metabolic and freeze-fracture studies. *J. Cell Biol.*, 91(3):706–715, 1981.

# 5 Appendix

## 5.1 Abbreviations

ADP	adenosine diphosphate
APS	ammonium persulfate
ATP	adenosine triphosphate
BM	bone marrow
BMC	bone marrow chimeras
bp	base pairs
BSA	bovine serum albumin
Ca/DAG-GEF	calcium and diacyl glycerol-regulated GEF
CLEC-2	C-type lectin-like receptor 2
CRP	collagen-related peptide
CVX	convulxin
DAG	diacylglycerol
DIC	differential interference contrast
DMEM	Dulbecco's modified Eagle's medium
DMS	demarcation membrane system
DMSO	dimethyl sulfoxide
dNTP	deoxynucleoside triphosphate
ECM	extracellular matrix
EDTA	ethylenediaminetetraacetic acid
EGF	epidermal growth factor
EGTA	ethylene glycol tetraacetic acid
ER	endoplasmic reticulum
ERK	extracellular-signal-regulated kinase
FACS	fluorescence-activated cell sorting
FcR	Fc receptor
FCS	fetal calf serum
FITC	fluorescein isothiocyanate
FLC	fetal liver cells
FSC	forward scatter
GDP	guanosine diphosphate
GEF	guanine nucleotide exchange factor
GP	glycoprotein

GPCR	G protein-coupled receptor
GPS	gray platelet syndrome
GTP	guanosine triphosphate
HCT	hematocrit
HEPES	4-(2-hydroxyethyl)-1-piperazineethanesulfonic acid
HGB	hemoglobin
HRP	horseradish peroxidase
IFI	integrated fluorescence intensity
IFN	interferon
Ig	immunoglobulin
IL	interleukin
IP	immunoprecipitation
IP <sub>3</sub>	inositol-1,4,5-trisphosphate
ITAM	immunoreceptor tyrosine-based activation motif
JAK	Janus kinase
LAT	linker for activation of T cells
mAb	monoclonal antibody
MCA	middle cerebral artery
MFI	mean fluorescence intensity
MK	megakaryocyte
MLC	myosin light chain
MMP	matrix metalloproteinase
MPV	mean platelet volume
mTOR	mammalian target of rapamycin
Nbeal2	neurobeachin like 2
NETs	neutrophil extracellular traps
PAR	protease-activated receptor
PCR	polymerase chain reaction
PE	phosphatidylethanolamine
PE	phycoerythrin
PF	platelet factor
PF4	platelet factor 4
PFA	paraformaldehyde
PGI <sub>2</sub>	prostacyclin
PH	pleckstrin homology
PI	phosphatidylinositol
PI3K	phosphoinositide-3-kinase
PIP2	phosphatidylinositol-4,5-bisphosphate
PIP5K	phosphatidylinositol 4-phosphate 5-kinase
PK	protein kinase
Plt	platelet

---

PMA	phorbol 12-myristate 13-acetate
PRP	platelet-rich plasma
PS	phosphatidylserine
PVDF	polyvinylidene difluoride
RBC	red blood cell
RC	rhodocytin
RhoGEF	Rho-specific guanine nucleotide exchange factor
RIAM	Rap1-GTP-interacting adapter protein
ROCK	RhoA kinase
rpm	rotations per minute
RT	room temperature
SD	standard deviation
SDS-PAGE	sodium dodecyl sulfate polyacrylamide gel electrophoresis
SERCA	sarco/endoplasmic reticulum $\text{Ca}^{2+}$ -ATPase
SH2	Src homology 2
SNARE	N-ethylmaleimide-sensitive fusion protein attachment protein receptors
SOCE	store-operated calcium entry
SSC	side scatter
Syk	spleen tyrosine kinase
TAE	TRIS acetate EDTA
TBS-T	TRIS-buffered saline containing Tween
TEMED	tetramethylethylenediamin
TEM	transmission electron microscopy
TF	tissue factor
tMCAO	transient middle cerebral artery occlusion
TNF	tumor necrosis factor
TRIS	tris(hydroxymethyl)aminomethane
TTC	2,3,5-triphenyltetrazolium chloride
TxA <sub>2</sub>	thromboxane A <sub>2</sub>
U46	U46619
vWF	von Willebrand factor
w/o	without
WBC	white blood cell
WT	wildtype

## 5.2 Acknowledgements

The work presented in this thesis was conducted in the group of Prof. Dr. Bernhard Nieswandt at the Department of Experimental Biomedicine, University Hospital and Rudolf Virchow Center, University of Würzburg. During my time as a PhD student (October 2011 – August 2015) many people helped and supported me. I would like to thank the following people:

- First and foremost I would like to thank my supervisor Prof. Dr. Bernhard Nieswandt who gave me the opportunity to work on the projects presented in this thesis and who always supported both my scientific and my professional development.
- Prof. Dr. Georg Krohne for being my second supervisor, for his support and especially for providing his expertise in electron microscopy.
- Dr. Paquita Nurden for her support and scientific advise, especially during the Nbeal2 project, in particular for her professional support and very fruitful discussions.
- Prof. Dr. Manfred Gessler who agreed to chair my thesis defense.
- Dr. David Stegner for supervision and support during several projects.
- Deya Cherpokova for great teamwork, support and encouragement.
- Prof. Dr. Guido Stoll and Dr. Peter Kraft from the department of neurology for the great and fruitful collaboration on several projects.
- Dr. Beate Eckes and Dr. Jan-Niklas Schulz from the department of dermatology at Cologne University for performing wound healing experiments.
- The Graduate School of Life Sciences for financial support and Dr. Gabriele Blum-Oehler, Bianca Putz and Jenny Heilig for always being there.
- All past and present members of the Nieswandt lab for making lab life so much fun. Sarah, Misch, Lizzie, Judith, Deya and David for proofreading this thesis.
- All of my friends in Frankfurt, Leer and everywhere for (non-)scientific discussions and the fun we had.
- Maria Trier ([www.mariatrier.de](http://www.mariatrier.de)) for help with designing the cover page.
- Als Letztes möchte ich ganz besonders meiner Familie danken, ohne deren Unterstützung ich es niemals soweit geschafft hätte.
- Think I forgot you, ha? Ute, love of my life! Thank you for everything.



## 5.3 Curriculum vitae

### PERSONAL DETAILS

---

Name: Carsten Deppermann  
Date of birth: May 7<sup>th</sup>, 1985  
Place of birth: Frankfurt/Main, Germany  
Nationality: German

### RESEARCH AND PROFESSIONAL EXPERIENCE

---

10/2011 - present      PhD student, Rudolf Virchow Center, Würzburg  
"The role of platelet granules in thrombosis, hemostasis, stroke  
and inflammation" in the laboratory of Prof. Dr. B. Nieswandt

09/2010 - 08/2011      Trainee Corporate Communications  
Boehringer Ingelheim, Ingelheim/Rhein

01/2010 - 08/2010      Diploma thesis, Institute for Neurology  
Goethe University Medical School, Frankfurt/Main  
"Interactions of the extracellular domains of the EGFR and  
 $\Delta$ EGFR" in the laboratory of Prof. Dr. M. Schmidt

### EDUCATION

---

10/2005 - 10/2010      Studies in biochemistry, Goethe University, Frankfurt/Main  
Majors: Cell biology, biochemistry and biophysical chemistry  
Final grade: 1.0 (with distinction)

09/2004 - 05/2005      Community service (School for physically handicapped children)  
Viktor-Frankl-Schule, Frankfurt/Main

06/2004                      A levels (Abitur), Elisabethengymnasium, Frankfurt/Main  
Majors: Mathematics and chemistry

## **HONORS AND AWARDS**

---

---

2012 - 2015	Fellowship of the Graduate School of Life Sciences, Würzburg
2015	ISTH Young Investigator Award 2015, Toronto, Canada
2014	ISTH Young Investigator Award 2014, Milwaukee, USA
2013	Hentschel Award for stroke research, Würzburg
2013	ISTH Young Investigator Award 2013, Amsterdam, The Netherlands

Würzburg, August 2015 \_\_\_\_\_

## 5.4 Publications

### 5.4.1 Research articles

Lowe K.L., Finney B.A., **Deppermann C.**, Hägerling R., Gazit S.L., Frampton J., Buckley C., Camerer E., Nieswandt B., Kiefer F. and Watson S.P. (2015). Podoplanin and CLEC-2 drive cerebrovascular patterning and integrity during development. *Blood*. 125 (24), 3769-3777

**Deppermann C.**, Cherpokova D., Nurden P., Schulz J., Thielmann I., Kraft P., Vögtle T., Kleinschnitz C., Dütting S., Krohne G., Eming S.A., Nurden A.T., Eckes B., Stoll G., Stegner D. and Nieswandt B. (2013). Gray platelet syndrome and defective thrombo-inflammation in Nbeal2-deficient mice. *J. Clin. Invest.* 123, 3331–3342.

**Deppermann C.**, Nurden P., Nurden A.T., Nieswandt B. and Stegner D. (2013). The Nbeal2<sup>-/-</sup> mouse as a model for the gray platelet syndrome. *Rare Diseases* 1:e26561

Stegner D.\*, **Deppermann C.\***, Kraft P., Morowski M., Kleinschnitz C., Stoll G. and Nieswandt B. (2013). Munc13-4 mediated secretion is essential for infarct progression but not intracranial haemostasis in acute stroke. *J. Thromb. Haemost.* 11, 1430–1433. \* Both authors contributed equally

Kraft P., Göb E., Schuhmann M.K., Göbel K., **Deppermann C.**, Thielmann I., Herrmann A.M., Lorenz K., Brede M., Stoll G., Meuth S.G., Nieswandt B., Pfeilschifter W. and Kleinschnitz C. (2013). FTY720 ameliorates acute ischemic stroke in mice by reducing thrombo-inflammation but not by direct neuroprotection. *Stroke*. 44, 3202–3210.

### 5.4.2 Selected talks and presentations

**Deppermann C.**, Kraft P., Wolf K., Nurden P., Stoll G., Stegner D. and Nieswandt B. (2015). Platelet granule release is crucial for vascular integrity in the ischemic brain but not in the inflamed skin or lung. Oral presentation at the ISTH congress 2015, Toronto, Canada

**Deppermann C.**, Wolf K., Stegner D. and Nieswandt B. (2014). Combined deficiency of platelet alpha and dense granules abrogates platelet aggregation and adhesion but has no effect on vascular integrity upon inflammation. Poster presentation at the ISTH SSC 2014 Milwaukee, USA

**Deppermann C.**, Cherpokova D., Nurden P., Thielmann I., Kraft P., Nurden A.T., Eckes B., Stoll G., Stegner D. and Nieswandt B. (2013). Nbeal2-deficient mice reveal a key role of platelet alpha-granules in arterial thrombosis, thromboinflammatory brain infarction and wound healing. Oral presentation at the ISTH congress 2013 Amsterdam, The Netherlands

**Deppermann C.**, Morowski M., Kraft P., Stoll G. and Nieswandt B. (2012). Munc13-4 is a major regulator of platelet degranulation. Poster presentation at the Joint Symposium „Cell-cell interactions in cardiovascular damage and healing“ of the SFB 688 together with the Comprehensive Heart Failure Center and the Rudolf Virchow Center, Würzburg

## 5.5 Affidavit

I hereby confirm that my thesis entitled "The role of platelet granules in thrombosis, hemostasis, stroke and inflammation" is the result of my own work. I did not receive any help or support from commercial consultants. All sources and/or materials applied are listed and specified in the thesis.

Furthermore, I confirm that this thesis has not yet been submitted as part of another examination process neither in identical nor in similar form.

Würzburg, August 2015 \_\_\_\_\_

## 5.6 Eidesstattliche Erklärung

Hiermit erkläre ich an Eides statt, die Dissertation "The role of platelet granules in thrombosis, hemostasis, stroke and inflammation" eigenständig, d.h. insbesondere selbständig und ohne Hilfe eines kommerziellen Promotionsberaters, angefertigt und keine anderen als die von mir angegebenen Quellen und Hilfsmittel verwendet zu haben.

Ich erkläre außerdem, dass die Dissertation weder in gleicher noch in ähnlicher Form bereits in einem anderen Prüfungsverfahren vorgelegen hat.

Würzburg, August 2015 \_\_\_\_\_